

## Content

- Topic 1:** Design and Composition of Orthodontic Bracket with  
Stainless Steel .....2  
*Ade Gratia Novalina Silaban*
- Topic2:** Preparation and Characterization of TiO<sub>2</sub>- based Planar-  
Heterojunction Perovskite Solar Cell.....41  
*Cho ChoThet*
- Topic 3:** Polybrominated diphenyl ethers (PBDEs),  
organophosphorus flame retardants (PFRs) and phthalates in floor  
and road dust from an e-waste dismantling facility and adjacent  
communities in Thailand.....60  
*Dudsadee Muenhor, Hyo-Bang Moon, Sunggyu Lee*
- Topic 4:** Eating Disorders and Weight Issues in Adolescents.....109  
*Frima Elda*
- Topic 5:** Resistive Switching Effect in Chromium Oxide Thin Film  
Probed by Conductive Atomic Force Microscopy.....128  
*Pham Kim Ngoc*
- Topic 6:** A Comprehensive Proteome Analysis of *Acinetobacter*  
*baumannii* Outer Membrane Vesicles Grown under Biofilm and  
Planktonic Conditions.....150  
*Vanitha Mariapan*

**Design and Composition of Orthodontic Bracket with Stainless Steel by Metal Injection Molding**

*Ade Gratia Novalina Silaban*

## **Theory of Metal Injection Molding**

### **Metal Powder Injection Molding (MIM) key trends and markets**

R. M. GERMAN, San Diego University, USA

#### **1. Introduction and Backgrounds**

Metal powder injection molding (MIM) is a subdivision of Powder injection molding (PIM) that relies on shaping metal particles and subsequently sintering those particles. Not like PIM, MIM product is nearly full density (because of the sintering process), has higher strength compared to die casting product, improved tolerances compared with investment or sand casting, and more shape complexity compared with most other forming routes. MIM has the capability to produce high complexity product with high production quantities, excellent performance, and often lower cost production compared to its competition. That's why, MIM has developed rapidly since its first demonstrations in 1970s until now, especially after 1990.

#### **2. History of success**

The development of powder injection molding was started after the development of plastic injection molding. Not long after the invention of Bakelite at about 1909. After this invention, many kind of thermoplastic such as polyethylene and polypropylene emerged to the industrial world, and soon after the machine to form them appeared. PIM first demonstration was in the USA and Germany during 1930s in the production of ceramic spark plug body, and then followed by the use of PIM in tableware production in the early 1960s. The MIM variant reached production in the 1970s. The advent of microprocessor-controlled processing equipment has allowed MIM to be applied in the industry, which enabled repeatable and defect-free cycles with tighter tolerances.

The first patent in MIM was made by Ron Rivers (Rivers) that used cellulose-water-glycerin as binder and proved to be unsuccessful. After that, the use of thermoplastic wax-based binders was introduced and able to reach production at several sites.

The most attractive development of MIM that expanded its use was when it won two design awards in 1979. It was for screw seal used in

Boeing jetliner and for a niobium alloy thrust-chamber and injection for a liquid-propellant rocket engine developed under an Air Force contract for Rocketdyne. After that, more patent were invented and the most useful of them was in 1980 by Ray Wiech. This era start many more patent, applications, and firms arose in MIM, especially in California. In the middle of 1980s, more companies used this production method without license by hiring former employees from the earlier firms to know the technology.

After so many years, the early binder patents have expired, but the wax-polymer system introduced by Ray Wiech is still mainly used in the industry. But in the mid-1990s, the use of paraffin wax has been replaced by other variants such as polyethylene glycol to give water solubility to part of the binder system.

Because of this development in the binder system, now MIM concept relies on plastic injection molding technology to shape powder-polymer feedstock into the desired shape. The shape must be oversized to accommodate the shrinkage during sintering that will remove the polymers and densified the metal particles. The result is a near full density product with smaller dimension of the molded shape that has performance attributes very close to the handbook values, usually far superior to that encountered in traditional press-sinter powder metallurgy and investment casting. This success is widely employed in small, complex, and high-value components, ranging from automotive fuel injectors to watch cases.

### **3. Market Opportunities**

There are so many products that have been manufactured by means of metal injection molding. These products are vary from electrical circuits component, firearm, medical devices and implants, even micro and nano robotics. Listed below are several often discussed market opportunities and some of the related information on growth aspects relative to MIM and its future.

- Cell phone, and computer, the use of MIM in the manufacturing of electronic components such as in hand-held devices such as cell phone and portable computer continue to increase since 2009. This components are small,

complex, and strong, applied to switches, buttons, hinges, latches, and decorative devices.

- Firearm industry, with its rapid escalation after the election of President Obama at 2008 due to fear of new restrictive gun laws; although that wave passed in North America, the temporary surge offset the economic decline seen in many other fields. Military procurement of firearm components has started to slow. However, smaller firearm manufacturers have started to embrace MIM.
- Industrial, hand tool, and household applications remain strong and steady, and include valve, plumbing, spraying, wrenches, multi-tools, pepper grinders, scissors, circular saws, nailing guns, and similar devices.
- Automotive applications for MIM started to escalate with use in turbochargers, fuel injectors, control components (clock mounts, entry locks, knobs, and levers), and valve lifters. This initiated in the USA for Buick and Chrysler application, but leadership shifted to Japan with Honda and Toyota applications from integrated vendors (Nippon Piston Rings) for turbocharger and valve applications. Subsequently, European MIM shops picked up on the materials and applications opened by the higher performance but smaller engines, and this wave has become global. There are many complaints over automotive parts production, but it generates large sales volumes that help to lower all costs and improve the field. All expectations are that MIM will continue to grow in the automotive sector.
- Medical applications are growing from an early base of endoscopic devices, and will become enormous as MIM becomes widely accepted. Much of the recent growth has been in minimally invasive surgical tools and robotic devices. Early frustrations were with the time to become qualified and the relatively small production lots on many surgical tools. Now adaptations to the market show that much higher prices allow for profitable MIM production in the smaller lots. For example, with knee implants in the USA, one million replacements are made per year, so that is an attractive opportunity. However, there are left and right

knees, and about 12 designs or styles. Thus the fragmentation show on average 40 000 per year of a design, and since there are three leaders in this market, any one company might only order 12 000 of each part per year. This is a low production volume application for MIM. However, pricing allows for sales that might reach \$4 million per design. So far only a few MIM firms are positioning for the production of implants, while many are seeking orders in surgical hand tools. Minimally invasive surgical tools are a prime opportunity for MIM. Micro-featured devices are frequently shown for new genetic sensors (micro-pillar, micro-texture and micro-array designs). These will be small devices, potentially used in enormous quantities for rapid blood testing and disease identification.

- Dental applications in this field long ago matured and today there are several firms involved in orthodontic bracket fabrication. However, new instrument and hand tool designs have opened up special opportunities for micro-featured designs. So MIM is moving from its strong historical position in orthodontic brackets into hand tools and special endodontic surgical devices.
- Aerospace applications for MIM have been demonstrated for 30 years. A new wave of efforts is now starting, driven by cost concerns and envisioned savings with MIM. About a dozen firms are active in this area. Like medical applications, the production volumes are often small, in the 10 000 per year range, but the unit prices are high.
- Lighting applications for MIM are limited to refractory metals and ceramics, and the developments in this area are in the hands of the big three – Sylvania, Philips, and General Electric. After much effort the MIM viability is in serious doubt to cost reduction and competing light-emitting diode (LED) devices. But cost will probably work against MIM.
- Sporting applications have persisted for 20 years, but it appears the cost points in this field do not match well with MIM and the penetration of MIM remains small. Past successes have included metal supports for football knee braces, dart bodies, golf clubs, and running cleats.

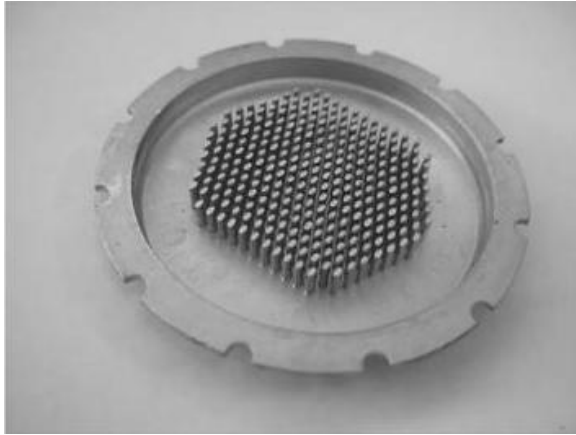
- Jewelry applications are new to MIM and could potentially grow rapidly as alternative materials (non-gold and non-silver) become accepted. These include titanium, high-polish stainless steel, tantalum, and even bronze.

Table 1 Percent of Global MIM sales for each market segment in 2011 <sup>[1]</sup>

Application field	Percentage
Aerospace	0
Automotive	14
Casting	0
Cell phone	4
Computer	4
Consumer	11
Cutting	0
Dental	9
Electronic	9
Firearm	7
Hand tool	3
Hardware	1
Household	0
Industrial	20
Jewelry	1
Lighting	0
Medical	8
Military	2
Sporting	2
Telecomm	0
Watch	2
Wear	0

The upside market size on a few of these is quite large, while others not listed above might grow, but the key actors are in place in Asia and it is doubtful if new entries can play a role.

Other future opportunities can be found from research and development (R&D) efforts that discussed in many conferences. One of it is ultra-high thermal conductivity composites (for example copper-diamond) for heat sinks. This heat sinks can reach 580 W/(m K) thermal conductivity that have been demonstrated by a Japan MIM firm for use in supercomputers, high end servers, phased array radar systems, military electronics, hybrid vehicle control systems, gaming computers, and other applications involving high-performance computing. One such device is pictured in Figure 1.



**Figure 1 A copper MIM heat transfer device used for electronic cooling (photograph courtesy of Lye King Tan).<sup>[1]</sup>**

There are some other related areas that were developed, one is vapor chamber design, typically from copper, where a closed internal chamber of porous metal is used to apply heat pipe technology to a similar problem requiring heat dissipation around electronics. The other one is LED heat sink, where copper arrays are used to mount the semiconductor, with reports of 100 g arrays with cost as low as \$0.75 per mount; these demonstrations have largely come from Asia.

Micro-miniature MIM for medical minimally invasive surgical tools is an area of development, involving very small components for end manipulators, such as cutters, grasps, and drug delivery. Most are made from stainless steel and example components are being sold in the range of \$2-\$15 each. Figure 2 shows one example used in shoulder repair.

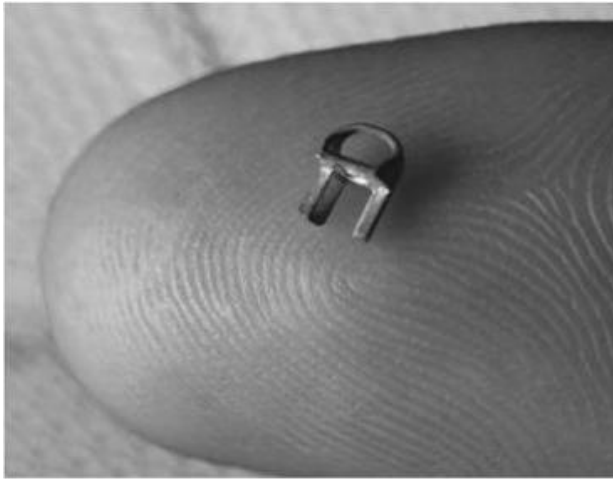


**Figure 2 Stainless steel MIM medical implant device (photograph courtesy of Metal Powder Industries Federation) <sup>[1]</sup>**

Other micro-miniature MIM applications involve components for cell phones, computers, hand-held electronic devices, and dental hand tools for endodontic use and dental cleaning. Implants such as dental tooth posts, components for ligament alignment, hearing canal (ear) reconstruction, drug delivery, heart valves, artificial knees, shoulders, and hips, are expected to be a billion dollar opportunity, but will require considerable dedication and resources to realize; Stryker and Medtronic have set up internal production, Zimmer and Biomed have elected to work with a few MIM shops, and Accellent and has elected to be fully qualified for any applications on a custom basis.

Microarray devices with hundreds to thousands of pins, posts, or holes for disposable lab-on-a-chip devices are used in blood testing, assessment of disease, analysis of DNA to predict disease, and protein tests. Hewlett-Packard and Oregon State University have a small MIM facility examining options, but activity is also on-going in Germany, Singapore and Japan.

Titanium biocompatible structures, such as for tissue affixation, implants, surgical tools, tool implants, and even sporting devices represent another development area. About 19 firms have some

variant of titanium, but few have focused on medical quality. Porous titanium by MIM offers the possibility of hydroxyapatite (bone) infusion; an example MIM device for tooth implants is shown in fig. 3

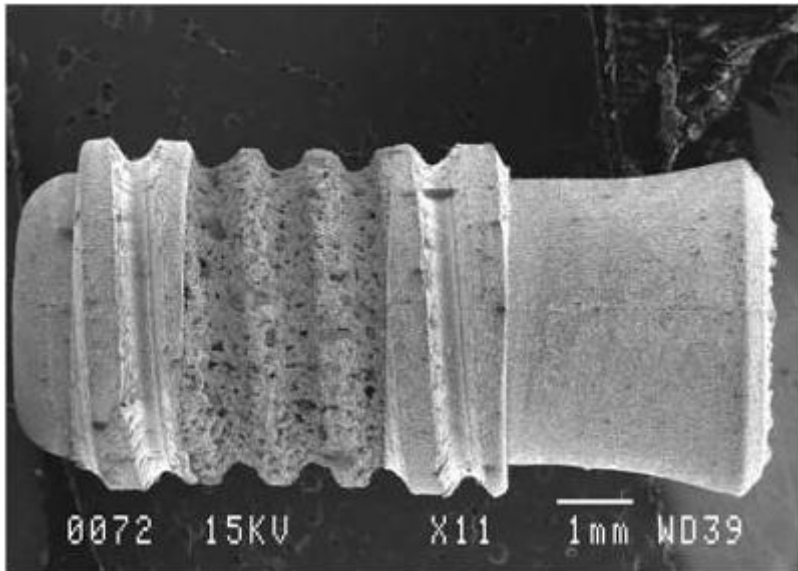


Figure 3 Titanium dental implant formed by MIM with an intentional porous region for bone in-growth (photograph courtesy of Eric Baril)<sup>[1]</sup>

## Designing for Metal Injection Molding (MIM)

D. F. Heaney, Advanced Powder Products, Inc., USA

### 4. Metal Injection Molding (MIM)

#### 4.1 Introduction

Micro injection molding is a process by which powder is shaped into complex components using tooling and injection molding machines that are very similar to those used in plastic injection molding. Therefore, the component's complexity is of the same magnitude as those seen in plastic injection molding. The artifacts associated with the injection molding process (gates, ejector pins, parting line) are also similar to those seen in plastic injection molding and must be accounted for in design. However, since the MIM process requires multiple post-molding debinding and sintering steps, some design considerations such as cross-sectional thickness and geometry features require consideration.

As a general rule of thumb, components that are less than approximately 100 g and fit into the palm of your hand could be good candidates for MIM technology. A mean size of 15 g is typical for a MIM component; however, components in the range around 0.030 g are possible. Table 2.1 compares the MIM process with other manufacturing processes. Notice that MIM is limited to smaller sizes, can provide thinner wall thicknesses, has excellent surface finish and is suited for high volumes. Table 2.2 reviews the upper and lower specifications of the MIM process.

Table 2. 1 Comparison of MIM attributes with other fabrication techniques

Attribute	MIM	Powder metallurgy	Casting	Machining
Component size (g)	0.030-300	0.1-10 000	1 +	0.1 +
Wall thickness range (mm)	0.025*-15	2 +	5 +	0.1 +
Percent theoretical density (%)	95-100	85-90	94-99	100
Percent theoretical strength (%)	95-100	75-85	94-97	100
Surface finish ( $\mu\text{m}$ )	0.3-1	2	3	0.4-2
Production volume	2000 +	2000 +	500 +	1 +

\*Features this small could have distortion.

Table 2. 2 Typical attributes produced by the MIM process

Attribute	Minimum	Typical	Maximum
Component mass (g)	0.030	10-15	300
Max. dimension (mm)	2 (0.08 in)	25 (1 in)	150 (6 in)
Min. wall thickness (mm)	0.025 (0.001 in)*	5 (0.2 in)	15 (0.6 in)
Tolerance (%)	0.2%	0.5%	1%
Density	93%	98%	100%
Production quantity	1000	100 000	100 000 000

\*Features this small could have distortion.

The following are some general design considerations which will be discussed in detail in this chapter.

- Avoid components over 12.5 mm (0.5 in) thick. This is a function of MIM technology and alloy, for example 4140 and alloys that use carbonyl powder can have thicker wall sections than those that use gas-atomized powders that have larger particles. Also modifications to binder systems can be made to allow thicker sections to debind.
- Avoid components over 100 g in mass; however, 300 g are possible for some technologies.

- Avoid long pieces without a draft (2°) to allow ejection.
- Avoid holes smaller than 0.1 mm (0.0039 in) in diameter.
- Avoid walls thinner than 0.1 mm (0.0039 in), although 0.030 mm walls are possible in some cases.
- Maintain uniform wall thickness; thin, slender sections attached to thick sections should be avoided to enhance flow during molding, to avoid sinks and voids, and to limit distortion during sintering.
- Core out thick areas to avoid sinks, warpage, and debinding defects.
- Avoid sharp corners. The desired radius is greater than 0.05 mm (0.002 in).
- Design with a flat surface to aid in sintering – otherwise custom ceramic setters required.
- Avoid inside closed cavities – although some technologies such as a chemically or thermally removable polymer core may be used but is not common.
- Avoid internal undercuts – although a collapsible core or extractible core mentioned above could be used but are not common.

## 4.2 Available materials and properties

Metal injection molding is available in many of the common structural materials for medical, military, hardware, electronic, and aerospace applications. If the powder is available in the appropriate size, less than 25 microns, and the powder sinters to a sufficiently high density, without change in alloy chemistry, the material can be manufactured using the MIM process. Table 2.3 provides an overview of available materials, applications, and specific features that make these metals desirable.

Table 2. 3 Overview of MIM materials, applications and features

Material Family	Applications	Specific alloys	Specific feature
Stainless steel	Medical, electronic, hardware, sporting goods, aerospace consumer products	17-4PH	Strength, heat treatable
		316L	Corrosion resistance, ductility, non-magnetic
		420, 440C	Hardness, wear resistance, heat treatable
		310	Corrosion and heat resistance

<b>Low-alloy steel</b>	Hardware, bearings, races, consumer goods, machine parts	1000 series 4000 series 52100	Case hardenable General purpose High wear resistance
<b>Tool steel</b>	Wood and metal cutting tools	M2/M4 T15 M42 S&	61-66 HRC 63-68 HRC 65-70 HRC 55-60 HRC
<b>Titanium</b>	Medical, aerospace, consumer products	Ti Ti-6Al-4V	Light weight Light weight, high strength
<b>Copper</b>	Electronic, thermal management	Cu W-Cu, Mo-Cu	High thermal and electrical conductivity High thermal conductivity, low thermal expansion
<b>Magnetic</b>	Electronics, solenoids, armatures, relays	Fe-3%Si Fe-50%Ni Fe-50%Co	Low core losses and high electrical resistivity High permeability and low coercive field Highest magnetic saturation
<b>Tungsten</b>	Military, electronic, sporting goods	W W heavy alloy	Density Density and toughness
<b>Hardmetals</b>	Cutting and wear applications	WC-5Co WC-10Co	Higher Hardness Higher toughness
<b>Ceramics</b>	Wear applications, nozzles, ferules	Alumina Zirconia	General purpose High wear resistance

Metal injection molding properties are superior to most cast products and slightly inferior to wrought products. Cast and MIM components both have microstructural pores or voids as a result of the processing methods, where the cast voids can be large and localized owing to the cooling of liquid to solid and the MIM voids are typically fine and well distributed across the microstructure after sintering. The large, localized voids of the cast material result in the inferior properties, whereas the distributed nature of the fine MIM pores provides a better microstructure of enhanced properties. Hot isostatic pressing ((HIPing) can be used to attain full density. Another attribute of the MIM process is that the final product will be annealed after the sintering operation, thus materials that show work hardening strengthening in the machined state may require some form of post-sinter operation to enhance the strength after the MIM sintering process. Table 2.4 provides typical data for many MIM structural materials.

Table 2. 4 MIM structural material properties

Material	Density (g/cm <sup>3</sup> )	YS (MPa)	UTS (MPa)	Elongation (%)	Unnotched Charpy impact energy (J)	Macro hardness	Young's modulus (GPa)
316L SS	7.8	180	520	40	190	67 HRB	185
17-4PH SS	7.6	740	900	6	140	27 HRC	190
17-4PH SS H9000	7.6	1100	1200	4	140	33 HRC	190
420 SS	7.5	1200	1370	-	40	44 HRC	190
440C SS	7.6	1600	1250	1	-	55 HRC	190
310 SS	7.5	-	-	-	-	-	185
Fe 2200 (2 Ni)	7.6	-	-	20	-	-	190
2700 (7.5 Ni)	7.6	125	280	35	135	45 HRB	190
2700 (7.5 Ni)	7.6	250	400	12	175	69 HRB	190
4605	7.55	210	440	15	70	62 HRB	200
4605 HT	7.55	1480	1650	1	55	48 HRC	210
4140 HT	7.5	1200	1600	5	75	46 HRC	200

Metal injection molding is an attractive method for the fabrication of soft magnetic materials. The MIM operation provides a net shape component that is in the annealed condition, which is a requirement for the best magnetic response. Table 2.5 provides data for soft magnetic applications. Each of these different alloys that has physical attributes which make them ideal for different applications. The 2200 alloy has magnetic properties similar to pure iron but with a greater strength. The Fe-50Ni alloy has a high permeability and low coercive field which makes it ideal for motors, switches, and relays. The Fe-50Co alloy has a very high magnetic saturation and is ideal for high magnetic flux density applications. Finally, if a good magnetic response is needed in conjunction with corrosion resistance, the 430L alloy would be the alloy of choice.

Table 2. 5 MIM soft magnetic alloy properties

Material	Density (g/cm <sup>3</sup> )	YS (MPa)	UTS (MPa)	Elongation (%)	Macro hardness (HRB)	Maximum permeability, $\mu$ max	Maximum H <sub>c</sub> (A/m)	B <sub>1,990</sub>
2200	7.6	120	280	35	45	2300	120	1.45
Fe-50Ni	7.7	165	450	30	50	45 000	10	1.40
Fe-3Si	7.6	380	535	24	80	8000	56	1.45
Fe-50Co	7.7	150	200	1	80	5000	120	2.00
430L	7.5	230	410	25	65	1500	140	1.15

Metal injection molding is a viable technique of the production of copper. The copper made with MIM exhibits good thermal and electrical conductivity, thus MIM copper is a viable option for electrical connectors and thermal management applications. Table 2.6 provides copper data in comparison to other forming methods. Generally speaking the electrical and thermal properties of MIM product are more affected by the density, provided a sintered closed pore condition is achieved.

Table 2. 6 Copper property comparison

Material	Cu MIM Grade 1	Cu MIM Grade 2	Wrought C11000	Cast 81100	Cast 83400
Density (g/cm <sup>3</sup> )	8.5	8.4	8.9	8.9	8.7
Thermal conductivity (W/m K)	330	290	380	350	180
Net shape capability	Excellent	Excellent	Difficult to machine	Difficult to cast	Easy to cast

The purpose of the controlled-expansion alloys is to insure good mating and/or sealing with other materials change temperature. Table 2.7 provides controlled-expansion alloy data for F-15 alloy, F-15 is also known as Kovar<sup>TM</sup> and consist of 29% nickel, 17% cobalt and the balance iron. F-15 has a coefficient of thermal expansion that matches borosilicate (Pyrex) and alumina ceramics and is primarily used for hermetically sealing applications. Other MIM control expansion such as Alloy 36, Alloy 42, and Alloy 48 exist and are basically iron with the percentage nickel added that matches the alloy number to adjust thermal expansion rate. Alloy 36 has a zero coefficient of thermal expansion until 100°C, Alloy 42 has low expansion until about 300°C and has thermal expansion behavior similar to many soft glasses. Alloy 48 has a thermal expansion behavior which matches soda lead and soda lime glasses.

Table 2. 7 Controlled-expansion alloys

Material	Density (g/cm <sup>3</sup> )	YS (MPa)	UTS (MPa)	Elongation (%)	Hardness (HRB)	CTE (100°C)	CTE (200°C)	CTE (300°C)
F-15	7.8	300	450	24	65	6.6	5.8	5.4

Implantation of MIM components is a growing market where the primary alloys in use are F-75, MP35N, and titanium-based alloys. Table 2.8 provides MIM biocompatible alloy data for F-75 and

MP35N. MIM titanium data exist, but are strongly dependent upon the manufacture of the product. MIM titanium and MIM titanium alloy properties are susceptible to carbon and oxygen impurities, thus, monitoring of these impurities in these alloys is paramount.

Table 2. 8 Bioimplantable alloys

Material	Density (g/cm <sup>3</sup> )	YS (MPa)	UTS (MPa)	Elongation (%)	Macro hardness (HRC)	Young's modulus (GPa)
<b>F-75</b>	7.8	520	1000	40	25	190
<b>MP35N</b>	8.3	400	900	10	8	-

The last class of alloys discussed here is the tungsten-based heavy alloys, which are of interest because of their high density. These alloys find application in military, medical, cell phone, inertia balancing, and sporting goods applications. Some specific applications are inertia penetrators, cell phone vibration weights, golfing club weights, medical electrodes, and fishing and hunting weights. Table 2.9 provides tungsten heavy alloy data.

Table 2. 9 Heavy alloys

Material	ASTM-B- 777-07	Density (g/cm <sup>3</sup> )	YS (MPa)	UTS (MPa)	Elongation (%)	Macro hardness (HRC)
<b>90W-7Ni- 3Fe</b>	Class 1	17	607	860	14	25
<b>90W-6Ni- 4Cu</b>	Class 1	17	620	758	8	24
<b>95W-3.5Ni- 1.5Fe</b>	Class 3	18	620	860	12	27
<b>95W-3.5Ni- 1.5Cu</b>	Class 3	18	586	793	7	27

### 4.3 Dimensional capability

Metal injection molding is a very repeatable process with variability in the range 0.2 – 0.5%. This dimensional variability is associated with the amount of shrinkage that the component experiences from the time that it is molded to after it is sintered. Components shrink about 1% during the molding operation and an additional 15-25% after sintering. Also the ceramic fixtures that are used for component support during sintering may have variability in them, which result in variability of the components from one fixture to the next. Some extreme cases may have greater variability if the particular feature

have a tendency to distort or if the feature lies along a parting line, ejector pin blemish, or a gate blemish. If a dimension of a component needs to have high precision, that feature should be embedded in one piece of steel and not have the negative effect of gates, parting lines, and ejector pins. Also, core pins that form holes may be tunneled into the far half of the tool to prevent the butt shut-off from forming flash that would cause variability in the inner diameter (ID) in that region. In general, MIM variability is superior to investment casting and inferior to high-precision machining.

#### **4.4 Surface finish**

Metal injection molding produces remarkable surface finish. Typically,  $0.8\ \mu\text{m}$  ( $32\ \mu\text{in}$ )  $R_a$  is achieved; however, a surface finish as smooth as  $0.3\text{-}0.5\ \mu\text{m}$  ( $12\text{-}20\ \mu\text{in}$ )  $R_a$  is possible. The surface finish is a function of the size and chemistry of powders that are used, the sintering conditions, and on any secondary operations, i.e. bead blasting or tumbling. Sandblast and beadblast have a tendency to increase surface roughness because of pitting, and tumbling has a tendency to decrease surface roughness. Component surface roughness can also be affected by the surface finish on the tooling used to manufacture the components. Electrical discharge machining (EDM) pits can be translated to the finished MIMed component.

## **Chapter 2. Micro Metal Injection Molding Final Design**

### **Explanation**

The result of this research is a machine that was designed to perform micro metal injection molding process with simple mechanism. It has relatively smaller dimensions (about 350 x 124 x 60 mm) compared to other MIM machines. It also has much lower manufacturing and operation cost due to its fewer parts number and the use of electric motors as driver. The use of electric motors has also made this machine very easy to operate and maintain compared to hydraulic or pneumatic system. The prototype is not fully automatic yet, so it can only allocate small production rate. But with the small and simple design, the next development can be directed to make a fully automatic, compact, and easy to use MIM.

The machine is consisted of about 29 parts (fasteners excluded) that were designed as simple as possible without forgetting their functions. The main parts of it are common in MIM machine such as screw, barrel, nozzle, hopper and heater parts. The idea was to build a micro-MIM machine that will only need a small place allocation, low cost, and easy to use and maintain. In this section, the explanation of the machine and its parts will be provided. First of all, we will look to the machine full assembly and then move to each parts.

As it has been told above, the machine is consisted of about 29 parts. They are mainly made of steel, except some insulators that are made of ebonite. The overall size of the assembly is 350 x 124 x 60 mm without raw material feeder, mold automatic placer and product release system that haven't been designed yet. Its parts assembly can be observed in **figure 1** and **2** below while the list of the component will be given in **table 1**.

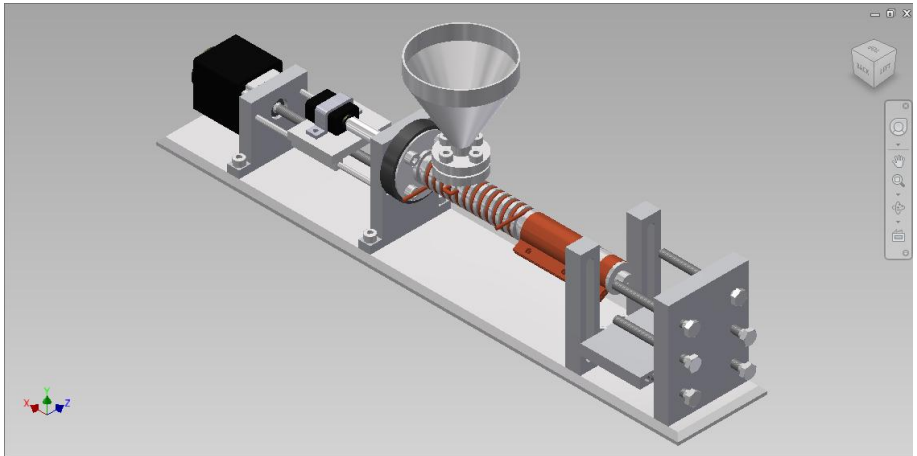


**Figure 4 Full Assembly Drawing of MIM Machine**

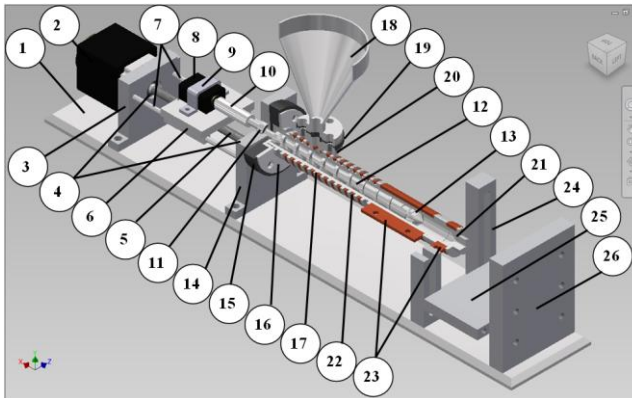


**Figure 5 MIM Machine Parts**

**Table 2 MIM Part List**

<b>No.</b>	<b>Part's Names</b>	<b>Quantity</b>	<b>Material Used</b>
1	Injector Base Plate	1	SUS304
2	Motor for Injecting Move	1	
3	Motor Mounting	1	SUS304

4	Lead Screw's Bearing	2	
5	Lead Screw	1	
6	Injector Screw Motor Mover	1	SUS304
7	Motor Mover Rail	2	SUS304
8	Injector Screw Motor	1	
9	Injector Screw Motor Mounting	1	SUS304
10	Motor and Screw Coupler	1	SUS304
11	Screw's Bearing	1	
12	Injector Screw	1	S45C
13	Injector Screw's Head	1	S45C
14	Main Mounting	1	SUS304
15	Main Insulation	1	Ebonite
16	Barrel Flange	1	S45C
17	Injector Barrel	1	S45C
18	Hopper	1	S45C
19	Hopper's Insulation	1	Ebonite
20	Hopper Mounting	1	S45C
21	Nozzle	1	S45C
22	Heater Coil	1	
23	Band Heater	2	
24	Front Mold Clamper	1	SUS304
25	Lower Mold Support	1	SUS304
26	Rear Mold Clamper	1	SUS304

The CAD drawings that will be explained in this section are the final design of the machine. Most of the parts have already been manufactured based on the earlier version of the drawings, but there were some miscalculating in the design, mostly in bolt head allocation space. That's why this new version of drawings was made to fix them and perfecting the earlier design. Each part design will be described below to give information about their function.

### **Injector Base Plate**

The base plate is made of steel with overall dimensions of 350 x 60 x 5 mm. Its main function is to become the standing place for the other parts, become the basis of the whole assemblies. To achieve this function, base plate must be rigid and have enough mass to stabilize the machine while it's operating. If the plate is not rigid and heavy enough, the machine may move due to the motor vibration, bend, or even worse, it can roll over if the center of gravity are not placed low enough. The CAD drawing of the base plate and the manufactured part are shown in **figure 3** below.

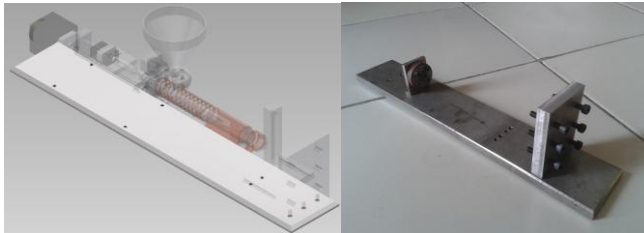


**Figure 6 Base Plate's CAD Drawing and Its Manufactured Product**

### **Main MIM Mounting**

The main mounting of this machine was design with a simple plate design having overall dimensions of 60 x 54 x 8 mm. This part is used as support for other parts such as barrel, screw, lead screw, and screw motor's rails. It is made of aluminum because it doesn't need a lot of mass and strength due to the light weight of the parts that supported by it. Having good rigidity will be sufficient for this part so that it won't move while the machine is operating. The rigidity is also very important because some parts like barrel and screw that have cantilever type of support need to be kept in line. The CAD

drawing and manufactured product from its earlier design will be shown in **figure 4** below.

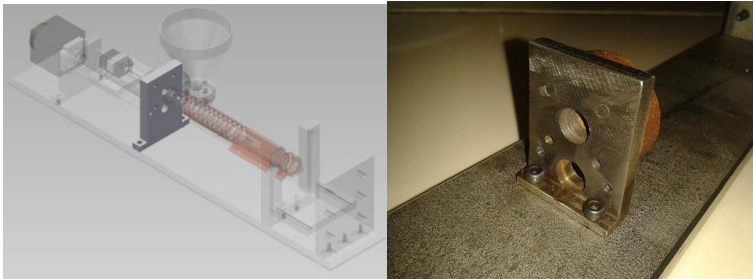


**Figure 7 Main Mounting's CAD Drawing and Its Manufactured Product**

### **Motor Mounting**

The Motor Mounting was made as the injecting motor support as well as the counterpart of the main mounting to support lead screw and screw motor's rails. It is also made of aluminum and having overall dimensions of about 40 x 54 x 8 mm. Similar with main mounting, it doesn't need a lot of mass and strength due to the small loads it receives. It only needs good rigidity to keep the parts it supports from moving while operating. The CAD drawing and manufactured product of earlier design of this part will be shown in **figure 5**.

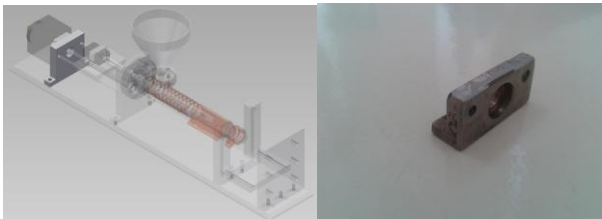


**Figure 8 Motor Mounting's CAD Drawing and Its Manufactured Product**

### **Motor for Injecting Move**

This motor is the driver for creating the forward movement of the screw to inject the molten material into the mold. The rotation torque from its shaft will be converted into axial force by the lead screw. Then the force will be applied to the screw in order to move it forward and push the molten material out of the nozzle. Because the nozzle has a very little opening (only 1 mm), so this motor needs to have high torque to achieve its function well. This will be the

important characteristic while choosing the motors. For this machine, servo motor will be used because it needs good accuracy to perform small movement to inject a very small volume of molten material.

### **Lead Screw**

As explained in the motor explanation section, the lead screw is used to convert the motor torque into axial force. This lead screw will not be manufactured, because it is very easy to get in many shop and available in various dimensions. For this machine, we need a lead screw with small rotation to movement ratio. This ratio means how far the screw (in mm) will move for every one rotation it moves. The smaller the ratio means the more accurate the machine will be to make very small movement (such as 0.1 mm) to inject very small volume of molten material. In this design, 5 mm of diameter lead screw is used.

### **Bearings**

For this machine, the total of three bearings are used, two with 5 mm of inner diameter and 11 mm of outer diameter for lead screw support, also one with 4 mm of inner diameter and 9 mm of outer diameter for injector screw support. The bearings are used as support for rotating parts so that they can rotate in their place smoothly. The locations of all the bearings are shown in **figure 6** below.

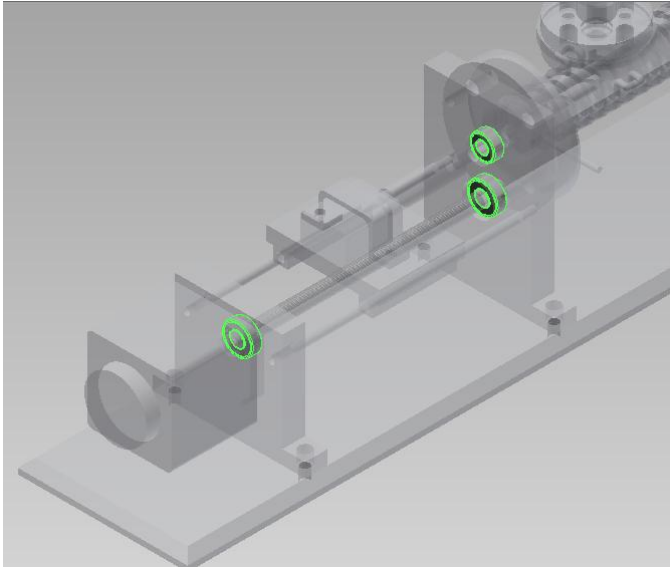


**Figure 9 Bearings Placement in the Machine**

### **Injector Screw Motor, Mounting and Coupler**

This motor is used to rotate the injector screw that will move the molten material from the bottom of the hopper into the nozzle. The screw doesn't need high rpm, so servo motor with medium torque will be enough for this function. The mounting design is depends on the motor design, it needs to be strong enough to keep the motor in place over the mover while operating. Then to connect the motor shaft to the screw, a coupling is needed. The coupling can be made as a simple hollow shaft whit an inner diameter suitable for motor shaft at one side, and injector screw at the other side. The location of these parts will be shown in **figure 7** below.

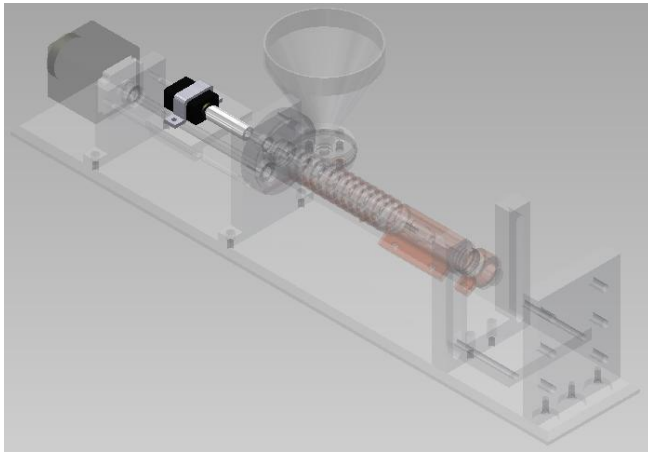


**Figure 10** Injector Screw Motor, Mounting, and Coupler Placement

### **Injector Screw Motor Mover and Rails**

This part's function is to transmit the movement of the lead screw to the injector screw motor. This part will slide on the rails forward as it pushes the molten material and backward as it returns to its original position. There are no particular characteristics needed for the mover material except for rigidity, but the rails need to be strong enough to not bend while be used. In this design, these parts are made of steel with overall dimensions of 40 x 30 x 10 mm for the mover and 3 mm of diameter and 90 mm length for each rail. The drawing will be shown in **figure 8** below.

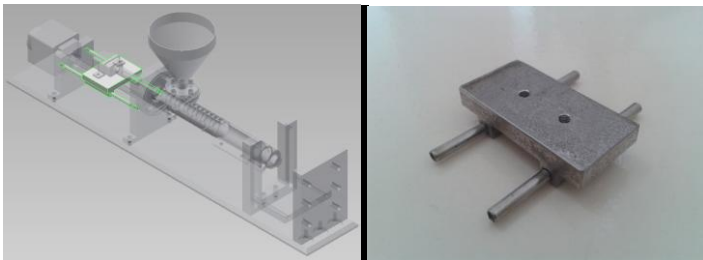


**Figure 11** Motor Mover and Its Rails CAD Drawing and the Manufactured Products

## Main and Hopper Insulation

Insulations are used to prevent the molten material leaks out of the barrel and damage other parts due to its high temperature. There are two insulations in the design, one is located between the barrel flange and main MIM mounting called main insulation, and the other is located between hopper and hopper bracket called hopper insulation. The main insulation has an opening with the size exactly the same with screw shaft, so the screw can move well through it without make any leakage. Both of the insulations are made of elastic material with high melting point (higher then molten material) such as silicon or ebonite. The CAD drawing and manufactured products of these parts are shown in **figure 9** below.

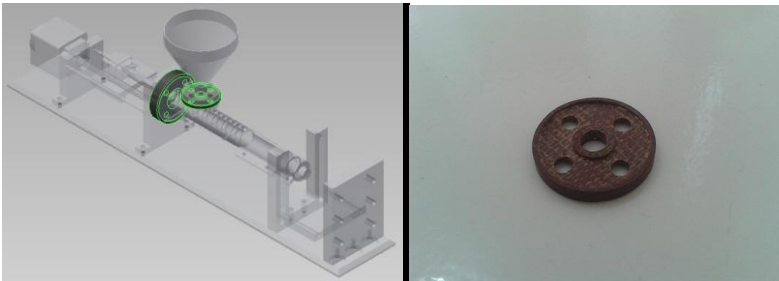


Figure 12 Main and Hopper Insulation's CAD Drawings

## Injector Barrel and Barrel's Flange

Barrel is the place where the raw material heated and melted to a certain point of temperature and viscosity. Inside barrel, the material will be heated to a very high temperature and then pushed with very high pressure to make them flow through small opening in the nozzle. That's why the barrel needs to be designed with high strength and high melting point. In this design, the barrel is made of S45C steel applied with hard chrome heat treatment process. The flange is used as barrel holder that is fixed to the main mounting. It is also made of the same material as the barrel and receives the same heat treatment. The CAD drawing and manufactured products of these part are shown in **figure 10** below.



**Figure 13 CAD Drawing and Manufactured Products of Injector Barrel and Flange**

### **Hopper and Mounting**

Hopper is the raw material gateway into the barrel. It has a funnel shape to ease material feeding process. It sits over the hopper mounting that is welded to the barrel. The hopper, insulation and mounting are tightened together using 4 bolts to make sure there won't be any leakage. The CAD drawing and manufactured product is shown in **figure 11** below (the mounting is shown in **figure 10** with together with the barrel).

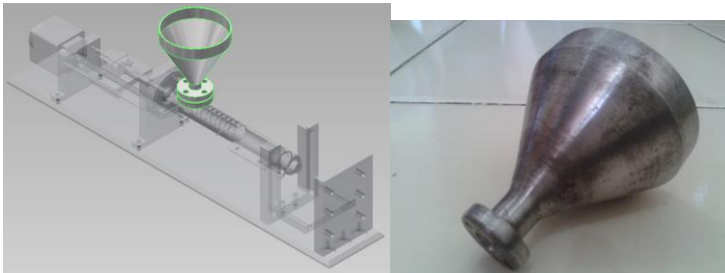


**Figure 14 CAD Drawing and Manufactured Product of Hopper and Its Mounting**

### **Injector Screw and Screw's Head**

Injector screw is one of the most important parts of MIM. It has two main functions, the first is to move the raw material from the bottom of hopper to the nozzle and the second is to heaten the material by means of friction. With these kinds of function and long but thin shape, screw needs to be highly strength in material. That's why the screw is made of S45C steel applied with hard chrome treatment. The same material is used for the screw's head because it is used to push the molten material into the mold through the nozzle. The drawing and finished products are shown in **figure 12** below.

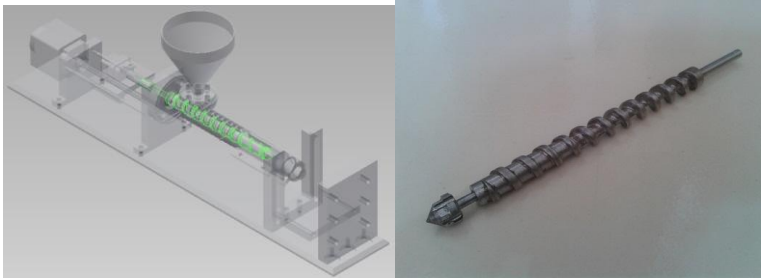


**Figure 15 CAD Drawing and Finished Products of Injector Screw and Its Head**

### **Nozzle**

Just like any other nozzle, this part of MIM is used to convert pressure into flow velocity. Its small opening will make pressure build-up at the inlet. Then, after a certain point, the material will burst with high velocity at the outlet into the mold. This velocity is needed to make sure the mold cavity is filled entirely. This part also has a funnel shape with a 1 mm of diameter tunnel, 7.5 mm length at the end of it. The drawing and finished products are shown in **figure 13** below.

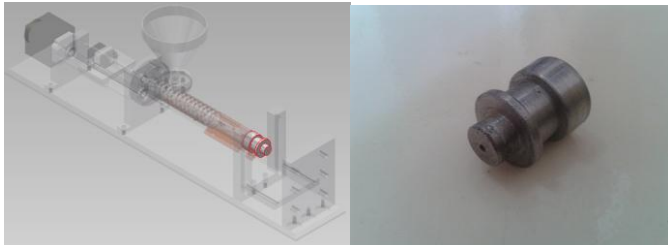


**Figure 16 CAD Drawing and Finished Products of Injector Nozzle**

### **Heater Elements**

To heaten the material, heater elements are placed along the barrel and nozzle. These elements are heater coil and heater band that are available in abundant in the market, made by many manufacturers. The parts placements are shown in **figure 14** below.

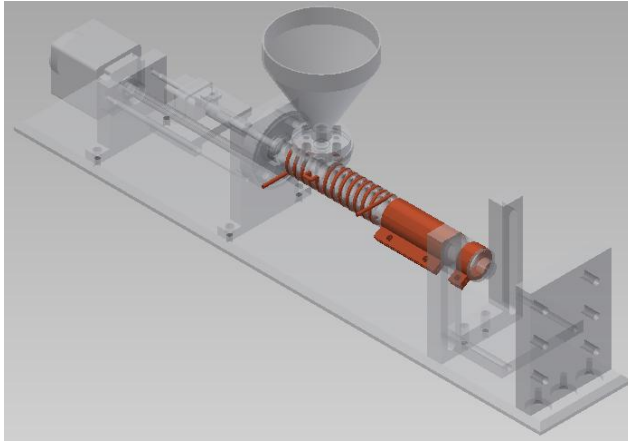


**Figure 17 Heater Elements Placement**

### **Mold Holders**

These parts function is the same as it sound, to hold the mold while the injection process going. There are three parts that build these holder mechanism, they are front mold clamber, lower mold support, and rear mold clamber. There are 6 M5 bolts placed in the rear clamber that can be tightened to push various sized of mold to the front clamber, while the lower support can be adjust up and down to bear the mold weight. The system is very simple, but it is designed to be able to hold various kind of mold with different size and shape.

### **How It Works**

The machine works like any common MIM machine available in the market, it melt the mixture raw material and binder in the barrel and then inject it into the mold. To do this, there are three subsystems that play roles in the whole operation. They are mold holder, raw material smelter, and the movement actuators. These three subsystems will be explained in this section, but first, the machine operation flow chart will be given in **figure 15** below.

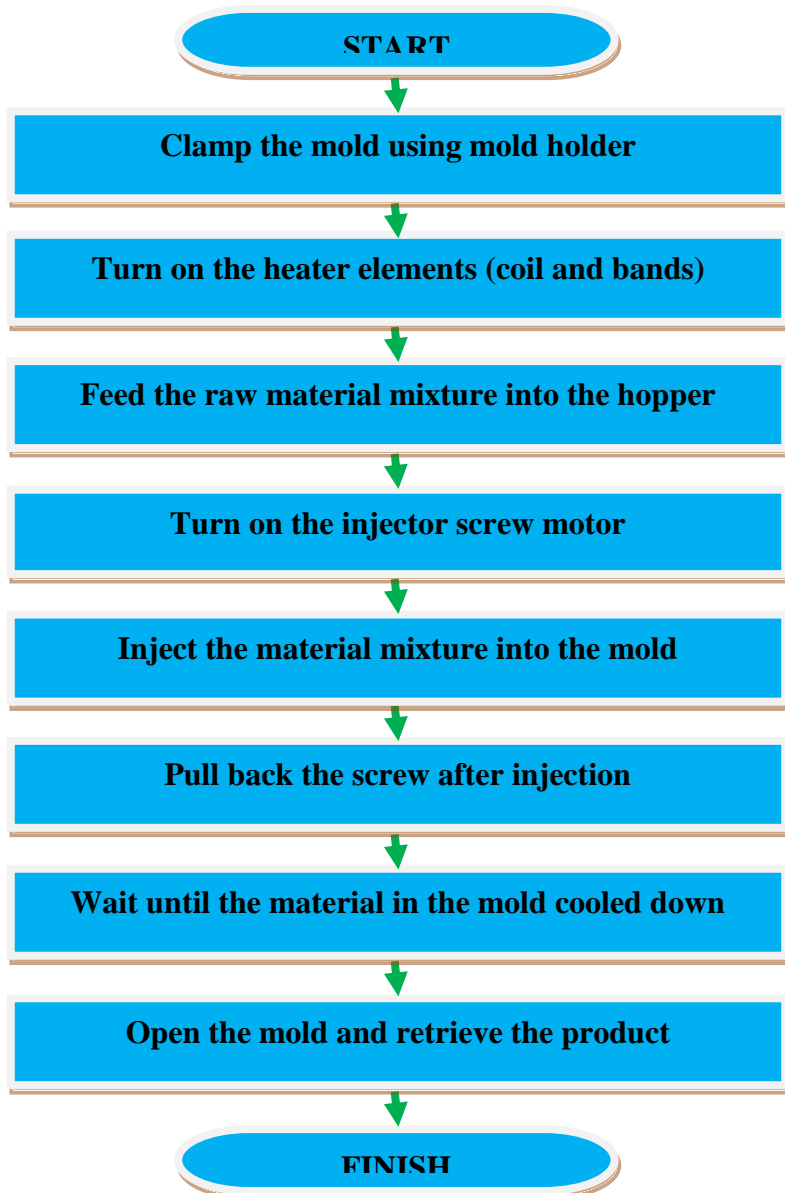
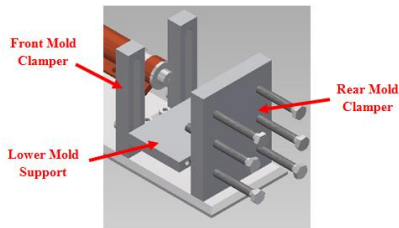


Figure 18 MIM Machine's Working Process Flowchart

## The Mold Holder Subsystem

The mold holder subsystem is consisted of three main parts, front mold clamper, lower mold support, and rear mold clamper (see **figure 16**). To hold the mold, we first need to insert the tip of the nozzle into a slot in the inlet side of the mold. The tip of the nozzle has a cylindrical shape with 10 mm of diameter and 5 mm of length (see **figure 17**). That's why, the mold that will be used in this machine also need to have a slot with 10 mm of diameter and 5 mm of depth in its inlet side.



**Figure 19** Mold Holder Subsystem's Parts

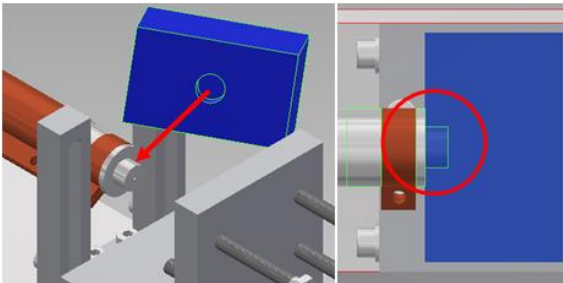


**Figure 20** the Assembly of Mold and Nozzle

After inserting the nozzle tip into the mold inlet slot, we need to adjust the lower support position so that the mold weight can be rest on it. The lower support is fastened with the front clamper by with two bolts. These bolts however, are put in a track-like slot that allows them to move up and down along it. To adjust the support position, we simply need to loosen the bolts, lift or drop the support, and then tighten the bolts again (see **figure 18**).

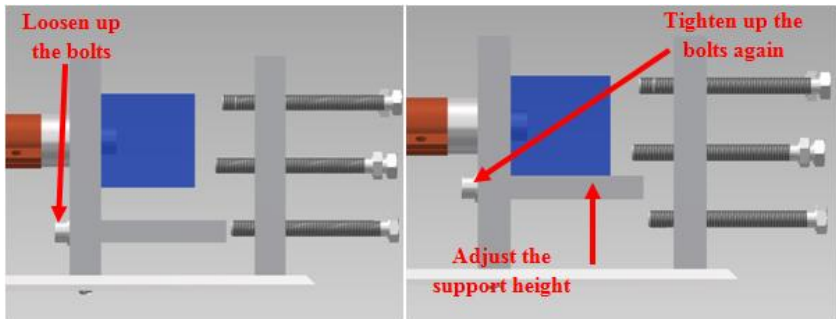


Figure 21 Steps to Adjust the Support

The last step is to tighten the bolts in the rear clamber so that they clamp the mold together with the front clamber. Tighten the bolts that can touch the mold surface only, as example, in the **figure 19** below, we can tighten up to 4 bolts. Only after the mold is held tight in its position, then the injection process can be started.

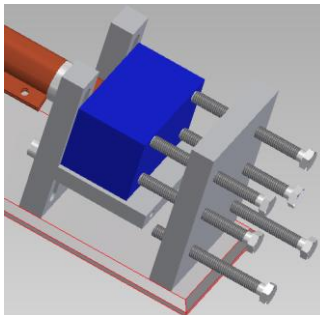
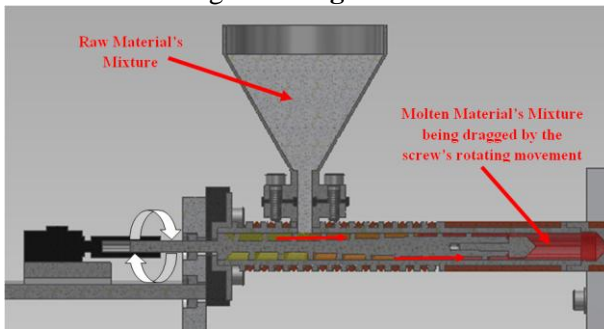


Figure 22 the Clamping Method of the Mold using Bolts

### Chapter 3. The Raw Material Mixture Smelter Subsystem

To be able to inject the raw material mixture, we need to heat it first until it has a certain value of viscosity and flow-ability sufficient to fill the mold cavity. The temperature needed to reach this point is vary depends on the material composition. To reach this temperature, several parts are working together to melt the mixture. These parts are injector barrel, screw, screw motor and heater elements.

First, we feed the material into the hopper. At the bottom of the hopper, the material will be dragged by the screw's rotation into the nozzle. The screw is rotated by the torque produced by the screw's motor. This drag movement will induce frictions between material molecules against each other and/or against screw's and barrel's surface. As a result, mixture's temperature will be raised to the melting point. To get the idea of the explained system better, a scheme has been given in **figure 20** below.



**Figure 23** The Material's Mixture Melting Scheme

The screw is not of constant diameter, this part has three main sections with different size designed to give more frictions to the mixture along the way. The screw is divided into three zones, feed zone, melt zone, and metering zone (see **figure 21**). The feed zone has a constant and smallest diameter along the screw work area. It has the biggest gap with the barrel inner surface to gather material and enriched it with air. The melt zone has increasing diameter, so the gap with the barrel surface will be decreases. This will make the mixture's volume becomes smaller and cause the material's molecules to rub even harder against each other to get higher temperature. The metering zone has a constant diameter but much

bigger than the feed zone. This zone acts as a pump to increase the pressure inside the nozzle. This mechanism, combined with heat energy produced by the heater coil and bands will melt the material and make it dilute enough to flow through the nozzle opening.

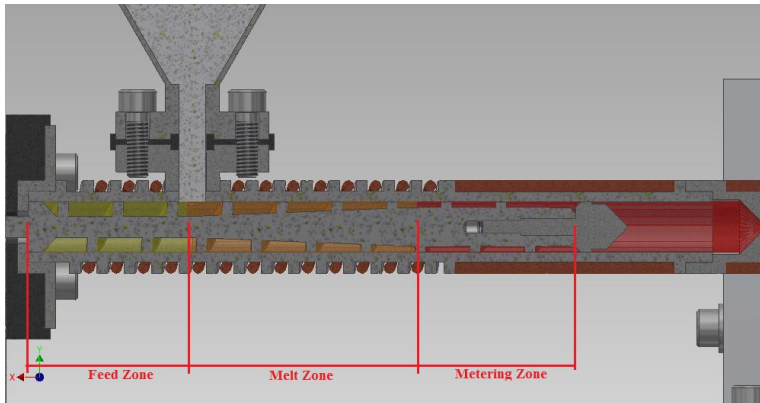
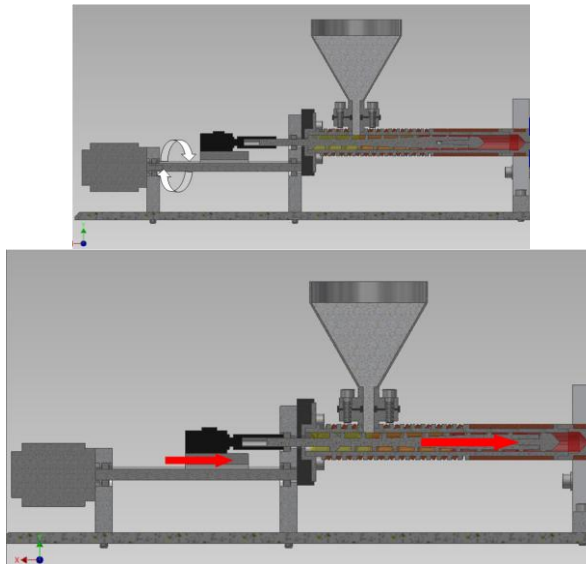


Figure 24 Feed, Melt, and Metering Zone in the Screw

### The Movement Actuators System

As has been explained before, this machine operates using two motors as its drivers. One motor is used to turn the screw, and the other is used to inject the material into the mold. After the mixture inside the nozzle reach high enough temperature and pressure, the injecting motor will rotate the lead screw. It will cause the motor mover attached to it to move forward carrying the screw motor. While this process going, screw's motor will stop rotating and push the screw into the nozzle, injecting a certain amount of mixture out of the nozzle and into the mold (see **figure 22**). After the mold cavity is fully loaded with molten material, the injecting and screw's motor will rotate in the other direction than before. Bring the screw back to its initial position while rotating with the counter direction then when the machine is melting the material. The next step is to wait until the product has cooled down to release from the mold, and then the injecting process can be repeated again.



**Figure 25 the Injecting Movement**

#### **Chapter 4. Design Evolution**

Since the first time it's been developed, this machine has been through a lot of design changes and improvements. The most major changes that have been made were focus on the actuator choice. I tried to avoid using hydraulic system as the injecting actuator that is actually very common in the MIM field. The reason is because one of the main goal that want to be achieved in this research is to make a small, simple, low cost, low power need micro-MIM that can be operated easily in a lab scale. That's why the use of hydraulic system is not an option because of its higher machine production and maintenance cost. It will also need bigger space allocation compared to other system. Several systems that have been considered as options were pneumatic system, combined electric motor and power screw system and double electric motor system. All of these systems will be described below.

#### **Pneumatic System**

The first considered option for the injecting movement actuator was the use of pneumatic system. The idea was to rotate the screw using an electric motor that is attached to a pneumatic actuator. The motor

will rotate the screw while the machine melting the material's mixture. Then when the molten material has been ready to be injected, the pneumatic actuator will push the motor along with the screw. The material will then be injected into the mold, and after that, the pneumatic will retract back to its initial position along with the motor and screw. For better illustration, the simple scheme will be given in **figure 23** below.

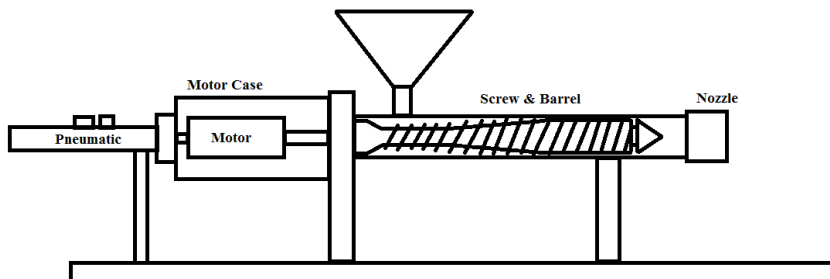


**Figure 26 MIM using Pneumatic Design Scheme**

But then, it is realized that this system has a very fatal weakness to be able to perform the injection process. This system lack the ability to control how far the distance of which the screw move, while it is one of the most important value in micro-MIM. This distance is the value we use to control the volume of material being injected into the mold. It becomes very important because when we work with micro processes, it means that we need to have a well controlled system with high accuracy to produce a very small part. That's why this idea was not used and change to the second one.

### **Combined Motor and Power Screw System**

The second idea was to use a combined motor and power screw to gain more control of the system. For this model, the barrel was modified to have an inner thread compatible with the screw thread. The idea was to employ the thread as the means to move screw forward and backward. As example, when we want to inject the material, the motor will rotate clockwise to move the screw forward. The screw then will push the material out of the nozzle into the mold cavity. After the mold cavity is fully filled, the motor will than rotate with the opposite direction to move the screw backward and repeat

the process. For better illustration, the cad drawing of the system is shown in **figure 24** below.

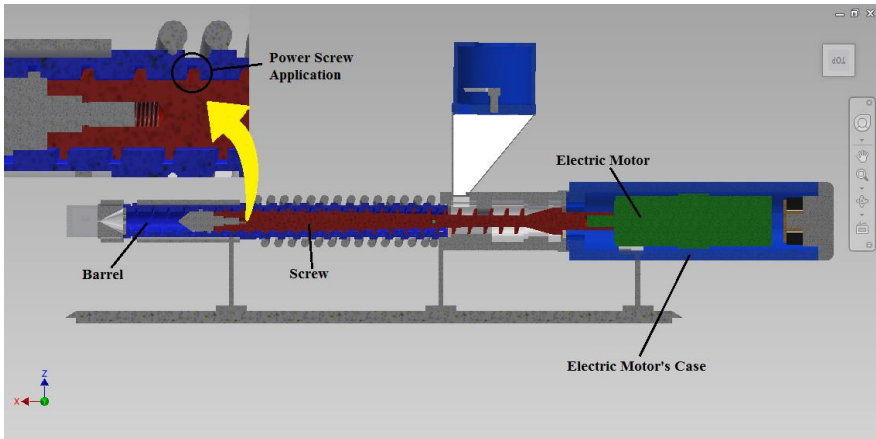


**Figure 27 MIM with Combined Electric Motor and Power Screw System**

Even though I thought the idea was good back then, but after a while I realize a fatal mistake in this design. The only mistake is that while melting the material, the screw need to rotate in place. But this system will always cause the screw to move either forward or backward if the motor rotates. So this design was rejected and the researched move on to the next design.

### **Double Electric Motors System First Version**

The third development of the design was more or less the same with the latest design in concept but with many miscalculations in bolt head space allocation. The mold holder subsystem was also designed specific for only one kind of mold configuration. But the concept was basically the same with the final design. It is to use double electric motor mechanism to gain more control in material injection accuracy and can accommodate the screw and injecting movement.

The explanation about the design has been described at the earlier section. The main point of this design is the use of one motor to rotate the screw at the material melting process and when the screw is retracted back after injecting, while the other motor is used to move the screw forward and backward at the injecting process by

means of lead screw. The miscalculations mostly take place in mounting and flange as it has been explained before. And also, the mold holder is required to be able to accommodate various configuration of mold. That's why this design has also been rejected and fixed in the second version. The design will be shown in **figure 25** below.

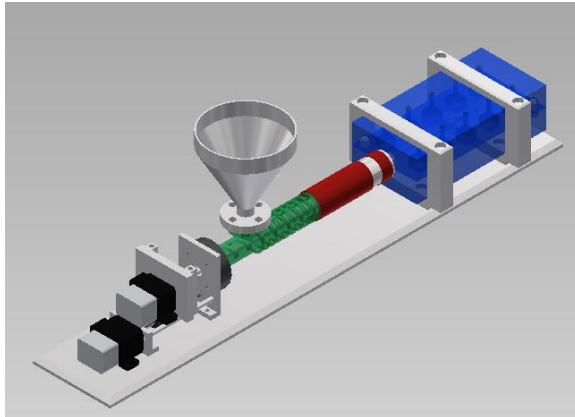


**Figure 28 MIM with Double Electric Motors System Version 1**

### **Double Electric Motors System Second Version**

The second version of double electric motors is the upgraded version from the first with mold holder system than can accommodate various configuration of mold. The mold holder system is identical with the final design. It holds the mold by means of clamping using 6 bolts. It is also the only design that has been manufactured so far. And the miscalculations of the bolts head allocation place were found only after all the parts had been manufactured. It occurred to the manufacturer when they tried to assemble all the parts. That's why, the sole purpose of the third version was to correct this miscalculations. The design of the second version is shown in **figure 26** below.

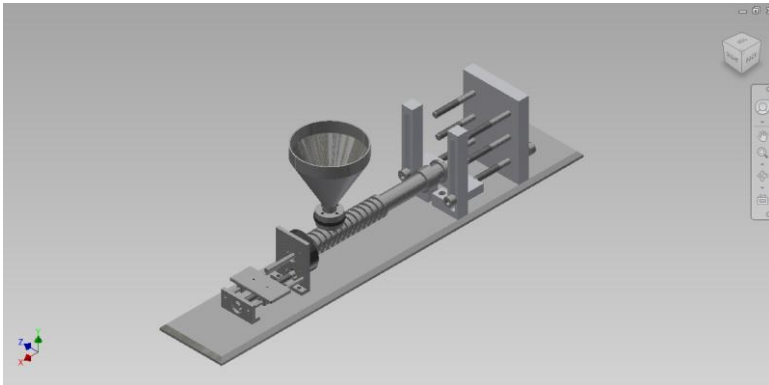


**Figure 29** the Second Version of MIM with Double Electric Motors System

### **Double Electric Motors System Third Version**

It is the current final design of the micro-MIM, and it is the repaired version of the second one for better assembly and bolt space allocation. The full explanation of the design has been described in the earlier version. It may still be able to be developed even further, but so far, this is my final design for this research and will be in my thesis. The full assembly of the design is shown in **figure 27**.

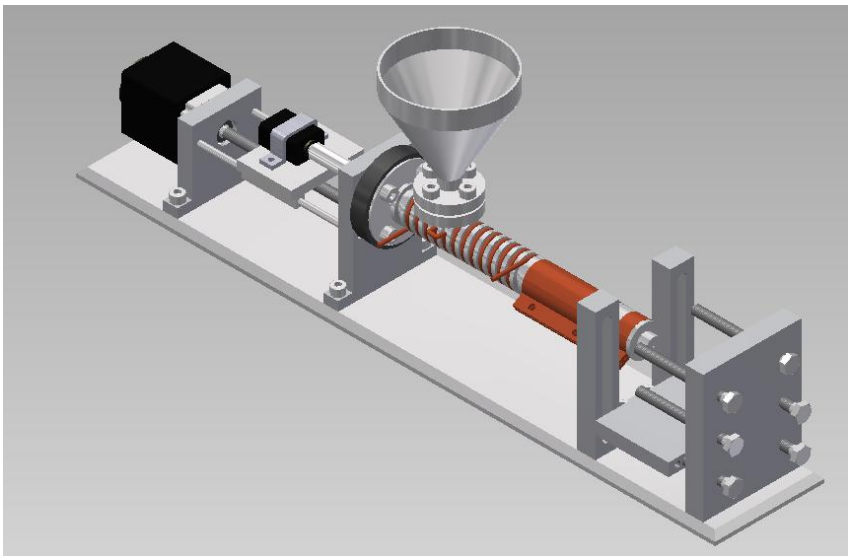


**Figure 30** The Final Design of the micro-MIM with Double Electric Motors System

## **Chapter 5. Conclusion**

### **The metal injection molding benefit the research evolution or the real sector**

As is clear from this research, 3 attributes are fundamental which is maintain from MIM process; shape complexity, high performance, and moderate to large production of quantities. This 3 fundamental are the benefit for the research evolution and for real industrial sector.

The growth of researches about MIM, is constantly balanced with competing technologies of die compaction, machining, slip casting, investment casting, tape casting, and cold process. New design guidelines from MIM products will help engineer identify more components for MIM processing, sustaining long term growth.

Besides bracket orthodontic, future applications based on MIM processing recognize that technology acceptance are requires motivation of development. Improved tolerances, a wider range of material, and lower production costs with fewer defects are major areas for improvement. Novel application are literally everywhere, because experience shows at least a 30% price reduction.

The application of MIM to orthodontic bracket came about due to miniaturization and improved aesthetics. Early bracket were in two pieces with welded mesh pads for adhesive attachment. Now the bracket are one piece constructions with a waffle pattern or porous layer for attachment. Several companies currently produce these devices, and most are fabricated by the dental supply companies for direct sale to the dentist.

The other applications area of MIM, they are; defense & aerospace, firearms, households, medical tools, dental tools, electronics, automotive and engines. Another growth area are, jewelry, cosmetic, sport tools, and wristwatch.

**Preparation and Characterization of TiO<sub>2</sub>- based Planar-  
Heterojunction Perovskite Solar Cell**

*Dr. Cho ChoThet*  
Lecturer  
Universities' Research Centre  
University of Yangon

## **Abstract**

Planar heterojunction perovskite solar cell had simply been fabricated by using TiO<sub>2</sub> as an electron collection layer (ECL). Low temperature solution process was carried out for the synthesis of TiO<sub>2</sub> NPs solution by using spin coating method. Methylammonium iodide (CH<sub>3</sub>NH<sub>3</sub>I) was simply sandwiched between the two layers of TiO<sub>2</sub> ECL and *SpiroOMeTAG*, hole transport layer (HTL) of the planar heterojunction solar cell. The optimum temperature for ECL layer was varied by changing by drying temperatures (150, 170 and 190 °C) at the different drying times (5, 10, 15, 20, 30 min) respectively. The characterization tools including UV, EDXRF, AFM, XRD, surface profilometer, KFM and solar simulator were conducted for specific purposes for each step of research. The optimum drying temperature for ECL was found out 170 °C for 15 min in air. The maximum efficiency for this optimum temperature was 7.65 % with the device parameters of V<sub>OC</sub> (0.92 V), J<sub>SC</sub> (15.26 mAcm<sup>-2</sup>), fill factor, FF (0.54) and power conversion efficiency, PCE (7.65 %).

## **Content**

### **Chapter I**

Theoretical Review

Perovskite solar cell

### **Chapter II**

Experimental Details

### **Chapter III**

Results and Discussion

Conclusions

# Chapter I

## Theoretical Review

### Perovskite solar cell

A solar cell which includes a perovskite absorber is called a perovskite solar cell. Most commonly materials used for perovskite absorber are a hybrid organic-inorganic lead or tin halide-based material. Since this absorber material is a light-harvesting active layer, it is an excellent candidate for use in photovoltaic solar cells. Organo-metal halide perovskite has several advantages including high absorption coefficient, optical band gap tuning, direct band gap, high stability and high carrier mobility, inexpensive and uncomplicated [1]. Charges in the perovskite material are predominantly present as free electrons and holes rather than as bound excitons since the exciton binding energy is low enough to enable charge separation at room temperature [2].

Perovskite solar cell structure is derived from the  $ABX_3$  crystal structure of the absorber materials. The most commonly perovskite absorber is methylammonium lead trihalide ( $CH_3NH_3PbX_3$ ) shown in Fig. 1.1 where X is a halogen ion such as I<sup>-</sup>, Br<sup>-</sup>, Cl<sup>-</sup>, with a bandgap between 2.3 eV and 1.57 eV depending on halide content [3]. Formamidinium lead trihalide ( $H_2NCH_2NH_3PbX_3$ ) is a newer material which has a bandgap between 2.23 eV and 1.48 eV. This minimum bandgap is closer to the optimal for a single-junction cell than methylammonium lead trihalide, so it should be capable of higher efficiencies. A common concern is the inclusion of lead as component of the perovskite materials; this has been addressed by Noel et al in 2014 with the introduction of a tin-based perovskite absorber,  $CH_3NH_3SnI_3$ , in which the lead is fully replaced with tin, yielding a power-conversion efficiency of more than 6% [4].

The fabrication methods are also very simple. The commonly used methods are solution processed, spin coating and printing at the low temperature. Therefore perovskite promises as superior materials for the current photovoltaic technologies such as organic PV, dye sensitized solar cell (DSSC) and even silicon solar cells. Beyond

these important properties, organo-metal halide perovskite does not require any restriction to specific solar cell architecture.

When light is absorbed by a dye in the DSSC, it injects excited electrons into semiconductor titanium dioxide nanoparticles which carry the charge away and ultimately generate current. Perovskites made attractive replacements for dyes because they absorb light efficiently over a broad spectrum since they are also excellent charge carriers in their own right. Therefore, perovskite absorbers could transform the fields of dye-sensitized, organic and thin film solar cells.

The working principle of perovskite solar cells was examined by time resolved spectroscopy techniques, ultrafast laser spectroscopy and microwave photoconductivity in order to determine how charges move across perovskite surfaces. There were two main dynamics. They are charge separation and charge recombination. In the first dynamic, the flow of electrical charges after sunlight reaches the perovskite light-absorber where takes place electron transfer at both junctions with titanium dioxide and the hole-transporting material on a sub-picosecond timescale [5].

In the latter, charge recombination is a detrimental process wasting the converted energy into heat and thus reducing the overall efficiency of the solar cell. The charge recombination was significantly slower for titanium oxide films rather than aluminum ones. Tuning the band alignment between the different layers in the device could reduce energy losses and recombination. Increasing the charge density in the metal oxide film would improve the charge separation and reduce the recombination rate.

In conclusion, all device improvements should entail low cost techniques in keeping with the trend of the third generation cells. The ability to use ambipolar properties of perovskite solar cell is definitely competitive advantages for high power conversion efficiencies solar cells.

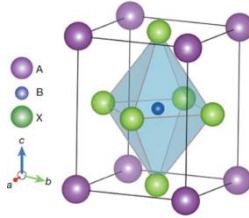


Fig.1 Crystal structure of the perovskite absorber adopting the perovskite  $ABX_3$  form, where A is methylammonium, B is Pb and X is I or Cl.

## CHAPTER II Experimental Details

### Synthesis of Materials

#### *Synthesis of $CH_3NH_3I$ solution*

$CH_3NH_3I$  was synthesized by reacting 27.86 mL methylamine (40% in methanol, Sigma-Aldrich) and 30 mL hydroiodic acid (57 wt%, Sigma-Aldrich) in a 250 mL round-bottomed flask at 0 °C for 2 h with stirring. A yellowish raw product ( $CH_3NH_3I$ ) was obtained using a rotary evaporator and re-dissolved in 80 mL absolute ethanol; a white-colored powder ( $CH_3NH_3I$ ) was formed via addition of 300 mL ethyl acetate. After filtration, the powder was washed repeatedly with ethyl acetate. Recrystallization from ethanol yielded a pure crystal of  $CH_3NH_3I$ . The crystal was collected and dried at 60 °C in a vacuum oven for 24 h [6]. A solution of  $CH_3NH_3I$  was prepared by using  $CH_3NH_3I$  crystal in 2-propanol ( $10 \text{ mgmL}^{-1}$ ) to form  $CH_3NH_3I$  solution

#### *Synthesis of $TiO_2$ solution*

In the synthesis of  $TiO_2$ , titanium isopropoxide (TTIP), 2-propanol and hydrochloric acid are used as the precursor, catalyst and solvent. Typically, the first solution of 0.0138 M, 2.53 mL 2-propanol (IPA) was mixed with 2 M, 35  $\mu\text{L}$  HCL (Sigma-Aldrich) were prepared. Then another solution of 0.23 M, 369  $\mu\text{L}$  titanium isopropoxide was prepared by adding 0.0138 M, 2.53 mL 2-propanol. The first solution is slowly added dropwise to the second solution and was stirred at 800 rpm. After being stirred for six hours at the room temperature, a clear and transparent  $TiO_2$  nanoparticle dispersion solution was successfully obtained [7].

### ***Preparing of PbI<sub>2</sub> solution***

A solution of PbI<sub>2</sub> was prepared by adding 460 mg of PbI<sub>2</sub> powder in 1 mL of DMF and stirring at 350 rpm at 80 °C for 12 hr.

### ***Preparing of Spiro OMeTAD solution***

A solution of a *spiro*-OMeTAD was prepared using (80 mg *spiro*-OMeTAD, 28.8  $\mu$ L 4-*tert*-butylpyridine, 17.5  $\mu$ L of a stock solution of 520 mgmL<sup>-1</sup> lithium bis(trifluoromethylsulphonyl)imide in acetonitrile, and 29  $\mu$ L of a stock solution of 300 mgmL<sup>-1</sup> tri(2-(1H-pyrazol-1-yl)-4-*tert*-butylpyridine)cobalt(III)bis (trifluoromethylsulphonyl) imide in acetonitrile in 1 mL chlorobenzene). The molecular structure of Spiro OMeTAG is shown in Fig. 2.1.

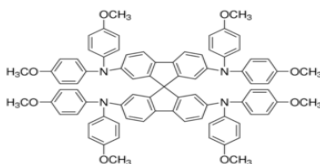


Fig. 2.1 Molecular structure of Spiro OMeTAD

### **Device fabrication**

Patterned ITO/glass substrates (15  $\Omega$ /sq) were cleaned with detergent, ultrasonicated in acetone and isopropyl alcohol, and subsequently dried overnight in an oven. For the electron-selective layer of the planar heterojunction (PHJ) perovskite solar cells, a sol-gel TiO<sub>2</sub> precursor solution was spincoated in air onto the pre-cleaned and UV/ozone-treated ITO/glass substrates at 2,000 rpm for 45 s. Then, the films were dried on a hot plate at 150°C in air at different drying times (5, 10, 15, 20, 30 min) respectively. After the TiO<sub>2</sub> thin film samples had been cooled to room temperature, they were transferred into a N<sub>2</sub>-filled glove box, where the thin PbI<sub>2</sub> films are spin-coated from a solution of PbI<sub>2</sub> at 3,000 rpm for 15 s and are dried for 80 °C for 10 min. The PbI<sub>2</sub> films spin coated from a solution of CH<sub>3</sub>NH<sub>3</sub>I to form CH<sub>3</sub>NH<sub>3</sub>PbI<sub>3</sub> perovskite films. The hole transport layer (HTL) is then deposited by spin coating a solution of a *spiro*-OMeTAD at 3,500 rpm for 30s. Finally, those samples were pumped down to a vacuum (1 $\times$ 10<sup>-7</sup>Torr), and an approximately 5 nm-thick

MoO<sub>x</sub> and 100 nm-thick Ag electrode (active area: 4.64 mm<sup>2</sup>) was deposited on top of the devices. In order to enhance the efficiency of perovskite solar cells, improving the electron transport/extraction is also very important. Therefore, the surface of the TiO<sub>2</sub> film was modified by incorporating 0.05 wt% of polyethylenimine (PEI) for better electron transport/extraction between the TiO<sub>2</sub> electron transport layer and the perovskite absorber. For the interfacial modification of the top surface of the TiO<sub>2</sub> layer, PEI was spin-coated onto the TiO<sub>2</sub> film at 5000 rpm for 10 s and then annealed at 80 °C for 5 min in air.

## CHAPTER III

### Experimental Results and Discussion

#### Ultraviolet-Visible (UV-Vis) Spectroscopy measurement

Ultraviolet–visible spectroscopy is a technique to determine concentrations (optical density of light) of absorbing samples in the ultraviolet-visible and near-infrared (NIR) by using the Beer–Lambert law. When a beam of monochromatic light is passed through a solution of an absorbing substance, the decreased intensity of radiation rate with thickness of the absorbing solution is proportional to both the incident radiation and the concentration of the solution. From UV spectroscopy,

$$A = \log (I_0/I) = Ecl$$

Where, A = absorbance

I<sub>0</sub> = intensity of light incident upon sample cell

I = intensity of light leaving sample cell

c = molar concentration of solute

k = length of sample cell (cm)

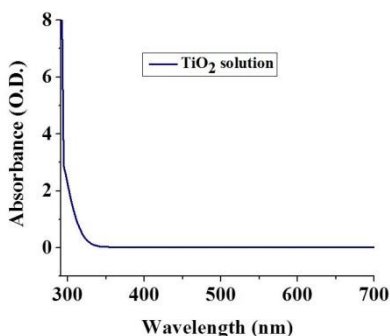
E = molar absorptivity

The more the number of molecules capable of absorbing light of a given wavelength, the greater the extent of light absorption is.

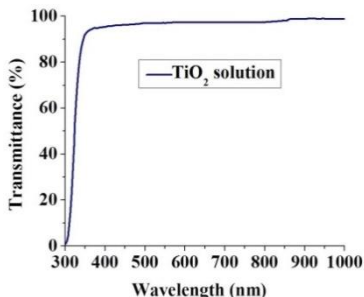


Fig.3.1 Lambda 750 UV/Vis/NIR Spectrophotometer

The optical properties of resulting  $\text{TiO}_2$  thin films were carried out by UV/Vis/NIR Abs. spectrometer detection wavelength: 200~3300 nm (Lambda) shown in Fig. 3.1. UV-Vis absorption spectrum of (a) as- synthesized  $\text{TiO}_2$  solution (b)  $\text{TiO}_2$  film on fused silica substrate (c) and (d) their transmission spectra are shown in Fig.3.2. Both the solution and film types of  $\text{TiO}_2$  show the high transmittance above 90% and have the absorption edges at 358.84 nm. The optical band gap ( $E_g$ ) of  $\text{TiO}_2$  film and  $\text{CH}_3\text{NH}_3\text{PbI}_3$  on  $\text{TiO}_2$  and  $\text{CH}_3\text{NH}_3\text{PbI}_3$  /PEI on  $\text{TiO}_2$  values are indicated in the UV spectrum of Fig.3.3 The optical band gap ( $E_g$ ) of  $\text{TiO}_2$  film was 3.456 eV and  $\text{CH}_3\text{NH}_3\text{PbI}_3$  on  $\text{TiO}_2$  and  $\text{CH}_3\text{NH}_3\text{PbI}_3$  /PEI on  $\text{TiO}_2$  values were 1.6 eV at their absorption wavelengths at 775 nm respectively as indicated in these graphs.



(a)



(c)

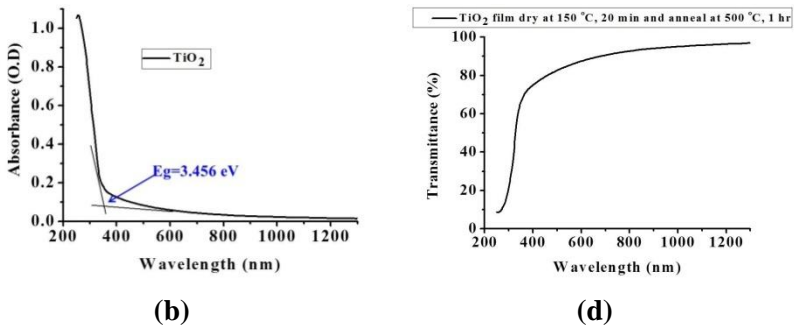


Fig. 3.2 UV-Vis spectra of TiO<sub>2</sub>

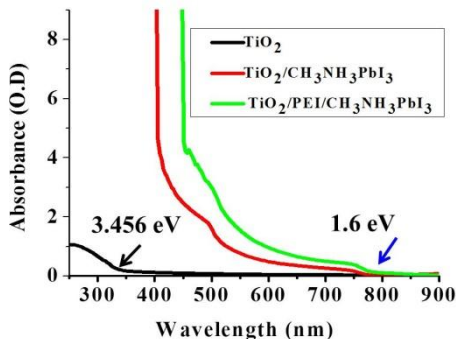


Fig.3.3 Optical band gap ( $E_g$ ) values of TiO<sub>2</sub> and perovskite on TiO<sub>2</sub> and perovskite on TiO<sub>2</sub>/PEI from UV-Vis absorption spectrum.

### Energy Dispersive XRF Spectrometer (EDXRF Spectrometer)

Energy dispersive X-ray fluorescence spectrometer is a nondestructive technique to determine the type and content of the elements comprising the samples. The fluorescent photons from the irradiated samples are excited by X-rays and the energy (wavelength) and intensity of the generated fluorescent X-rays are measured. The elements from sodium (Na) through to uranium (U) can be simultaneously detected within a few minutes. Each peak of the element occurs at a known fixed position and concentrations can be detected from the range of 100% down to a few parts per million (ppm).

Both of the qualitative and quantitative results can be observed from this technique. When a sample is irradiated with X-rays, the atoms in

the sample generate fluorescent X-rays. Qualitative analysis can be performed by investigating these wavelengths of the fluorescent X-rays since their unique wavelength and energy are characteristic of each element that generates them. Besides, as the intensity of fluorescent X-ray is also a function of the concentration, quantitative analysis can be measured from the amount of X-rays at the specific wavelength to each element. It is useful for the elemental analysis of solid, powder and liquid samples as well as rapid, non-destructive testing for harmful elements in printed circuit boards and electronic devices. The elemental analysis of  $\text{TiO}_2$  film was measured by Shimadzu EDX 720 (Fig.3.4). The aim of EDXRF investigation is to observe quantitative concentration of oxide percentage in the synthesized solution. The observed EDXRF spectrum of  $\text{TiO}_2$  film is shown in Fig. From the EDXRF measurement, the synthesized solution was highly purify since titanium dioxide ( $\text{TiO}_2$ ) peak can only be observed in the XRF spectrum of Fig. 3.5.



Fig. 3.4 Shimadzu EDX 720

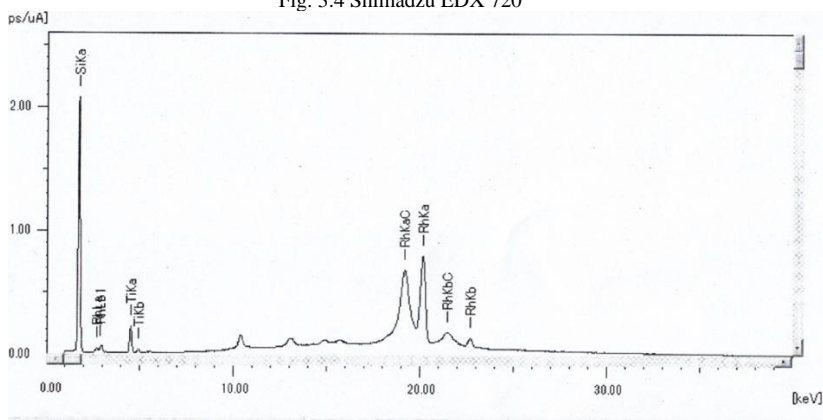


Fig.3.5 EDX spectrum of  $\text{TiO}_2/\text{Si}$  film

Table of quantitative result of TiO<sub>2</sub> solution (oxide form)

Compound	Percentage (%)
SiO <sub>2</sub>	99.837
TiO <sub>2</sub>	0.163

### **Atomic Force Microscopy (AFM)**

Atomic force microscopy is a powerful microscope for the observation of matter at nano scale. The AFM provides a 3D surface profile and can analyze heights at the sub-nm level. A photo of AFM is shown in Fig.3.6. The AFM machine consists of a cantilever, a tip, laser beam, photo diode (detector), and feedback electronics. The van der Waals force between the tip and the sample causes deflection of the cantilever. The deflection can be measured using a laser beam reflected off the back of the cantilever onto the photodetectors array. The feedback mechanism is responsible for adjusting the tip-to-sample distance in order to avoid the physical contact between them during scanning.

The AFM can operate in three modes: contact mode, non-contact mode, and dynamic contact mode or tapping mode. In the contact mode operation, a constant deflection is maintained to keep the force constant during the scanning. In the non-contact mode, the cantilever is oscillated externally in order to avoid tip-sample contact. In the dynamic contact or tapping mode, the cantilever is oscillated so that the tip comes into contact with the sample in each period of scanning. Frequency and amplitude modulations provide surface information in the non-contact and the dynamic contact modes. The change in oscillation frequency provides information of the sample while the change in amplitude provides topographic information of the sample. The surface morphologies of films were measured by AFM (Park systems corp., XE-100).

The purpose of AFM scanning is in order to study the surface morphology of samples. The size distribution of TiO<sub>2</sub> nano particles (NPs) from AFM analysis is used to determine the size homogeneity of NPs. AFM topographic images of a TiO<sub>2</sub> dried at (a) 5min (b) 10 min and (c) 30 min at 150 °C at the room temperature were shown in Fig. 3.7. Root mean square roughness's are observed (a) 0.234 nm

(b) 0.271 nm and (c) 0.416 nm respectively. Since the surface roughness's values  $\text{TiO}_2$  film are less than 1 nm,  $\text{TiO}_2$  is very good for electron collection layer of fabricated devices.



Fig. 3.6 Atomic force microscope (AFM)

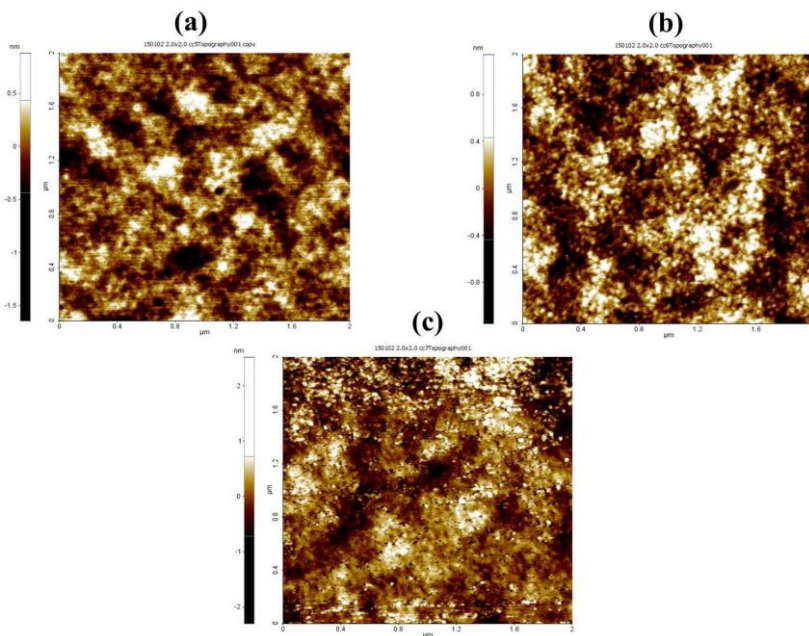


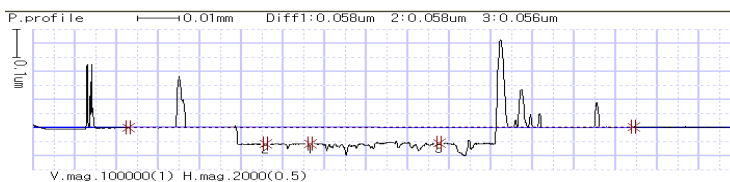
Fig. 3.7 AFM topographic images of a  $\text{TiO}_2$  dried at (a) 5min (b) 10 min and (c) 30 min at  $150^\circ\text{C}$  at room temperature

## Thickness Measurement by Surface Profilometer

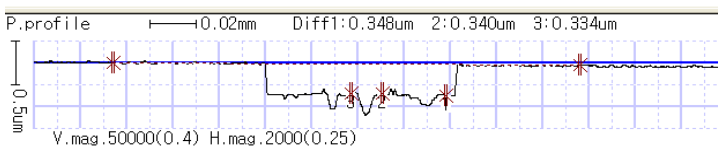
ET 3000 surface profilometer is capable of accurately tracing very small forms of precision parts with a nanometer levels. All necessary contour elements can be analyzed. The system is also suitable for components or sample that is made from a soft material since ET 3000 utilizes low force stylus. Measuring force is ranging from 10 up to 500  $\mu\text{N}$ . ET 3000 has a vertical measuring range of 600  $\mu\text{m}$  and horizontal measuring range of 100 mm. The thickness of the  $\text{TiO}_2$  electron collection layer and perovskite layer were measured by *alpha-step* profilometer (Surfcorder ET3000, Kosaka Laboratory Ltd.) shown in Fig. 3.8. Figure 3.9 showed that the thicknesses of  $\text{TiO}_2$  film and perovskite layer were found about 60 nm and 350 nm respectively.



Fig.3.8 Alpha-stepprofilometer



(a)



(b)

Fig. 3.9 Thicknesses of (a)  $\text{TiO}_2$  film and (b) perovskite layer measured by surface profilometer

## X-ray Diffraction (XRD)

X-ray diffraction is a technique used to determine material structures and phases of a sample. In addition to structural and phase analysis, other application for XRD includes semi-quantitative phase analysis relative degree of crystallinity measurement, particle analysis film thickness analysis and stress analysis.

The operating principles of XRD can be explained by the Bragg's law. When a sample is irradiated with a parallel beam of monochromatic X-rays, the X-ray beams are diffracted to specific angles from the atomic lattice of the sample which acts as a 3D diffraction grating. Each detected X-ray signal from the diffraction pattern corresponds to coherent reflection, called a Bragg reflection, from successive planes of the sample for which Bragg's law is satisfied

$$2d\sin\theta=n\lambda$$

Where  $d$  = atomic spacing between the plane,  $\theta$  = angle that X-ray beam makes with respect to the plane,  $\lambda$  = wavelength of the X-rays  
 $n = 1, 2, 3, \dots$

In this work, XRD measurements are carried out using Philips X'pert pro Multipurpose Diffract meter (MPD) and XPERT XRD with X'celerator Detector shown in Fig.3.10 (a) and (b). It is used to determine the crystal structures of TiO<sub>2</sub> electron collection layer and CH<sub>3</sub>NH<sub>3</sub>PbI<sub>3</sub> perovskite layer.



Fig.3.10(a) X'Pert pro Multipurpose Diffractometer (MPD)



Fig.3.10(b) XPERT XRD with X'celerator Detector for thin film

The typical XRD pattern of TiO<sub>2</sub> thin film (dried at 150 °C for 15 min and annealed at 500 °C for 1 hr) and CH<sub>3</sub>NH<sub>3</sub>PbI<sub>3</sub> layer on this TiO<sub>2</sub> film are shown in Fig.3.11(a) and (b). All the diffraction peaks are indexed to the anatase phase of TiO<sub>2</sub> indicating that the obtained product is pure anatase TiO<sub>2</sub>.

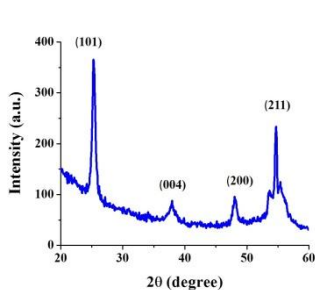


Fig. 3.11(a) XRD spectrum of TiO<sub>2</sub> thin film

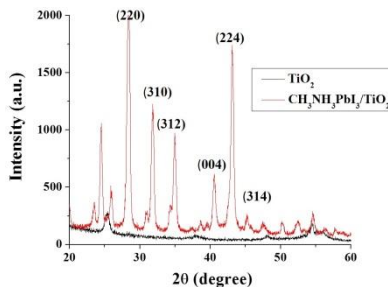


Fig. 3.11(b) XRD spectra of TiO<sub>2</sub> and CH<sub>3</sub>NH<sub>3</sub>PbI<sub>3</sub>/TiO<sub>2</sub> layer

## Kelvin Probe Force Microscopy (KFM)

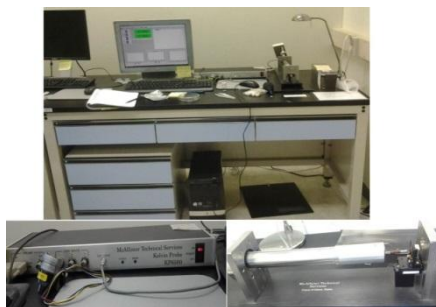


Fig. 3.12 Kelvin Probe Force Microscope (KFM)

The Kelvin Probe (KP) method is a non-contact technique used to measure work function of fabricated devices. Work function is the energy difference between the vacuum potential level and the Fermi level which is located between valence band (VB) and conduction band (CB) of the energy gap.

KP system is a McAllister Technical Services KP 6500 shown in Fig. 3.12. The probe is positioned in a port of the smaller chamber

oriented at 45° with respect to the sample actuator. In order to keep the surfaces of the KP tip and the sample parallel, the tip is customized to face at 45° from the longitudinal axis of the tip. The tip can probe a 2 mm diameter area. The sample to tip distance is varied manually using a linear translator attached to the Kelvin probe chamber. The fine adjustment to the sample to tip distance and the tip oscillation is done by means of the computer-controlled voice coil system.

Calibration is carried out to obtain the work function of the sample by measuring the position of the Fermi level of the sample relative to the reference tip. Calibration is performed using the known work function reference electrode (graphite). The resulting tip work function value is 4.58 eV. The measured work function values of the samples for the different conditions were determined shown in table. The annealing temperature for ECL was 500 °C.

Sample	Contact Potential Difference (V)	Work Function (eV)
ITO	-0.30883	4.89
TiO <sub>2</sub>	-0.47414	5.05
TiO <sub>2</sub> /PEI	0.357802	4.22
TiO <sub>2</sub> (anneal)	-0.46157	5.04
TiO <sub>2</sub> (anneal)/PEI	0.403931	4.18
TiO <sub>2</sub> (anneal)/perovskite	0.125495	4.45
TiO <sub>2</sub> (anneal)/PEI /perovskite	-0.33974	4.92

### **JV Measurement**

The J-V characteristics were measured using a Keithley 237 source measure unit in an N<sub>2</sub> atmosphere. The solar-cell parameters were obtained using an AM 1.5 G solar simulator with an irradiation intensity of 100 mWcm<sup>-2</sup> shown in Fig. 3.13. The lamp was calibrated with an NREL-calibrated KG5 filtered silicon reference cell. The light intensity of the lamp was modulated by using neutral density filters with a various optical density.



Fig. 3.13 AM 1.5 solar simulator system

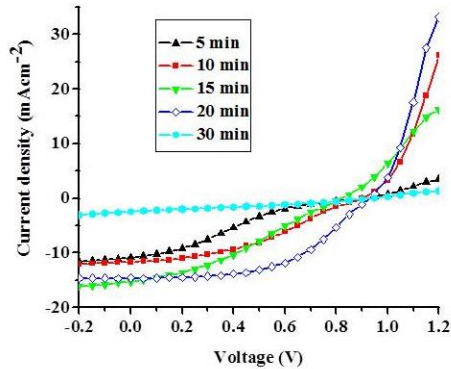


Fig.3.14 Current density-voltage characteristics of the planar-heterojunction perovskite solar cells for various drying times of  $\text{TiO}_2$  ECL at  $150^\circ\text{C}$  in air

The current density-voltage characteristics of the planar-heterojunction perovskite solar cells with various drying times of  $\text{TiO}_2$  layer (5, 10, 15, 20, 30 min) at  $150^\circ\text{C}$  in air were shown in Fig 3.14. The device structure was  $\text{ITO}/\text{TiO}_2/\text{CH}_3\text{NH}_3\text{PbI}_3/\text{Spiro OMeTAD}/\text{Ag}$  which was measured under AM 1.5G irradiation at  $100\text{ mW cm}^{-2}$ . The devices were measured with illumination time and the performances of the device increase with the illumination time. It was found out that the optimum drying time for ECL was 20 min at  $150^\circ\text{C}$ .

Again, the optimum temperature for ECL was investigated by varying the drying temperatures (150, 170 and 190 °C) as shown in Fig. 3.15. The optimum temperature was 170 °C for the drying time at 15 min. The power conversion efficiency for this perovskite solar cell device was 7.65% as shown in Fig.3.16.

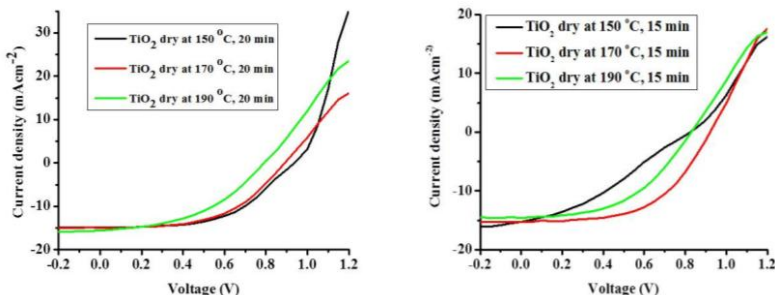


Fig. 3.15 Current density-voltage performance of the planar-heterojunction perovskite solar cells

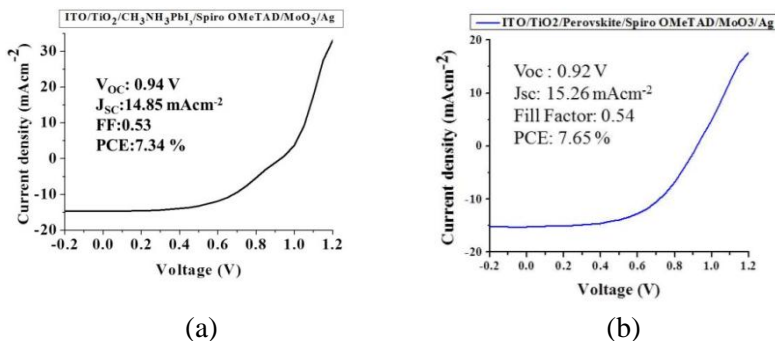


Fig. 3.16 Current density-voltage characteristics of the planar-heterojunction perovskite solar cells with a structure of ITO/TiO<sub>2</sub> NP/CH<sub>3</sub>NH<sub>3</sub>PbI<sub>3</sub>/Spiro OMeTAD/Ag

## Conclusions

In conclusion, TiO<sub>2</sub> electron collection layer was synthesized by low temperature solution method. The optimum conditions for ECL layer were investigated by varying the drying temperatures and times. The planar heterojunction perovskite solar cells with a power conversion efficiency of 7.65% by using a sol-gel processed TiO<sub>2</sub> electron collection layer were fabricated. The synthesis of TiO<sub>2</sub> NPs was confirmed by UV-vis and the elemental analysis was observed by EDXRF. AFM measurement was performed to reference the surface roughness of ECL layer. The crystal structures of ECL layer and

perovskite layer were determined by XRD. The thicknesses of fabricated devices were conducted by surface profilometer. The JV characteristics of fabricated devices were measured by solar simulator. The optimum drying temperature of the TiO<sub>2</sub> ECL layer was 170 °C for 20 min in air and the maximum efficiency of the ITO/TiO<sub>2</sub>/(CH<sub>3</sub>NH<sub>3</sub>PbI<sub>3</sub>)/Spiro OMe TAD/MoO<sub>3</sub>/Ag was found out to be 7.65 %.

## References

1. Gamliel Shany and Etgar Lioz. (2014). Organo-metal perovskite based solar cells: sensitized versus planar architecture. RSC Advances. RSC Adv.4, 29012
2. D'Innocenzo Valerio, Grancini Giulia, Alcocer Marcelo J. P., Kandada Ajay Ram Srimath, Stranks Samuel D., Lee, Michael M., Lanzani Guglielmo, Snaith Henry J. (8 April 2014). Excitons versus free charges in organo-lead tri-halide perovskites. Nature Communications 5. doi:10.1038/ncomms458
3. Liu Mingzhen, Johnston Michael B. and Snaith Henry J. (19 September 2013). Efficient planar heterojunction perovskite solar cells by vapour deposition, Letter 501, Edoi:10.1038/nature12509
4. Noel Nakita K., Stranks Samuel D., Abate Antonio, Wehrenfennig Christian, Guarnera Simone, Haghighirad Amir-Abba, Sadhanala Aditya, Eperon Giles E., Pathak Sandeep K., Johnston Michael B., Petrozza Annamaria, Herz Laura M., Snaith Henry J. (1 May 2014). Lead-free organic-inorganic tin halide perovskites for photovoltaic applications. Energy & Environmental Science 7 (9) 3061. doi:10.1039/C4EE01076K.
5. Marchioro Arianna, Teuscher Joël, Friedrich Dennis, Kunst Marinus, Kroel Roel van de, Moehl Thomas, Grätzel Michael and Moser Jacques-E. (2014) Unravelling the mechanism of photoinduced charge transfer processes in lead iodide perovskite solar cells, Nature Photonics 8, 250-255.
6. Liu Diany and Kelly Timothy L. (2014) Perovskite solar cells with a planar heterojunction structure prepared using room-temperature solution processing techniques, Nat. Photon 8, 133-138.
7. Docampo Pablo, Hanusch Fabian C, Giesbrecht Nadja, Angloher Philipp, Ivanova Alesja, and Bein Thomas. (2014) Influence of the orientation of methylammonium lead iodide perovskite crystals on solar cell performance, APL Materials 2, 081508.

**Polybrominated diphenyl ethers (PBDEs), organophosphorus flame retardants (PFRs) and phthalates in floor and road dust from an e-waste dismantling facility and adjacent communities in Thailand**

*Dr. Dudsadee Muenhor;  
Assoc. Prof. Dr. Hyo-Bang Moon;  
Mr. Sunggyu Lee*

Dudsadee Muenhor<sup>1,2,\*</sup>, Hyo-Bang Moon<sup>3</sup> and Sunggyu Lee<sup>3</sup>

<sup>1</sup>*Faculty of Environmental Management, Prince of Songkla University, Hat Yai Campus, Hat Yai, Songkhla 90110, Thailand*

<sup>2</sup>*Center of Excellence on Hazardous Substance Management (HSM), Bangkok 10330, Thailand*

<sup>3</sup>*Department of Marine Sciences and Convergent Technology College of Science and Technology, Hanyang University, Ansan, Republic of Korea*

## Abstract

This study investigates concentrations of PBDEs, PFRs and phthalates in settled floor dust (n=40) and road dust (n=20) from an electronic and electrical waste (e-waste) dismantling facility, two homes and a Buddhist temple in Thailand. Concentrations of  $\Sigma 22$  PBDEs,  $\Sigma 10$  PFRs and  $\Sigma 6$  phthalates in floor dust from an e-waste dismantling facility varied between 1200-43000 ng g<sup>-1</sup>, 36-1700 ng g<sup>-1</sup> and 86-790  $\mu\text{g g}^{-1}$ , whereas those from adjacent communities were found to lie in the range 6.6-2200 ng g<sup>-1</sup>, 13-9200 ng g<sup>-1</sup> and 44-2700  $\mu\text{g g}^{-1}$  respectively. Concentrations of  $\Sigma 22$  PBDEs (43000 ng g<sup>-1</sup>) were highest in floor dust collected from the facility, while the highest concentration of  $\Sigma 10$  PFRs (9200 ng g<sup>-1</sup>) and  $\Sigma 6$  phthalates (2700  $\mu\text{g g}^{-1}$ ) was detected in floor dust sampled from a house with no prevailing winds, suggesting that the treated consumer and commercial products at homes represent a source of PFRs and phthalates to the indoor environment. The upwind PBDE concentrations at a house and a Buddhist temple exceed those observed at a house with no prevailing winds and PBDE concentrations decreased with increasing distance from the facility, revealing that the facility might be a source of PBDEs to the surrounding environments.

Concentrations of  $\Sigma 22$  PBDEs,  $\Sigma 10$  PFRs and  $\Sigma 6$  phthalates in road dust from the facility varied from 26-21000 ng g<sup>-1</sup>, 1100-2100 ng g<sup>-1</sup> and 40-670  $\mu\text{g g}^{-1}$ , whilst those from the adjacent residences were about 5.4-63 ng g<sup>-1</sup>, 650-2000 ng g<sup>-1</sup> and 27-650  $\mu\text{g g}^{-1}$  respectively. Levels of  $\Sigma 22$  PBDEs (21000 ng g<sup>-1</sup>),  $\Sigma 10$  PFRs (2100 ng g<sup>-1</sup>) and  $\Sigma 6$  phthalates (670  $\mu\text{g g}^{-1}$ ) were highest in road dust taken at the facility. Under realistic high-end scenarios of occupational exposure to BDE-99, workers in the facility were exposed above a recently-published Health Based Limit Value for this congener. Reassuringly, estimated exposures to BDE-209 were below the U.S. EPA's reference dose for this congener.

## 1. Introduction

Polybrominated diphenyl ethers (PBDEs), organophosphorus flame retardants (PFRs) and phthalates are polymer additives present in a diverse array of household and industrial goods. They have become ubiquitous pollutants observed in both indoor and outdoor environments especially indoor dust throughout the world (Besis and Samara, 2012; van der Veen and de Boer, 2012; Kang *et al.*, 2012).

PBDEs have been utilized broadly as flame retardants in construction and building materials, furniture, textiles, automotive and aeronautic parts as well as plastics, including plastic casings of electrical and electronic devices (BSEF, 2015).

PFRs are considered to be suitable alternatives to PBDE formulations (deca-BDE, octa-BDE and penta-BDE) that have been recently restricted or phased out because of deleterious health consequences, persistence, bioaccumulation and biomagnification. Therefore, the manufacture and application of these chemicals has been growing remarkably during the recent decade (Morris *et al.*, 2014). PFRs have a large variety of utilizations, with the predominant use of several as flame retardants, plasticizers, stabilizers, lubricants, polyurethane foams (PUFs) and floor polish (van der Veen and de Boer, 2012; Marklund *et al.*, 2005). For example, chlorinated organophosphorus compounds tris (2-chloroethyl)-phosphate (TCEP), tris (1-chloro-2-propyl)-phosphate (TCPP or TCIPP) and tris (1,3-dichloro-2-propyl) phosphate (TDCPP or TDCIPP) are penta-BDE replacements utilized primarily as FRs in both flexible and rigid PUFs deployed in chairs, sofas, vehicle upholstery and relevant products (van der Veen and de Boer, 2012; Dodson *et al.*, 2012; Stapleton *et al.*, 2009; Marklund *et al.*, 2003). TCEP is also principally applied to polyvinyl chloride (PVC) material and polyester resins (Marklund *et al.*, 2003; WHO, 1998). On the one hand, non-chlorinated organophosphates triphenyl phosphate (TPP or TPHP) and tricresyl phosphate (TCP or TMPP) are extensively used as FRs in PVC, tents, electrical cables, synthetic leather and conveyor belts (TOPL, 2015; van der Veen and de Boer 2012; Meeker and Stapleton, 2010). They are also applied as lubricants in hydraulic fluids (van der Veen and de Boer 2012; Solbu

*et al.*, 2007). The non-chlorinated organophosphorus compounds used chiefly as plasticizers are 2-ethylhexyl diphenyl phosphate (EHDP) and tris (2-ethylhexyl) phosphate (TEHP) (Saito *et al.*, 2007; Marklund *et al.*, 2003), the former being chiefly used in PVC, hydraulic fluids and food packaging (van der Veen and de Boer 2012). Moreover, triethyl phosphate (TEP) is applied as FRs in rigid urethane foam (Tajima *et al.*, 2014). Tris (2-butoxyethyl) phosphate (TBEP or TBOEP) is typically utilized as an additive in synthetic rubber, e.g. in soles of shoes, seals, hoses and gaskets as well as as a levelling agent in paper coating and floor waxes and polishes (Marklund *et al.*, 2003; 2005; WHO, 2000). Tributyl phosphate (TBP) is mainly used as a plasticizer in vinyl resins and plastics, as a solvent for lacquers, cellulose esters and natural gums, and as a base stock in the formulation of fire-resistant (aircraft) hydraulic fluids (WHO, 1991a).

Phthalates (otherwise known as phthalate diesters, phthalic acid esters (PAEs) and dialkyl phthalate esters) are synthetic diesters of phthalic acid that can be broadly categorized into lighter molecular weight (dimethyl phthalate (DMP), diethyl phthalate (DEP), and di-*n*-butyl phthalate (DBP or DnBP), and greater molecular weight (benzyl butyl phthalate (BBP, BzBP or BBzP), di-*n*-octyl phthalate (DOP or DnOP), di-2-ethylhexyl phthalate (DEHP), diisononyl phthalate (DiNP), and diisodecyl phthalate (DiDP)) (North *et al.*, 2014; Takaro *et al.*, 2010). The eight most ordinarily-applied congeners of these compounds include DMP, DEP, DBP, BBP (BBzP or BzBP), DOP (or DnOP), DEHP, DiNP and DiDP (Takaro *et al.*, 2010). Phthalates are used in PVC (to make it soft and flexible), food packaging, cosmetics, personal and baby care products, solvents for paints and inks, adhesives, lacquers, lubricants, clothing, plastics toys, enteric coating of pharmaceuticals, medical devices, pharmaceuticals, dentures, construction materials (including wall paper and flooring), domestic furnishings and cleaning products (Takaro *et al.*, 2010; Hauser and Calafat, 2005). The lower molecular weight congeners (DMP, DEP and DBP) are utilized mostly in pharmaceuticals, cosmetics, adhesives, solvents, inks, waxes and insecticides (Takaro *et al.*, 2010). DBP is also applied to the enteric coatings of some medications. Higher congeners (DEHP, DiNP, DOP (or DnOP) and DiDP) are utilized in clothing, building material

and furnishings, but their greatest use is as plasticizers (Takaro *et al.*, 2010; ATSDR, 2002; ATSDR, 1997). Roughly 90% of phthalates produced, especially the greater congeners, are applied as plasticizers in the manufacture of polymeric materials, e.g., PVC, polyvinyl acetate and polystyrene (Xu *et al.*, 2009). BBP (BBzP or BzBP) is extensively utilized in the manufacture of foamed PVC, which is applied greatly to floorings (Guo *et al.*, 2011).

Resulting from the widespread use of PBDEs, PFRs and phthalates in indoor applications, levels of all these chemicals are substantially greater in indoor environments than in outdoor environment (Wensing *et al.*, 2005; Wilford *et al.*, 2004; Carlsson *et al.*, 1997). PBDEs may also be found in recycled items (Ma *et al.*, 2009; Directorate-General Environment, 2005). Human exposure to PBDEs, PFRs and phthalates can occur via three primary pathways including inhalation of air and airborne particles, dietary ingestion and dermal contact (Frederiksen *et al.*, 2009; Fromme *et al.*, 2009; Abb *et al.*, 2009; Heudorf *et al.*, 2007; Wormuth, *et al.*, 2006; Wensing *et al.*, 2005; Hauser *et al.*, 2004). Nonetheless, ingestion of indoor dust has also been considered a predominant exposure pathway for humans particularly for infants and toddlers (Jones-Otazo, *et al.*, 2005; Wilford *et al.*, 2005; Weschler and Nazaroff, 2008; Johnson-Restrepo and Kannan, 2009; Mercier *et al.*, 2011; Harrad *et al.*, 2010; Lioy *et al.*, 2002; Guo, *et al.*, 2011). Furthermore, occupational exposure to PBDEs via indoor dust ingestion may occur in workplaces where electrical and electronic devices are repaired or dismantled, or where PBDE-treated goods are recycled (Ma *et al.*, 2009; Stapleton *et al.*, 2008a; ATSDR, 2004).

PBDEs, PFRs and phthalates are not chemically bound to the polymeric matrix; thus, they can relatively readily leach out, evaporate, migrate or abrade from the treated products, and then spread out into the surrounding air or adsorbed on airborne particulates and settled dust over time (Gevao *et al.*, 2013; Kang *et al.*, 2012; Abb *et al.*, 2009; Heudorf *et al.*, 2007; Harrad *et al.*, 2006; Wormuth, *et al.*, 2006; U.S. EPA, 2005; Wensing *et al.*, 2005; Fromme *et al.*, 2004; Marklund *et al.*, 2003; Fujii *et al.*, 2003). Because domestic dust is produced virtually ubiquitously in residences or offices, it is an integral sample of indoor

microenvironments. The residential dust is typically retained in vacuum bags by using a vacuum cleaner and hence the representative chemical samples of a specific house or office might be obtained from the vacuum cleaning (Abb *et al.*, 2009).

PBDE, PFR and phthalate exposures have adverse health effects. For instance, PBDEs possibly cause cancer as well as affect detrimentally thyroid hormones, endocrine systems, neurobehavioral development, reproduction and birth outcomes (Eskenazi *et al.*, 2013; Noyes *et al.*, 2013; Johnson *et al.*, 2012; Hoffman *et al.*, 2012; Harley *et al.*, 2011; Herbstman *et al.*, 2010; Harley *et al.*, 2010; ATSDR, 2004; Branchi *et al.*, 2003; Darnerud, 2003; McDonald, 2002).

Limited data is available on the toxicity of PFRs. Nevertheless, it is known that TDCPP (or TDCIPP) and TCEP are animal carcinogens, as well as TBEP (TBOEP) and TCPP (TCIPP) are suspected carcinogens (WHO 2000; 1998). TCEP also affects adversely fetal development (Sato *et al.*, 1997; Chapin *et al.*, 1997). Neurotoxic effects have been documented for TCEP, TPP (or TPHP), TCP (or TMPP) (WHO, 2000; 1991a; 1990). TDCPP, TCEP, TCPP, TBEP, TEHP and TBP can cause skin irritation in experimental animals (WHO, 2000; WHO, 1998; WHO, 1991a; 1991b). TDCPP, TCEP, TCPP and TPP also have reported hemolytic effects (Sato *et al.*, 1997). TPP Exposures have been linked to contact dermatitis (Camarasa and Serra-Baldrich, 1992). TDCPP and TPP may be associated with reduced sperm quality, and TDCPP was significantly inversely related to free thyroxin T4, one of the thyroid function indicator (Meeker and Stapleton, 2010). Increases in TDCPP and TCPP levels were correlated with increased risk of atopic dermatitis (Araki *et al.*, 2014).

Based on the toxicological and epidemiological research conducted to date, the health concerns of phthalates generally fall into two major categories: cancer and reproductive effects (Meeker *et al.*, 2012; Sathyanarayana, 2008; Swan *et al.*, 2005; Kavlock *et al.* 2002a, 2002b, 2002c, 2002d, 2002e, 2002f, 2002g). However, there have also been correlations between phthalate exposures and asthma's development (Jaakkola and Knight, 2008; Bornehag *et al.*, 2004; Oie *et al.* 1997), precocious puberty and pre-mature thelarche

(breast development) in girls (Colon *et al.*, 2004; Wolff *et al.*, 2010) as well as allergic symptoms (Jaakkola and Knight, 2008; Kolarik *et al.*, 2008a; Bornehag *et al.*, 2004), neurodevelopment (Kim *et al.*, 2011; Jurewicz and Hanke, 2011) and pathogenesis of bronchial obstruction in children (Jaakkola *et al.* 1999). According to the International Agency for Research on Cancer (IARC), these chemicals are not classifiable as to their carcinogenicity to humans (Group 3) (Grosse *et al.*, 2011). DBP, DEP, BBP (BzBP or BBzP) and DEHP affect deleteriously the mobility of human male sperm (Liu *et al.*, 2012; Main *et al.*, 2006; Hauser *et al.*, 2006: Duty *et al.*, 2005a, 2003; Becker *et al.*, 2004). DBP, BBP and DEHP may also disturb the expression luteinizing hormone (LH) and therefore human testosterone levels (Mendiola *et al.*, 2011; Main *et al.*, 2006; Jonsson *et al.*, 2005; Duty *et al.*, 2005b, 2003; Becker *et al.*, 2004). DEHP is a carcinogenic, endocrine and teratogenic toxicant in animals (Morgenroth, 1993; WHO 1992). It can cause damage to liver and particularly testes based on animal studies (Hauser and Calafat, 2005), and has been demonstrated to lessen the duration of human pregnancy (Latini *et al.*, 2003). In addition, DEHP in domestic dust has been associated with asthma and allergies in children (Jaakkola and Knight, 2008; Kolarik *et al.*, 2008a; Bornehag *et al.*, 2004). Raised levels of DEHP metabolites were observed in autistic (Testa *et al.*, 2012) and school children with IQ scores and lower vocabulary (Cho *et al.*, 2010). Moreover, a study by Toft *et al.* (2012) shows the relationship between periconceptional urinary level of MEHP (the principal urinary metabolite of DEHP) and pregnancy loss.

The application of PBDEs, PFRs and phthalates in Thailand is not strictly regulated; hence all these compounds may be found in a wide range of consumer and commercial products and wastes, particularly electrical and electronic waste (e-waste). In 2007, the total e-waste produced in Thailand was estimated at roughly 308, 845 tons. Televisions, air conditioners, refrigerators, washing machines, personal computers, VCD players, DVD players, cellular phones and digital cameras accounted for 27.49, 19.50, 17.13, 16.00, 14.65, 3.50, 1.24, 0.44 and 0.05% of total e-waste, respectively. The generation of household hazardous and e-waste in the country is expected to increase to about 573, 463 tons by 2017 (Pollution Control Department, 2008). Because of the lack of appropriate e-waste

management in Thailand, workers at e-waste dismantling facilities and populations living nearby the facilities may be exposed to PBDEs via contaminated dust.

This study reports concentrations of PBDEs, PFRs and phthalates in floor and road dust samples collected from an e-waste dismantling facility and adjacent communities in Thailand. Tri- to deca-BDEs (BDEs 17, 28, 47, 66, 71, 85, 99, 100, 119, 126, 138, 153, 154, 183, 184, 190, 191, 196, 197, 206, 207 and 209), PFRs (TEP, TBP, TCEP, TCPP, TDCPP, TBEP, TPP, EHDPP, TEHP and TCP) and phthalates (DMP, DEP, DBP, BBP, DEHP and DOP) were determined in dust. The main objectives were: (i) to obtain comprehensive data on contamination of PBDEs, PFRs and phthalates in an e-waste dismantling facility and adjacent communities in Thailand; (ii) to compare levels of PBDEs, PFRs and phthalates in this study with those published previously elsewhere in the world to elucidate differences in contamination of indoor settled dust among countries; (iii) to estimate occupational exposure to all these pollutants via dust ingestion within the e-waste dismantling facility; and (iv) to assess non-occupational exposure to all these contaminants via dust ingestion within the adjacent communities for both adults and children as appropriate.

## **2. Experimental section**

This study was performed at an e-waste dismantling facility and adjacent communities ranged over a distance of 350 m. (a house 1 predominantly upwind of a facility located 10 m. west of the facility, a house 2 with no prevailing winds located 350 m. northeast of the facility as well as a Buddhist temple predominantly upwind of a facility located 300 m. east of the facility) in Phatthalung Province, Southern Thailand between May 3-15, 2014. Floor and road dust samples were taken from each studied microenvironment (Table 1-2), and were later analyzed for PBDEs, PFRs and phthalates at Hanyang University, Republic of Korea between November 1-December 31, 2014.

### **2.1 Dust sampling methods**

In total, 60 samples of floor (n=40) and road dust (n=20) were collected from an e-waste dismantling facility and adjacent

communities in Phatthalung Province (Fig. 1) using a standardized protocol described previously by Muenhor and Harrad (2012), Muenhor *et al.* (2010) and Harrad *et al.* (2008a). Briefly, dust samples were collected from an e-waste dismantling facility and adjacent communities (Table 1-2) using Hitachi CV-BM16 RE 1600W vacuum cleaners. The vacuum cleaners were modified to sample dust into a 25 µm pore size nylon sock and were cleaned between sample collections to avoid cross contamination. In each sampling area, four m<sup>2</sup> of bare floor/road surface or one m<sup>2</sup> of carpeted floor were thoroughly and evenly vacuumed for exactly 4 or 2 minutes respectively. After collection, dust samples will be stored at -20 °C. All dust samples will be passed through a pre-cleaned and hexane rinsed 500 µm mesh sieve, homogenized thoroughly, weighed, immediately transferred to hexane rinsed glass vials and refrigerated at -20 °C until chemical analysis. Moreover, floor dust sampling questionnaires will be used to collect basic information about the studied houses and a Buddhist temple (e.g. room ventilation, types and number of electrical and electronic appliances in the sampling rooms, number of sponge containing chairs and number of sofas, as presented in Questionnaire 1).

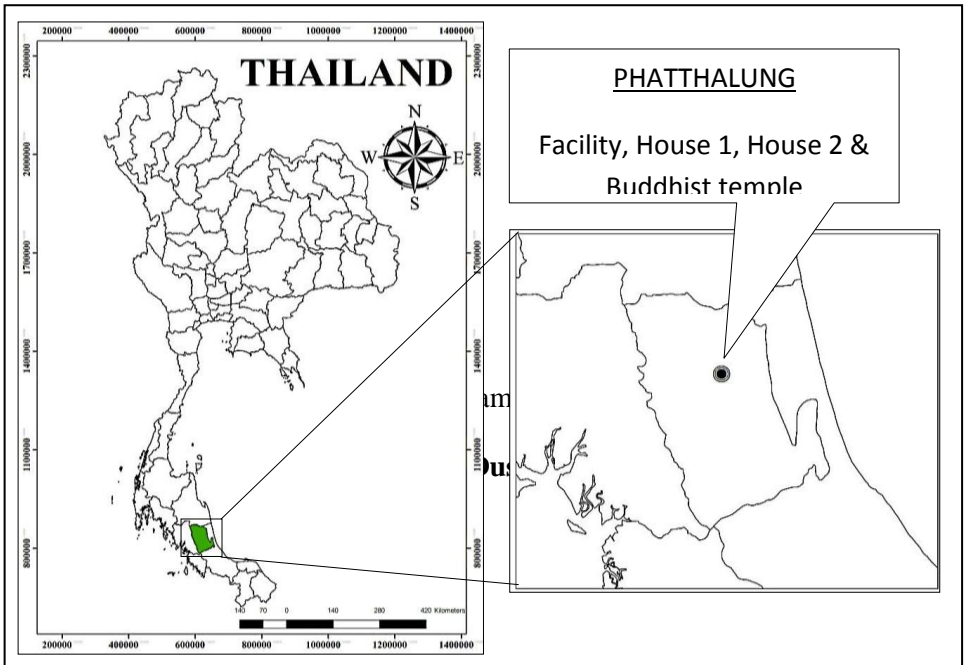
**Table 1** Studied microenvironments for floor dust sampling.

Microenvironments for floor dust sampling	No. of samples	Sampling date
1. An e-waste dismantling facility, Phatthalung Province, Southern Thailand	10	3, 6, 9, 12 & 15 May 2014
2. Adjacent communities (communities sampled ranged over a distance of 350 m.)		
2.1 A house predominantly upwind of a facility located 10 m. west of the facility (House 1)	5	3, 6, 9, 12 & 15 May 2014
2.1.1 Living room	5	
2.1.2 Bedroom	10	
2.2 A Buddhist temple predominantly upwind of a facility located 300 m. east		

of the facility		
2.3 A house with no prevailing winds located 350 m. northeast of the facility (House 2)	5	
2.3.1 Living room	5	
2.3.2 Bedroom		
Total	40	

**Table 2** Studied microenvironments for road dust sampling.

Microenvironments for road dust sampling	No. of samples	Sampling date
1. An e-waste dismantling facility, Phatthalung Province, Southern Thailand	5	3, 6, 9, 12 & 15 May 2014
2. Adjacent communities (communities sampled ranged over a distance of 350 m.)	5	
2.1 A house predominantly upwind of a facility located 10 m. west of the facility (House 1)	5	3, 6, 9, 12 & 15 May 2014
2.2 A Buddhist temple predominantly upwind of a facility located 300 m. east of the facility	5	
2.3 A house with no prevailing winds located 350 m. northeast of the facility (House 2)		
Total	20	



Type of indoor microenvironment:  Office  Home  Other

Sample taken in:  Living Room  Bedroom  Other

Date sample taken:

Approximate time since last vacuumed:  
(if smooth floor please leave at least 2 days since last vacuuming)

Room specifications:  
(Details of the room sampled)

1. Room ventilation:  Natural  Air conditioned

2. Is the room carpeted?

3. Number of sponge containing chairs: How old?

4. Number of sofas: How old?

5. Number of beds: How old?
6. Number of computers: How old?
7. Number of fridges/freezers: How old?
8. Number of TVs: How old?
9. Number of other electronics (i.e., printers, stereos, microwaves, VCD/DVD players, etc.). List them and add how old they are:

## **2.2 Analytical protocols**

### **2.2.1 Target compounds**

In this study, 22 PBDEs, 10 PFRs and 6 phthalates were measured in dust samples. We defined  $\Sigma 22$  PBDEs,  $\Sigma 10$  PFRs and  $\Sigma 6$  phthalates as the sum of BDEs 17, 28, 47, 66, 71, 85, 99, 100, 119, 126, 138, 153, 154, 183, 184, 190, 191, 196, 197, 206, 207 and 209; TEP, TBP, TCEP, TCPP, TDCPP, TBEP, TPP, EHDPP, TEHP and TCP; and DMP, DEP, DBP, BBP, DEHP and DOP, respectively.

### **2.2.2. Analysis of PBDEs, PFRs and phthalates in dust samples**

At Ansan, Republic of Korea, concentrations of PBDEs were quantified in each dust sample using methods described previously (Lee *et al.*, 2013). In summary, accurately weighed 0.15-0.20 g aliquots of each sample were spiked with 2 ng of surrogate standards (MBDE-MXE, Wellington Laboratories), and extracted in a Soxhlet apparatus using 200 mL of 50% dichloromethane (DCM; Ultra residue analysis, J.T. Baker, Phillipsburg, NJ, USA): hexane (Ultra residue analysis, J.T. Baker) (3:1, v:v) for 16-18 h. Following extraction, the crude extracts were concentrated using a rotary evaporator and made up to 5 mL in hexane. A 100  $\mu$ L aliquot of concentrate was transferred to a tube and redissolved in 400  $\mu$ L of acetone for instrumental analysis of PFRs and phthalates. For PBDE analysis, the concentrate was purified by passage through a multi-layer silica gel column with 150 mL of 15% DCM in hexane using the Dioxin Cleanup System (DAC695/DPU8; GL Sciences). The eluates were concentrated to approximately 1 mL and were then

evaporated at room temperature to 50-100  $\mu\text{L}$ . The residues were resolubilized in 100  $\mu\text{L}$  of nonane for instrumental analysis.

Identification and measurement of twenty-two PBDE congeners, ten PFRs and six phthalates was conducted by GC/MS (ECNI), GC/MS (EI) and GC/MS/MS, respectively.

### **2.2.3 Quality control**

To assess contamination occurred during sample analysis, a procedural blank comprising 0.2 g of pre-extracted sodium sulfate (treated in the same way as the samples) was included with each batch of ten samples. These procedural blanks contained <5% of the target compounds in dust samples and the data presented here are thus not blank-corrected. Average  $\pm$  standard deviation percent recoveries of surrogate standards in all samples were:  $81\pm 23$ ,  $97\pm 21$ ,  $105\pm 14$ ,  $103\pm 18$ ,  $94\pm 18$ ,  $102\pm 10$ ,  $92\pm 14$ ,  $110\pm 14$ ,  $112\pm 15$ ,  $107\pm 18$  and  $110 \pm 11\%$  for  $^{13}\text{C}$ - BDE 209, BDE 77, TCEP-d12, TCPP-d18, TDCPP-d15, TPP-d15, DMP-d4, DEP-d4, DBP-d4, DEHP-d4 and DOP-d4 respectively. For the purposes of calculating descriptive statistics, concentrations below the limits of quantitation (LOQs) were assumed to equal half the LOQ. LOQs for all target compounds are given in Table 3.

**Table 3** Mean concentrations (ng g<sup>-1</sup>; range in parentheses) of PBDEs in floor dust samples from an e-waste dismantling facility, houses and a Buddhist temple in Thailand.

Compound	LOQ	Facility (n=10 <sup>a</sup> )	House 1 Upwind (n=10 <sup>b</sup> )	Temple Upwind (n=10 <sup>a</sup> )	House 2 No winds (n=10 <sup>b</sup> )	All studied residences (House 1+ Temple + House 2) (n=30)
<u>PBDEs</u>						
BDE-17	0.07	25 (<0.07-150)	0.21 (0.07-0.56)	0.11 (<0.07-0.54)	0.02 (<0.07-0.10)	0.11 (<0.07-0.56)
BDE-28	0.07	2700 (61-16000)	8.7 (0.46-51)	1.4 (0.24-3.7)	1.7 (0.30-9.8)	3.9 (0.24-51)
BDE-47	0.07	5000 (260-23000)	16 (4.5-53)	3.2 (0.42-9.1)	1.4 (0.80-2.2)	6.9 (0.42-53)
BDE-66	0.07	230 (<0.07-1200)	3.3 (1.2-12)	0.56 (<0.07-2.2)	0.09 (<0.07-0.50)	1.3 (<0.07-12)
BDE-71	0.07	65 (<0.07-410)	2.2 (<0.07-8.9)	<0.07 (<0.07-<0.07)	<0.07 (<0.07-<0.07)	0.74 (<0.07-8.9)
BDE-85	0.07	49 (<0.07-360)	0.85 (<0.07-2.9)	<0.07 (<0.07-<0.07)	<0.07 (<0.07-<0.07)	0.28 (<0.07-2.9)
BDE-99	0.07	1300 (48-6700)	15 (4.4-44)	2.5 (0.14-6.9)	0.99 (0.38-2.3)	6.2 (0.14-44)
BDE-100	0.07	71 (3.8-500)	1.7 (0.6-5.1)	0.12 (<0.07-0.69)	0.09 (<0.07-0.21)	0.63 (<0.07-5.1)

BDE-119	0.07	11 (<0.07-76)	2.5 (0.79-6.6)	<0.07 (<0.07- <0.07)	0.09 (<0.07- <0.74)	0.88 (<0.07-6.6)
BDE-126	0.07	39 (<0.07-310)	<0.07 (<0.07- <0.07)	<0.07 (<0.07- <0.07)	<0.07 (<0.07- <0.07)	<0.07 (<0.07- <0.07)
BDE-153	0.07	240 (4.7-1400)	4.1 (0.88-9.6)	0.84 (<0.07-2.3)	0.29 (<0.07- 0.95)	1.7 (<0.07-9.6)
BDE-154	0.07	34 (1.0-140)	0.96 (0.36-2.6)	0.08 (<0.07- 0.33)	0.13 (<0.07- 0.38)	0.39 (<0.07-2.6)
BDE-183	0.07	91 (3.6-250)	1.7 (0.38-5.0)	0.35 (<0.07- 0.87)	0.26 (<0.07-1.5)	0.78 (<0.07-5.0)
BDE-184	0.07	7.4 (<0.07-32)	0.35 (<0.07- 0.94)	<0.07 (<0.07- <0.07)	0.02 (<0.07- 0.23)	0.12 (<0.07-0.94)
BDE-196	0.33	57 (7.7-110)	2.2 (<0.33-9.3)	0.51 (<0.33-1.0)	0.11 (<0.33- 0.71)	0.92 (<0.33-9.3)
BDE-197	0.33	42 (8.5-80)	2.0 (<0.33-6.2)	0.46 (<0.33-1.1)	0.14 (<0.33- 0.75)	0.86 (<0.33-6.2)
BDE-206	0.33	520 (52-960)	23 (1.8-140)	5.1 (1.5-8.8)	2.3 (1.3-9.0)	10 (1.3-140)
BDE-207	0.33	200 (26-330)	12 (1.4-49)	4.2 (0.64-6.3)	1.7 (0.64-8.6)	6.1 (0.64-49)
BDE-209	3.33	7400 (640- 11000)	290 (20-1900)	32 (3.4-66)	16 (3.3-130)	114 (3.3-1900)
Σ22 PBDEs	-	18000 (1200- 43000)	390 (45-2200)	51 (6.6-93)	26 (8.0-170)	156 (6.6-2200)

Note: <sup>a</sup> All samples taken from same two sampling areas.

<sup>b</sup> All samples taken from same bedroom and living room.

**Table 4** Mean concentrations (ng g<sup>-1</sup>; range in parentheses) of PFRs in floor dust samples from an e-waste dismantling facility, houses and a Buddhist temple in Thailand.

Compound	LOQ	Facility (n=10 <sup>a</sup> )	House 1 Upwind (n=10 <sup>b</sup> )	Temple Upwind (n=10 <sup>a</sup> )	House 2 No winds (n=10 <sup>b</sup> )	All studied residences (House 1+ Temple + House 2) (n=30)
<u>PFRs</u>						
TEP	2.5	<2.5 (<2.5- <2.5)	<2.5 (<2.5- <2.5)	<2.5 (<2.5- <2.5)	1.3 (<2.5-5.5)	0.42 (<2.5-5.5)
TBP	2.5	<2.5 (<2.5- <2.5)	3.0 (<2.5-9.0)	<2.5 (<2.5- <2.5)	<2.5 (<2.5- <2.5)	1.0 (<2.5-9.0)
TCEP	2.5	3.3 (<2.5-14)	1.9 (<2.5-5.8)	0.88 (<2.5- 3.1)	0.62 (<2.5- 3.3)	1.1 (<2.5-5.8)
TCPP	2.5	30 (<2.5-100)	30 (<2.5-60)	28 (<2.5-58)	50 (8.1-76)	36 (<2.5-76)
TDCPP	2.5	20 (6.8-55)	12 (6.0-51)	5.9 (4.0-7.7)	6.3 (5.2-7.8)	8.0 (4.0-51)

---

TBEP	25	130 (<25-1200)	230 (<25-720)	2200 (<25-4500)	4400 (1500-9100)	2300 (<25-9100)
TPP	0.5	150 (19-480)	1.1 (<0.5-9.0)	<0.5 (<0.5-<0.5)	0.15 (<0.5-1.5)	0.43 (<0.5-9.0)
EHDPP	0.5	1.5 (<0.5-2.4)	0.48 (<0.5-1.3)	1.0 (<0.5-3.0)	0.76 (<0.5-1.5)	0.75 (<0.5-3.0)
TEHP	0.5	0.84 (<0.5-8.4)	<0.5 (<0.5-<0.5)	<0.5 (<0.5-<0.5)	<0.5 (<0.5-<0.5)	<0.5 (<0.5-<0.5)
TCP total	0.1	26 (10-48)	7.7 (6.4-11)	6.4 (5.0-9.2)	5.1 (1.3-10)	6.4 (1.3-11)

---

Σ10 PFRs	-	370 (36-1700)	290 (27-760)	2300 (13-4500)	4500 (1500-9200)	2400 (13-9200)
----------	---	---------------	--------------	----------------	------------------	----------------

**Note:** <sup>a</sup> All samples taken from same two sampling areas' All samples taken from same bedroom and living room.

**Table 5** Mean concentrations ( $\mu\text{g g}^{-1}$ ; range in parentheses) of phthalates in floor dust samples from an e-waste dismantling facility, houses and a Buddhist temple in Thailand.

Compound	LOQ	Facility (n=10 <sup>a</sup> )	House 1 Upwind (n=10 <sup>b</sup> )	Temple Upwind (n=10 <sup>a</sup> )	House 2 No winds (n=10 <sup>b</sup> )	All studied residences (House 1+ Temple + House 2) (n=30)
<u>Phthalates</u>						
DMP	0.005	1.2 (0.40-3.6)	1.6 (0.85-4.3)	2.3 (0.83-4.0)	2.4 (1.4-5.0)	2.1 (0.83-5.0)
DEP	0.005	0.62 (<0.005-0.77)	1.1 (0.54-2.1)	1.3 (0.73-3.6)	0.99 (0.84-1.3)	1.1 (0.54-3.6)
DBP	0.005	5.4 (<0.005-8.0)	14 (4.3-40)	6.9 (4.1-17)	4.9 (3.4-6.3)	8.4 (3.4-40)
BBP	0.002	0.43 (<0.002-1.1)	0.69 (0.41-0.94)	0.22 (0.01-0.62)	0.17 (0.10-0.28)	0.36 (0.01-0.94)
DEHP	0.05	550 (79-780)	900 (460-1900)	380 (39-590)	580 (200-2700)	620 (39-2700)

DOP	0.01	0.48 (0.18-0.89)	3.8 (1.1-15)	0.36 (0.11-0.77)	0.91 (0.22-2.2)	1.7 (0.11-15)
Σ6 phthalates	-	550 (86-790)	920 (470-1900)	390 (44-600)	590 (210-2700)	630 (44-2700)

Note: <sup>a</sup> All samples taken from same two sampling areas.

<sup>b</sup> All samples taken from same bedroom and living room.

**Table 6** Mean concentrations (ng g<sup>-1</sup>; range in parentheses) of PBDEs in road dust samples from an e-waste dismantling facility, houses and a Buddhist temple in Thailand.

Compound	LOQ	Facility (n=5 <sup>a</sup> )	House 1 Upwind (n=5 <sup>a</sup> )	Temple Upwind (n=5 <sup>a</sup> )	House 2 No winds (n=5 <sup>a</sup> )	All studied residences (House 1+ Temple + House 2) (n=15)
<u>PBDEs</u>						
BDE-17	0.07	7.3 (0.10-30)	0.09 (<0.07-0.16)	0.04 (<0.07-0.10)	<0.07 (<0.07-<0.07)	0.04 (<0.07-0.16)
BDE-28	0.07	190 (1.3-960)	2.1 (<0.07-3.1)	2.4 (0.36-3.7)	0.34 (0.12-0.59)	1.6 (<0.07-3.7)
BDE-47	0.07	840 (1.7-4200)	1.2 (0.69-2.0)	1.1 (0.69-2.0)	0.60 (0.42-0.95)	0.98 (0.42-2.0)
BDE-66	0.07	250 (<0.07-1200)	0.17 (<0.07-0.41)	0.08 (<0.07-0.39)	<0.07 (<0.07-<0.07)	0.08 (<0.07-0.41)

BDE-71	0.07	0.73 (<0.07-2.5)	0.14 (<0.07-0.69)	<0.07 (<0.07-<0.07)	<0.07 (<0.07-<0.07)	0.05 (<0.07-0.69)
BDE-85	0.07	<0.07 (<0.07-<0.07)	<0.07 (<0.07-<0.07)	<0.07 (<0.07-<0.07)	<0.07 (<0.07-<0.07)	<0.07 (<0.07-<0.07)
BDE-99	0.07	730 (1.4-3600)	0.85 (0.29-1.9)	1.1 (0.3-2.4)	0.20 (<0.07-0.47)	0.72 (<0.07-2.4)
BDE-100	0.07	45 (<0.07-220)	0.15 (<0.07-0.21)	0.09 (<0.07-0.45)	<0.07 (<0.07-<0.07)	0.08 (<0.07-0.45)
BDE-119	0.07	<0.07 (<0.07-<0.07)	0.10 (<0.07-0.48)	<0.07 (<0.07-<0.07)	<0.07 (<0.07-<0.07)	0.03 (<0.07-0.48)
BDE-126	0.07	<0.07 (<0.07-<0.07)	<0.07 (<0.07-<0.07)	<0.07 (<0.07-<0.07)	<0.07 (<0.07-<0.07)	<0.07 (<0.07-<0.07)
BDE-153	0.07	160 (0.74-770)	0.31 (0.21-0.44)	0.33 (<0.07-0.98)	<0.07 (<0.07-<0.07)	0.21 (<0.07-0.98)
BDE-154	0.07	35 (<0.07-180)	0.10 (<0.07-0.21)	0.08 (<0.07-0.23)	<0.07 (<0.07-<0.07)	0.06 (<0.07-0.23)
BDE-183	0.07	16 (0.54-71)	0.80 (<0.07-2.6)	0.16 (<0.07-0.81)	<0.07 (<0.07-<0.07)	0.32 (<0.07-2.6)
BDE-184	0.07	2.4 (<0.07-11)	0.06 (<0.07-0.32)	<0.07 (<0.07-<0.07)	<0.07 (<0.07-<0.07)	0.02 (<0.07-0.32)
BDE-196	0.33	16 (<0.33-77)	0.35 (<0.33-1.7)	0.14 (<0.33-0.69)	<0.33 (<0.33-<0.33)	0.16 (<0.33-1.7)
BDE-197	0.33	25 (0.33-120)	0.35 (<0.33-1.3)	0.14 (<0.33-0.72)	<0.33 (<0.33-<0.33)	0.16 (<0.33-1.3)
BDE-206	0.33	150 (1.8-700)	2.3 (1.7-4.1)	2.5 (1.6-5.2)	1.8 (1.00-2.1)	2.2 (1.0-5.2)
BDE-207	0.33	110 (1.2-530)	1.7 (1.1-3.6)	1.8 (0.85-4.6)	0.98 (0.54-1.3)	1.5 (0.54-4.6)

BDE-209	3.33	1700 (10-8000)	7.4 (5.4-10)	12 (3.3-42)	3.7 (3.33-4.28)	7.6 (3.3-42)
Σ22 PBDEs	-	4200 (26-21000)	18 (13-27)	22 (7.6-63)	7.6 (5.41-9.38)	16 (5.4-63)

Note: <sup>a</sup> All samples taken from same sampling area.

**Table 7** Mean concentrations (ng g<sup>-1</sup>; range in parentheses) of PFRs in road dust samples from an e-waste dismantling facility, houses and a Buddhist temple in Thailand.

Compound	LOQ	Facility (n=5 <sup>a</sup> )	House 1 Upwind (n=5 <sup>a</sup> )	Temple Upwind (n=5 <sup>a</sup> )	House 2 No winds (n=5 <sup>a</sup> )	All studied residences (House 1+ Temple + House 2) (n=15)
<u>PFRs</u>						
TEP	2.5	<2.5 (<2.5-<2.5)	<2.5 (<2.5-<2.5)	<2.5 (<2.5-<2.5)	<2.5 (<2.5-5.5)	<2.5 (<2.5-5.5)
TBP	2.5	<2.5 (<2.5-<2.5)	<2.5 (<2.5-<2.5)	<2.5 (<2.5-<2.5)	<2.5 (<2.5-<2.5)	<2.5 (<2.5-<2.5)
TCEP	2.5	5.6 (3.5-12)	4.4 (3.1-5.0)	3.9 (3.3-4.5)	4.2 (3.2-5.0)	4.1 (3.1-5.0)
TCPP	2.5	48 (12-171)	28 (11-43)	1.8 (<2.5-6.6)	1.8 (<2.5-6.3)	10 (<2.5-43)
TDCPP	2.5	12 (5.3-33)	5.9 (5.4-6.4)	5.8 (5.4-6.1)	5.7 (5.2-5.9)	5.8 (5.2-6.4)
TBEP	25	1300 (1100-1600)	1200 (920-1300)	1200 (900-2000)	871 (640-1100)	1100 (640-2000)
TPP	0.5	110 (<0.5-300)	<0.5 (<0.5-<0.5)	<0.5 (<0.5-<0.5)	<0.5 (<0.5-<0.5)	<0.5 (<0.5-<0.5)

EHDPP	0.5	<0.5 (<0.5-<0.5)	<0.5 (<0.5-<0.5)	0.56 (<0.5-2.8)	<0.5 (<0.5-<0.5)	0.19 (<0.5-2.8)
TEHP	0.5	<0.5 (<0.5-<0.5)	<0.5 (<0.5-<0.5)	<0.5 (<0.5-<0.5)	<0.5 (<0.5-<0.5)	<0.5 (<0.5-<0.5)
TCP total	0.1	10 (1.6-42)	2.8 (1.2-6.4)	0.58 (0.49-0.74)	0.47 (0.44-0.51)	1.3 (0.44-6.4)
Σ10 PFRs	-	1500 (1100-2100)	1200 (960-1300)	1200 (920-2000)	880 (650-1100)	1100 (650-2000)

Note: <sup>a</sup> All samples taken from same sampling area.

**Table 8** Mean concentrations ( $\mu\text{g g}^{-1}$ ; range in parentheses) of phthalates in road dust samples from an e-waste dismantling facility, houses and a Buddhist temple in Thailand.

Compound	LOQ	Facility (n=5 <sup>a</sup> )	House 1 Upwind (n=5 <sup>a</sup> )	Temple Upwind (n=5 <sup>a</sup> )	House 2 No winds (n=5 <sup>a</sup> )	All studied residences (House 1+ Temple + House 2) (n=15)
<u>Phthalates</u>						
DMP	0.005	0.62 (0.27-0.83)	0.81 (0.67-0.89)	1.2 (0.55-3.2)	0.65 (0.47-0.91)	0.88 (0.47-3.2)
DEP	0.005	0.68 (0.64-0.80)	0.79 (0.63-1.0)	0.83 (0.72-0.94)	0.79 (0.71-0.96)	0.80 (0.63-1.0)
DBP	0.005	3.2 (2.7-4.1)	4.6 (3.2-6.6)	4.2 (2.7-6.3)	4.4 (2.9-6.2)	4.4 (2.7-6.6)

BBP	0.002	0.08 (0.02-0.27)	0.03 (0.02-0.05)	0.06 (0.03-0.17)	0.04 (0.03-0.09)	0.04 (0.02-0.17)
DEHP	0.05	170 (36-670)	26 (22-32)	150 (31-640)	70 (42-110)	85 (22-640)
DOP	0.01	0.19 (0.05-0.54)	0.07 (0.05-0.13)	0.25 (0.09-0.52)	0.42 (0.27-0.77)	0.25 (0.05-0.77)
Σ6 phthalates	-	170 (40-670)	32 (27-40)	170 (36-650)	76 (50-120)	91 (27-650)

Note: <sup>a</sup> All samples taken from same sampling area.

**Table 9** Summary of concentrations (ng g<sup>-1</sup>) of selected BDEs in indoor dust samples from this and selected other studies.

Location (reference)	Statistical parameter / compound	BDE-28	BDE-47	BDE-99	BDE-100	BDE-153	BDE-154	BDE-183	BDE-206	BDE-207	BDE-209	ΣBDE <sup>a</sup>
Thailand, this study,	Average	2700	5000	1300	71	240	34	91	520	200	7400	18000
	Median	300	1000	720	11	100	15	72	540	200	7500	13000
An e-waste	Minimum	61	260	48	3.8	4.7	1.0	3.6	52	26	640	1200

dismantling facility, n=10	Maximum	1600 0	2300 0	6700	500	1400	140	250	960	330	11000	43000
Thailand, this study, Three residences, n=30	Average	3.9	6.9	6.2	0.63	1.7	0.39	0.78	10	6.1	114	156
	Median	1.1	2.3	2.1	0.19	0.88	0.22	0.41	4.6	3.3	23	46
	Minimum	0.24	0.42	0.14	<0.07	<0.07	<0.07	<0.07	1.3	0.64	3.3	6.6
	Maximum	51	53	44	5.1	9.6	2.6	5.0	140	49	1900	2200
Thailand, Four e-waste storage facilities, n=25 (Muenhor <i>et al.</i> , 2010)	Average	8.3	410	870	130	380	160	1800	1900	1700	33000	43000
	Median	6.8	160	380	52	130	49	1700	910	1000	20000	28000
	Minimum	<0.5	6.9	10	2.4	2.6	<0.5	11	<10	<10	250	320
	Maximum	33	1800	4600	680	3300	1100	6700	1400 0	9500	250000	290000
Shanghai, China, e-waste recycling workshop floor, n =5 (Ma <i>et al.</i> , 2009)	Average	85	310	270	29	65	18	-	-	-	30000	31000
	Minimum	11	70	24	15	23	12	-	-	-	5600	6300
	Maximum	170	530	510	42	110	28	-	-	-	81000	82000
Japan, Two homes (Takigami <i>et</i>	Average	<0.03	2.5	2.8	0.54	2.0	0.99	-	-	-	390	-

<i>al.</i> , 2009)												
Birmingham , UK, Homes, n=30 <sup>b</sup> (Harrad <i>et</i> <i>al.</i> , 2008b)	Average	0.70	15	36	5.6	14	4.4	71	-	-	260000	260000
	Median	<0.5	10	20	3.4	5.0	2.8	4.2	-	-	8100	8500
	Minimum	<0.5	1.2	2.8	<0.5	<0.5	<0.5	<2.0	-	-	<3.0	12
	Maximum	2.1	58	180	17	110	16	550	-	-	220000	220000
											0	0
Canada, Homes, n=10 <sup>c</sup> (Harrad <i>et</i> <i>al.</i> , 2008a)	Average	6.6	300	510	120	71	69	13	-	-	670	1400
USA, Homes, n=20 <sup>d</sup> (Harrad <i>et</i> <i>al.</i> , 2008a)	Average	25	810	1400	240	240	240	28	-	-	1600	4800
USA, Homes, n=30 (Stapleton <i>et</i> <i>al.</i> , 2014)	GM	0.77	452	741	98.6	40.6	56.8	1.0	-	-	1720	-
	Minimum	<0.07	55	8.0	9.0	7.0	5.0	<0.06	-	-	441	-
	Maximum	30.9	2472	3621	1023	3407	3061	4.5	-	-	76130	-
			0	0	0							
Sweden, Homes, n=5 (Karlsson <i>et</i> <i>al.</i> , 2007)	Average	2.2	51	79	24	4.9	3.9	4.8	22	16	470	-

Germany, Homes, n=34 (Fromme <i>et al.</i> , 2009)	Average	3.4	24	35	6.5	5.0	3.6	9.2	-	-	350	-
Germany, Homes, n=20, GC/MS (Fromme <i>et al.</i> , 2014)	Average	0.2	11.7	19.6	3.3	4.5	2.1	90.7	-	-	1233	-
	Minimum	<0.1	1.3	1.7	0.3	0.2	0.1	0.7			10	
	Maximum	1.0	52.3	79.7	12.4	25.6	6.8	1494			3748	
Germany, Homes, n=6 (Brommer <i>et al.</i> , 2012)	Average	-	2.1	2.6	-	-	-	1.5	-	-	45	52
Australia, Homes, n=10 (Toms <i>et al.</i> , 2009a)	Average	-	91	184	38	23	-	100	-	-	380	-
Australia, Homes & offices, n=9 (Toms <i>et al.</i> , 2009b)	Average	-	54	77	15	13	7.3	25	-	-	620	-
New Zealand,	Average	0.86	36	87	16	9.8	8.7	-	-	-	-	-

Homes,  
n=20  
(Harrad *et al.*, 2008a)

<sup>a</sup> Sum of PBDEs 17, 28, 47, 66, 71, 85, 99, 100, 119, 126, 138, 153, 154, 183, 184, 190, 191, 196, 197, 206, 207 and 209 (this study only).

<sup>b</sup> Thirty samples analyzed for tri-hexa-BDEs; eighteen samples analyzed for  $\Sigma$ BDE.

<sup>c</sup> Ten samples analyzed for tri-hexa-BDEs; seven samples analyzed for  $\Sigma$ BDE.

<sup>d</sup> Twenty samples analyzed for tri-hexa-BDEs; seventeen samples analyzed for  $\Sigma$ BDE.

**Table 10** Summary of concentrations (ng g<sup>-1</sup>) of selected PFRs in indoor dust samples from this and selected other studies.

Location (reference)	Statistical parameter/ compound	TCEP	T CPP	TDCPP	TBEP	TPP	EHDPP	TEHP	TCP total	$\Sigma$ PFRs <sup>a</sup>
Thailand, this study, An e-waste dismantling facility, n=10	Average	3.3	30	20	130	150	1.5	0.84	26	370
	Median	3.3	20	15	<25	160	1.7	<0.5	25	240
	Minimum	<2.5	<2.5	6.8	<25	19	<0.5	<0.5	10	36
	Maximum	14	100	55	1200	480	2.4	8.4	48	1700
Thailand, this study, Three residences, n=30	Average	1.1	36	8.0	2300	0.43	0.75	<0.5	6.4	2400
	Median	<2.5	38	6.4	2300	<0.5	0.68	<0.5	6.3	2300
	Minimum	<2.5	<2.5	4.0	<25	<0.5	<0.5	<0.5	1.3	13
	Maximum	5.8	76	51	9100	9.0	3.0	<0.5	11	9200
Assiut, Egypt, Homes,	Average	49	53	147	86	101	52	-	-	310

n=20 (Abdallah and Covaci, 2014)	Median	22	28	72	18	67	42	-	-	189
	Minimum	<LOQ	<LOQ	<LOQ	<LOQ	8	<LOQ	-	-	38
	Maximum	132	123	557	305	289	102	-	-	962
The Netherlands, Around electronics, n=8 (Brandsma <i>et al.</i> , 2014)	Median	1300	1300	280	22000	820	350	-	110	27000
	Minimum	220	480	70	4600	680	300	-	<50	7400
	Maximum	6900	3800	3200	159000	11000	2000	-	180	167000
New Zealand, Homes, Living room floors, n=34 (Ali <i>et al.</i> , 2012)	Median	110	350	230	4020	600	-	-	120	-
	Average	200	740	<80	730	380	-	-	94	3000
	Minimum	140	370	<80	<60	180	-	-	<40	800
Germany, Homes, n=6 (Brommer <i>et al.</i> , 2012)	Maximum	280	960	110	2800	1300	-	-	240	6000
	GM	32	-	-	-	110	110	130	13	550
	Minimum	<0.44	-	-	-	8.5	8.0	4.1	<0.27	21
Malate, The Philippines, Homes, n=17 (Kim <i>et al.</i> , 2013)	Maximum	1200	-	-	-	2100	770	970	25	4300
	GM	6.4	-	-	-	73	45	30	7.5	253
	Minimum	<0.44	-	-	-	13	7.7	<0.17	<0.27	55
Payatas, The Philippines, Homes, n=20 (Kim <i>et al.</i> , 2013)	Maximum	140	-	-	-	440	560	370	140	880
	GM	348	3440	2730	-	-	-	-	-	-
	Minimum	20	217	621	-	-	-	-	-	-
USA, Homes, n=30 (Stapleton <i>et al.</i> , 2014)	Maximum	6920	67810	13110	-	-	-	-	-	-

<sup>a</sup> Sum of PFRs TEP, TBP, TCEP, TCPP, TDCPP, TBEP, TPP, EHDPP, TEHP and TCP (this study only).

**Table 11** Summary of concentrations ( $\mu\text{g g}^{-1}$ ) of selected phthalates in indoor dust samples from this and selected other studies.

Location (reference)	Statistical parameter/ compound	DMP	DEP	DBP	BBP	DEHP	DOP	$\Sigma$ Phthalates <sup>a</sup>
Thailand, this study, An e-waste dismantling facility, n=10	Average	1.2	0.62	5.4	0.43	550	0.48	550
	Median	0.77	0.68	5.7	0.33	590	0.42	600
	Minimum	0.40	<0.005	<0.005	<0.002	79	0.18	86
	Maximum	3.6	0.77	8.0	1.1	780	0.89	790
Thailand, this study, Three residences, n=30	Average	2.1	1.1	8.4	0.36	620	1.7	630
	Median	1.8	0.95	5.7	0.23	490	0.74	500
	Minimum	0.83	0.54	3.4	0.01	39	0.11	44
	Maximum	5.0	3.6	40	0.94	2700	15	2700
Sweden, Homes, n=346 (Bornehag <i>et al.</i> , 2005)	Average	-	31	226	319	1310	-	-
	Median	-	0	150	135	770	-	-
	Minimum	-	0	0	0	0	-	-
	Maximum	-	2425	5446	45549	40459	-	-
Kuwait, Homes, n=21 (Gevao <i>et al.</i> , 2013)	GM	0.01	1.5	51	6.4	1700	14	2100
	Median	0.03	1.8	45	8.6	2256	14	2400
	Minimum	<d.l.	0.1	8.3	<d.l.	380	<d.l.	470
	Maximum	0.1	16	160	160	7800	1300	7800
Bulgary, Homes, n=177 (Kolarik <i>et al.</i> , 2008b)	GM	260	350	7860	320	960	250	-
	Median	280	340	9930	340	1050	300	-
	Minimum	210	290	6590	280	790	200	-
	Maximum	320	420	9360	380	1170	300	-

China, Homes, n=75 (Guo and Kannan, 2011)	Median	0.2	0.4	20.1	0.2	228	0.2	295
	Minimum	nd	nd	1.5	nd	9.9	nd	24.4
	Maximum	8.2	45.5	1160	12	8400	45.7	8590
Albany, USA, Homes, n=33 (Guo and Kannan, 2011)	Median	0.08	2.0	13.1	21.1	304	0.4	396
	Minimum	nd	0.7	4.5	3.6	37.2	nd	87.1
	Maximum	3.3	11.8	94.5	393	9650	14.1	9670
Canada, Homes, Household vacuum dust (HD), n=126 (Kubwabo <i>et al.</i> , 2013)	Median	0.12	2.0	16.8	42.3	462	-	-
	Minimum	<MDL	<MDL	<MDL	0.57	36	-	-
	Maximum	22	193	1392	944	3836	-	-

<sup>a</sup> Sum of phthalates DMP, DEP, DBP, BBP, DEHP and DOP (this study only)

### 3. Results and discussion

#### 3.1. Concentrations of PBDEs PFRs and phthalates in floor dust samples

Concentrations of  $\Sigma 22$  PBDEs,  $\Sigma 10$  PFRs and  $\Sigma 6$  phthalates in floor dust from an e-waste dismantling facility were 1200-43000 ng g<sup>-1</sup>, 36-1700 ng g<sup>-1</sup> and 86-790  $\mu\text{g g}^{-1}$ , while those from adjacent communities ranged between 6.6-2200 ng g<sup>-1</sup>, 13-9200 ng g<sup>-1</sup> and 44-2700  $\mu\text{g g}^{-1}$  respectively (Table 3-5). PBDE congener pattern for floor dust from the facility was predominated by BDEs 28, 47 and 209, whereas that for residential floor dust was dominated by BDEs 206 and 209. The prominent PFR and phthalate in all forty floor dust samples was TBEP and DEHP respectively.

Levels of  $\Sigma 22$  PBDEs (43000 ng g<sup>-1</sup>) were highest in floor dust collected from the facility, whilst the highest level of  $\Sigma 10$  PFRs (9200 ng g<sup>-1</sup>) and  $\Sigma 6$  phthalates (2700  $\mu\text{g g}^{-1}$ ) was both observed in floor dust sampled from a house with no prevailing winds located 350 m. northeast of the facility, revealing that the treated consumer and commercial items at homes represent a source of PFRs and phthalates to the indoor environment. The upwind PBDE concentrations at a house (House 1) and a Buddhist temple exceed those detected at a house with no prevailing winds (House 2) and PBDE levels decreased with increasing distance from the facility, indicating that the facility might be a source of PBDEs to the outdoor environment.

The PBDE concentrations in floor dust presented here were significantly lower than those found in e-waste treatment facilities in Thailand and China (Muenhor *et al.*, 2010; Ma *et al.*, 2009). We believe that the much lower dust PBDE levels in this study are partly because of the design of the facility studied, which consisted of open barns with no walls, which provide good air ventilation and indoor-outdoor air exchange, and partly due to the fact that unlike in the other studies, in the small informal facility studied here, e-waste was dismantled mechanically by using simple methods and hand tools such as power drill, screwdriver, hammer, plier, wrench, shears and knife.

Concentrations of all BDE congeners found in residential dust in this study were lower than the concentrations reported in many countries around the world including the United Kingdom, the United States,

Canada, Germany, Sweden, Australia and New Zealand (Table 9) (Harrad *et al.*, 2008a,b; Stapleton *et al.*, 2014; Fromme *et al.*, 2009; 2014; Karlsson *et al.*, 2014; Toms *et al.*, 2009a,b). However, the levels of BDE-28, 47, 99 and 100 reported here were higher than those present in homes in Japan (Takigami *et al.*, 2009). The possible reasons for the low PBDE levels in domestic dust in this study are most likely owing to greater use of BFRs like TBBP-A in Thailand, as well as differences in use patterns and household characteristics such as furnishings, non-carpeted rooms/floor and the small number of electrical and electronic goods (particularly laptops and personal computers) in rural Thai residences.

PFR levels observed in indoor dust in this study were lower than the concentrations reported in Egypt, the Netherlands, New Zealand, Germany, the Philippines and the United States (Table 10) (Abdallah and Covaci, 2014; Brandsma *et al.*, 2014; Ali *et al.*, 2012; Brommer *et al.*, 2012; Kim *et al.*, 2013; Stapleton *et al.*, 2014). Nevertheless, the concentrations of TBEP reported here exceeded those detected in houses in Egypt and Germany (Abdallah and Covaci; Brommer *et al.*, 2012). The low PFR concentrations in floor dust in this study could possibly be ascribed to the differences in application of PFR-treated materials and the small number of consumer and commercial products in rural Thai homes and Buddhist temples.

Phthalate concentrations seen in settled dust in this study were lower than the levels reported in Sweden, Kuwait and Bulgaria (Table 11) (Bornehag *et al.*, 2005; Gevao *et al.*, 2013; Kolarik *et al.*, 2008b). Nonetheless, the levels of DMP, DEP, BBP, DEHP and DOP reported here were greater than those measured in homes in China (Guo and Kannan, 2011). The low phthalate levels in dust samples in this study may be due to the differences in utilization of phthalate-treated items and the small number of household and industrial products in rural residences in Thailand.

### **3.2. Concentrations of PBDEs PFRs and phthalates in road dust samples**

Levels of  $\Sigma 22$  PBDEs,  $\Sigma 10$  PFRs and  $\Sigma 6$  phthalates in road dust from the facility fell in the range 26-21000 ng g<sup>-1</sup>, 1100-2100 ng g<sup>-1</sup> and 40-670  $\mu$ g g<sup>-1</sup>, whilst those from the adjacent residences varied from 5.4-63 ng g<sup>-1</sup>, 650-2000 ng g<sup>-1</sup> and 27-650  $\mu$ g g<sup>-1</sup> respectively (Table 6-8).

BDEs 47, 99 and 209 were the abundant congeners measured in road dust samples from the facility, whereas BDEs 209 was the major congener in road dust samples from the communities. The main PFR and phthalate in both road dust from the facility and residences was TBEP and DEHP respectively. Concentrations of  $\Sigma 22$  PBDEs ( $21000 \text{ ng g}^{-1}$ ),  $\Sigma 10$  PFRs ( $2100 \text{ ng g}^{-1}$ ) and  $\Sigma 6$  phthalates ( $670 \text{ } \mu\text{g g}^{-1}$ ) were highest in road dust taken at the facility.

### **3.3. Occupational exposure to PBDEs via floor dust ingestion**

It has been documented that PBDEs may detrimentally affect workers exposed occupationally via ingestion of indoor dust (Julander *et al.*, 2005). Hence, in order to evaluate occupational exposure to PBDEs within the Thai e-waste dismantling facility, we have assumed 100% absorption of intake. Assuming that indoor dust ingestion occurs only during waking hours (average 16 h per day), we have used average adult dust ingestion figures of  $1.25 \text{ mg h}^{-1}$ , and high dust ingestion figures for adults of  $3.13 \text{ mg h}^{-1}$  (Jones-Otazo *et al.*, 2005). We also have used an average male and female adult weight for the Thai population of 68.83 and 57.40 kg (Size Thailand, 2015), and assumed that occupational exposure occurs for 8 h daily. Based on these assumptions, we have created a number of exposure scenarios. These variously estimate exposure at average and high-end dust ingestion rates and where exposure is assumed to be due to dust contaminated at either the median or 95<sup>th</sup> percentile concentrations reported here. Table 12 presents these occupational exposure assessments of male and female workers to BDE-99 and BDE-209 via indoor dust ingestion.

These values are compared with currently available health-based limit values (HBLVs) for PBDEs. For BDE-99, a preliminary HBLV of 0.23-0.30 ng/kg bw/day has been derived by Netherlands researchers (Bakker *et al.*, 2008). Additionally, for BDE-209, the U.S. EPA's Integrated Risk Information System (IRIS) Toxicological Evaluation recommends a reference dose (RfD) of daily oral exposure to BDE-209 of  $7 \text{ } \mu\text{g/kg bw/day}$  that is considered to be without appreciable risk of adverse effects (U.S. EPA, 2008). The exposure estimates for BDE-99 calculated from the Thai dust (0.62-1.87 ng/kg bw/day) exceeded the HBLV cited above when the dust to which exposure occurred was

contaminated at or above the 95th percentile concentration (4300 ng g<sup>-1</sup>), regardless of the assumed dust ingestion rate. By comparison all exposure estimates for BDE-209 were lower than the U.S. EPA's RfD.

**Table 12** Estimated exposures (ng/kg bw/day) of male and female workers in Thai e-waste dismantling facility to BDE-99 and BDE-209 via indoor dust ingestion

Exposure pathway	BDE-99		BDE-209	
	Male	Female	Male	Female
<u>Average dust ingestion rate<sup>a</sup></u>				
- Median concentration	0.10	0.12	1.09	1.30
- 95 <sup>th</sup> percentile concentration	0.62	0.75	1.54	1.84
<u>High-end dust ingestion rate<sup>b</sup></u>				
- Median concentration	0.26	0.31	2.72	3.26
- 95 <sup>th</sup> percentile concentration	1.56	1.87	3.85	4.62
Health-based limit value	0.23-0.30 <sup>c</sup>	0.23-0.30 <sup>c</sup>	7,000 <sup>d</sup>	7,000 <sup>d</sup>

<sup>a</sup> 1.25 mg hr<sup>-1</sup>.

<sup>b</sup> 3.13 mg hr<sup>-1</sup>.

<sup>c</sup> Bakker *et al.*, 2008.

<sup>d</sup> U.S. EPA, 2008.

#### 4. Conclusion

The present study is the first to provide a preliminary database for PBDE, PFR and phthalate contamination in a Thai e-waste dismantling facility, homes and a Thai Buddhist temple. Floor dust levels are substantially lower than reported elsewhere, but in some instances exceeded those reported for household dust in other countries. The evidence of this preliminary study indicates that inappropriate dismantling of e-waste may constitute a source of PBDEs to the surrounding environments. Of potential concern is that under some high-end, but plausible scenarios, exposure of workers to BDE-99 at an e-waste dismantling facility in this study exceeds a health-based limit value proposed recently by Netherlands researchers. Whilst there is a growing database relevant to the environmental occurrence, fate,

distribution and behavior of PBDEs, PFRs and phthalates, there remains an urgent need to examine PBDE contamination of workers involved in the processing of e-waste. Specific issues that require addressing are: the importance of indoor dust ingestion as occupational and non-occupational exposure pathways; the factors influencing PBDE, PFR and phthalate contamination of workplace and residential environments; and the potential health impact of occupational and non-occupational exposure to PBDEs, PFRs and phthalates.

### **Acknowledgements**

Dr. Dudsadee Muenhor is grateful to the Korean Association of Southeast Asian Studies (KASEAS) and the ASEAN University Network (AUN) for the ASEAN-ROK academic exchange fellowship funding. Miss Jariya Khwanthong and Miss Phiyachat Nookongbut are acknowledged gratefully for sample processing. The authors acknowledge gratefully the cooperation from the owners and workers at the Thai e-waste dismantling facility as well as the study participants for permitting us enter into the Buddhist temple and their houses.

### **References**

- Abb, M., Heinrich, T., Sorkau E. and Lorenz, W. 2009. Phthalates in house dust. Environment International, 35: 965-70.
- Abdallah, M. A.-E. and Covaci, A. 2014. Organophosphate Flame Retardants in Indoor Dust from Egypt: Implications for Human Exposure. Environmental Science and Technology, 48: 4782-9.
- Ali, N., Dirtu, A. C., Van den Eede, N., Goosey, E., Harrad, S., Neels, H., Mannetje, A., Coakley, J., Douwes, J. and Covaci, A. 2012. Occurrence of alternative flame retardants in indoor dust from New Zealand: Indoor sources and human exposure assessment Chemosphere, 88: 1276-82.
- Araki, A., Saito, I., Kanazawa, A., Morimoto, K., Nakayama, K., Shibata, E., Tanaka, M. Takigawa, T., Yoshimura, T., Chikara, H., Saijo, Y. and Kishi, R. 2014. Phosphorus flame retardants in indoor dust and their relation to asthma and allergies of inhabitants. Indoor Air, 24: 3-15.
- ATSDR. 1997. Toxicological profile for di-n-octyl phthalate (DnOP). Agency for Toxic Substances and Disease Registry; Atlanta, GA, The United States; 1997. September. Available online: <http://www.atsdr.cdc.gov/toxprofiles/tp95.pdf> (Accessed: 11 April 2015).

- ATSDR. 2002. Toxicological profile for di (2-ethylhexyl) phthalate (DEHP). Agency for Toxic Substances and Disease Registry; Atlanta, GA, The United States; 2002. September. Available online: <http://www.atsdr.cdc.gov/toxprofiles/tp9.pdf> (Accessed: 11 April 2015).
- ATSDR. 2004. Toxicological profile for polybrominated biphenyls and polybrominated diphenyl ethers. Agency for Toxic Substances and Disease Registry; Atlanta, GA, The United States; 2004. September. Available online: <http://www.atsdr.cdc.gov/toxprofiles/tp68.pdf> (Accessed: 10 April 2015).
- Bakker, M. I., de Winter-Sorkina, R., de Mul, A., Boon, P. E., van Donkersgoed, G., van Klaveren, J. D., Baumann, B. A., Hijman, W. C., van Leeuwen, S. P. J., de Boer, J. and Zeilmaker, M. J. 2008. Dietary intake and risk evaluation of polybrominated diphenyl ethers in The Netherlands. Molecular Nutrition & Food Research, 52: 204-16.
- Becker, K., Seiwert, M., Angerer, J., Heger, W., Koch, H. M., Nagorka, R., Rosskamp, E., Schluter, C., Seifert, B. and Ullrich, D. 2004. DEHP metabolites in urine of children and DEHP in house Dust. International Journal of Hygiene and Environmental Health, 207: 409-17.
- Besis, A. and Samara, C. 2012. Polybrominated diphenyl ethers (PBDEs) in the indoor and outdoor environments-A review on occurrence and human exposure. Environmental Pollution, 169: 217-29.
- Bornehag, C. -G., Sundell, J., Weschler, C. J., Sigsgaard, T., Lundgren, B., Hasselgren, M. and Hagerhed-Engman, L., 2004. The association between asthma and allergic symptoms in children and phthalates in house dust: a nested case-control study. Environmental Health Perspectives, 112, 1393-7.
- Bornehag, C. -G., Lundgren, B., Weschler, C. J., Sigsgaard, T., Hagerhed-Engman, L. and Sundell, J. 2005. Phthalates in Indoor Dust and Their Association with Building Characteristics. Environmental Health Perspectives, 113 (10): 1399-1404.
- Branchi, I., Capone, F., Alleva, E. and Costa, L. G. 2003. Polybrominated diphenyl ethers: Neurobehavioral effects following developmental exposure. Neuro Toxicology, 24: 449-62.

- Brandsma, S. H., de Boer, J., van Velzen, M. J. M. and Leonards, P. E. G. 2014. Organophosphorus flame retardants (PFRs) and plasticizers in house and car dust and the influence of electronic equipment. Chemosphere, 116: 3-9.
- Brommer, S., Harrad, S., Van den Eede, N. and Covaci, A. 2012. Concentrations of organophosphate esters and brominated flame retardants in German indoor dust samples. Journal of Environmental Monitoring, 14: 2482-7.
- BSEF (Bromine Science and Environmental Forum). 2015. Our substances: Deca-BDE. <http://www.bsef.com/our-substances/deca-bde/applications> (accessed 19 April 2015).
- Camarasa, J. G. and Serra-Baldrich, E. 1992. Allergic contact dermatitis from triphenyl phosphate. Contact Dermatitis, 26: 264-5.
- Carlsson, H., Nilsson, U., Becker, G. and Ostman, C., 1997. Organophosphate ester flame retardants and plasticizers in the indoor environment: analytical methodology and occurrence. Environmental Science and Technology, 31: 2931-36.
- Chapin, R. E., Sloane, R. A. and Haseman, J. K. 1997. The relationships among reproductive endpoints in Swiss mice, using the reproductive assessment by continuous breeding database. Fundamental and Applied Toxicology, 38: 129-42.
- Cho, S.-C., Bhang, S.-Y., Hong, Y.-C., Shin, M.-S., Kim, B.-N., Kim, J.- W., Yoo, H.-J. 4 Cho, I. H. and Kim, H.-W. 2010. Relationship between environmental phthalate exposure and the intelligence of school-age children. Environmental Health Perspectives, 118: 1027-32.
- Colon, I., Caro, D., Bourdony, C. J. and Rosario, O. 2004. Identification of phthalate esters in the serum of young Puerto Rican girls with premature breast development. Environmental Health Perspectives, 112, A541-3.
- Darnerud, P. O. 2003. Toxic effects of brominated flame retardants in man and in wildlife. Environment International, 29: 841-53.
- Directorate-General Environment. 2005. RoHS substances (Hg, Pb, Cr (VI), Cd, PBB and PBDE) in electrical and electronic equipment in Belgium. Final report. Federal Public Service Health, Food Chain, Safety and Environment. Directorate-General Environment; Brussels, Belgium; 2005 November.
- Dodson, R. E., Perovich, L. J., Covaci, A., Van den Eede, N., Ionas, A. C., Dirtu, A. C., Brody, J. G. and Rudel, R. A. 2012.

- After the PBDE phase-out: a broad suite of flame retardants in repeat house dust samples from California. Environmental Science and Technology, 46:13056-66.
- Duty, S. M., Ackerman, R. M., Calafat, A. M. and Hauser, R. 2005b. Personal care product use predicts urinary concentrations of some phthalate monoesters. Environmental Health Perspectives, 113: 1530-5.
- Duty, S. M., Calafat, A. M., Silva, M. J., Ryan, L. and Hauser, R. 2005a. Phthalate exposure and reproductive hormones in adult men. Human Reproduction, 20: 604-10.
- Duty, S. M., Silva, M. J., Barr, D. B., Brock, J. W., Ryan, L., Chen, Z., Herrick, R. F., Christiani, D. C. and Hauser, R. 2003. Phthalate exposure and human semen parameters. Epidemiology, 14: 269-77.
- Eskenazi, B., Chevrier, J., Rauch, S. A., Kogut, K., Harley, K. G., Johnson, C., Trujillo, C., Sjödin, A. and Bradman, A. 2013. In utero and childhood polybrominated diphenyl ether (PBDE) exposures and neurodevelopment in the CHAMACOS study. Environmental Health Perspectives, 121: 257-62.
- Frederiksen, M., Vorkamp, K., Thomsen, M. and Knudsen, L. E. 2009. Human internal and external exposure to PBDEs-a review of levels and sources. International Journal of Hygiene and Environmental Health, 212: 109-34.
- Fromme, H., Hilger, B., Kopp, E., Miserok, M. and Völkel, W. 2014. Polybrominated diphenyl ethers (PBDEs), Hexabromocyclododecane (HBCD) and “novel” brominated flame retardants in house dust in Germany. Environment International, 64: 61-8
- Fromme, H., Korner, W., Shahin, N., Wanner, A., Albrecht, M., Boehmer, S., Parlar, H., Mayer, R., Liebl, B. and Bolte, G. 2009. Human exposure to polybrominated diphenyl ethers (PBDEs), as evidenced by data from a duplicate diet study, indoor air, house dust and biomonitoring in Germany. Environment International, 35: 1125-35.
- Fromme, H., Lahrz, T., Piloty, M., Gebhart, H., Oddoy, A. and Ruden, H. 2004. Occurrence of phthalates and musk fragrances in indoor air and dust from apartments and kindergartens in Berlin (Germany). Indoor Air, 14: 188-95.
- Fujii, M., Shinohara, N., Lim, A., Otake, T., Kumagai, K. and Yanagisawa, Y. 2003. A study on emission of phthalate

- esters from plastic materials using a passive flux sampler. Atmospheric Environment, 37: 5495-504.
- Gevao, B., Al-Ghadban, A.N., Bahloul, M., Uddin, S. and Zafar, J. 2013. Phthalates in indoor dust in Kuwait: implications for non-dietary human exposure. Indoor Air, 23: 126-33.
- Grosse, Y., Baan, R., Secretan-Lauby, B., El Ghissassi, F., Bouvard, V., Benbrahim-Tallaa, L., Guha, N., Islami, F., Galichet, L. and Straif, K. 2011. Carcinogenicity of chemicals in industrial and consumer products, food contaminants and flavourings, and water chlorination byproducts. Lancet Oncology, 12, 328-9.
- Guo, Y., Wu, Q. and Kannan, K. 2011. Phthalate metabolites in urine from China, and implications for human exposures. Environment International, 37: 893-8.
- Guo, Y. and Kannan, K. 2011. Comparative assessment of human exposure to phthalate esters from house dust in China and the United States. Environmental Science and Technology, 45: 3788-94.
- Harley, K. G., Marks, A. R., Chevrier, J., Bradman, A., Sjödin, A., and Eskenazi, B. 2010. PBDE concentrations in women's serum and fecundability. Environmental Health Perspectives, 118: 699-704.
- Harley, K.G., Chevrier, J., Schall, R. A., Sjodin, A., Bradman, A. and Eskenazi, B. 2011. Association of prenatal exposure to polybrominated diphenyl ethers and infant birth weight. American Journal of Epidemiology, 174: 885-92.
- Harrad, S., de Wit, C. A., Abdallah, M. A.-E., Bergh, C., Bjorklund, J. A., Covaci, A., Darnerud, P. O., de Boer, J., Diamond, M., Huber, S., Leonards, P., Mandalakis, M., Ostman, C., Haug, L. S., Thomsen, C. and Webster, T. F. 2010. Indoor contamination with hexabromocyclododecanes, polybrominated diphenyl ethers, and perfluoroalkyl compounds: An important exposure pathway for people. Environmental Science and Technology, 44(9): 3221-31.
- Harrad, S., Hazrati, S. and Ibarra, C. 2006. Concentrations of polychlorinated biphenyls in indoor air and polybrominated diphenyl ethers in indoor air and dust in Birmingham, United Kingdom: implications for human exposure. Environmental Science and Technology, 40: 4633-8.
- Harrad, S., Ibarra, C., Diamond, M., Melymuk, L., Robson, M., Douwes, J., Roosens, L., Dirtu, A. C. and Covaci, A. 2008a.

- Polybrominated diphenyl ethers in domestic indoor dust from Canada, New Zealand, United Kingdom and United States. Environment International, 34: 232-8.
- Harrad, S., Ibarra, C., Abdallah, M. A.-E., Boon, R., Neels, H. and Covaci, A. 2008b. Concentrations of brominated flame retardants in dust from United Kingdom cars, homes, and offices: Causes of variability and implications for human exposure. Environment International, 34: 1170-5.
- Hauser, R. and Calafat, A. M. Phthalates and human health. 2005. Occupational and Environmental Medicine, 62: 806-18.
- Hauser, R., Duty, S., Godfrey-Bailey, L. and Calafat, A. M. 2004. Medications as a source of human exposure to phthalates. Environmental Health Perspectives. 112: 751-3.
- Hauser, R., Meeker, J. D., Duty, S., Silva, M. J. and Calafat, A. M. 2006. Altered semen quality in relation to urinary concentrations of phthalate monoester and oxidative metabolites. Epidemiology, 17: 682-91.
- Herbstman, J. B., Sjödin, A., Kurzon, M., Lederman, S. A., Jones, R. S., Rauh, V., Needham, L. L., Tang, D., Niedzwiecki, M., Wang, R. Y. and Perera, F. 2010. Prenatal exposure to PBDEs and neurodevelopment. Environmental Health Perspectives, 118: 712-9.
- Heudorf, U., Mersch-Sundermann, V. and Angerer, J. 2007. Phthalates: Toxicology and exposure. International Journal of Hygiene and Environmental Health, 210: 623-34.
- Hoffman, K., Adgent, M., Goldman, B. D., Sjödin, A. and Daniels, J. L. 2012. Lactational exposure to polybrominated diphenyl ethers and its relation to social and emotional development among toddlers. Environmental Health Perspectives, 120: 1438-42.
- Jaakkola, J. J. K. and Knight, T. L. 2008. The role of exposure to phthalates from polyvinyl chloride products in the development of asthma and allergies: a systematic review and meta-analysis. Environmental Health Perspectives, 116: 845-53.
- Jaakkola, J. J. K., Oie, L., Nafstad, P., Botten, G., Samuelsen, S. O. and Magnus, P. 1999. Interior surface materials in the home and the development of bronchial obstruction in young children in Oslo, Norway. American Journal of Public Health, 89:188-92.

- Jones-Otazo, H., Clarke, J. P., Diamond, M. L., Archbold, J. A., Ferguson, G., Harner, T., Richardson, G. M., Ryan, J.J. and Wilford, B. 2005. Is house dust the missing exposure pathway for PBDEs? An analysis of the urban fate and human exposure to PBDEs. Environmental Science and Technology, 39: 5121-30.
- Johnson, P. I., Altshul, L., Cramer, D. W., Missmer, S. A., Hauser, R. and Meeker, J. D. 2012. Serum and follicular fluid concentrations of polybrominated diphenyl ethers and in-vitro fertilization outcome. Environment International, 45: 9-14.
- Johnson-Restrepo, B. and Kannan, K. 2009. An assessment of sources and pathways of human exposure to polybrominated diphenyl ethers in the United States. Chemosphere, 76: 542-8.
- Jonsson Bo, A. G., Richthoff, J., Rylander, L., Giwercman, A. and Hagmar, L. 2005. Urinary phthalate metabolites and biomarkers of reproductive function in young men. Epidemiology, 16: 487-93.
- Julander, A., Westberg, H., Engwall, M. and van Bavel, B. 2005. Distribution of brominated flame retardants in different dust fractions in air from an electronics recycling facility. Science of the Total Environment, 350: 151-60.
- Jurewicz, J. and Hanke, W. 2011. Exposure to phthalates: reproductive outcome and children health. A review of epidemiological studies. International Journal of Occupational Medicine and Environmental Health, 24: 115-41.
- Kang, Y., Man, Y. B., Cheung, K. C. and Wong, M. H. 2012. Risk assessment of human exposure to bioaccessible phthalate esters via indoor dust around the Pearl River Delta. Environmental Science and Technology, 46: 8422-30.
- Karlsson, M., Julander, A., van Bavel, B. and Hardell, L. 2007. Levels of brominated flame retardants in blood in relation to levels in household air and dust. Environment International, 33: 62-9.
- Kavlock, R., Boekekheide, K., Chapin, R., Cunningham, M., Faustman, E., Foster, P., Golub, M., Henderson, R., Hinberg, I., Little, R., Seed, J., Shea, K., Tabacova, S., Tyl, R., Williams, P. and Zacharewski, T. 2002 a. NTP Center for the Evaluation of Risks to Human Reproduction: phthalates expert panel report on the reproductive and developmental toxicity of butyl benzyl phthalate. Reproductive Toxicology, 16: 453-87.

- Kavlock, R., Boekelheide, K., Chapin, R., Cunningham, M., Faustman, E., Foster, P., Golub, M., Henderson, R., Hinberg, I., Little, R., Seed, J., Shea, K., Tabacova, S., Tyl, R., Williams, P. and Zacharewski, T. 2002 b. NTP Center for the Evaluation of Risks to Human Reproduction: phthalates expert panel report on the reproductive and developmental toxicity of di-*n*-butyl phthalate. Reproductive Toxicology, 16: 489-527.
- Kavlock, R., Boekelheide, K., Chapin, R., Cunningham, M., Faustman, E., Foster, P., Golub, M., Henderson, R., Hinberg, I., Little, R., Seed, J., Shea, K., Tabacova, S., Tyl, R., Williams, P. and Zacharewski, T. 2002 c. NTP Center for the Evaluation of Risks to Human Reproduction: phthalates expert panel report on the reproductive and developmental toxicity of di (2-ethylhexyl phthalate). Reproductive Toxicology, 16: 529-653.
- Kavlock, R., Boekelheide, K., Chapin, R., Cunningham, M., Faustman, E., Foster, P., Golub, M., Henderson, R., Hinberg, I., Little, R., Seed, J., Shea, K., Tabacova, S., Tyl, R., Williams, P. and Zacharewski, T. 2002d. NTP Center for the Evaluation of Risks to Human Reproduction: phthalates expert panel report on the reproductive and developmental toxicity of di-isodecyl phthalate. Reproductive Toxicology, 16: 655-78.
- Kavlock, R., Boekelheide, K., Chapin, R., Cunningham, M., Faustman, E., Foster, P., Golub, M., Henderson, R., Hinberg, I., Little, R., Seed, J., Shea, K., Tabacova, S., Tyl, R., Williams, P. and Zacharewski, T. 2002 e. NTP Center for the Evaluation of Risks to Human Reproduction: phthalates expert panel report on the reproductive and developmental toxicity of di-isononyl phthalate. Reproductive Toxicology, 16: 679-708.
- Kavlock, R., Boekelheide, K., Chapin, R., Cunningham, M., Faustman, E., Foster, P., Golub, M., Henderson, R., Hinberg, I., Little, R., Seed, J., Shea, K., Tabacova, S., Tyl, R., Williams, P. and Zacharewski, T. (2002 f). NTP Center for the Evaluation of Risks to Human Reproduction: phthalates expert panel report on the reproductive and developmental toxicity of di-*n*-hexyl phthalate. Reproductive Toxicology, 16: 709-19.

- Kavlock, R., Boekelheide, K., Chapin, R., Cunningham, M., Faustman, E., Foster, P., Golub, M., Henderson, R., Hinberg, I., Little, R., Seed, J., Shea, K., Tabacova, S., Tyl, R., Williams, P. and Zacharewski, T. 2002 g. NTP Center for the Evaluation of Risks to Human Reproduction: phthalates expert panel report on the reproductive and developmental toxicity of di-*n*-octyl phthalate. Reproductive Toxicology, 16: 721-34.
- Kim, J.-W., Isobe, T., Sudaryanto, A., Malarvannan, G., Chang, K.-H., Muto, M., Prudente, M. and Tanabe, S. 2013. Organophosphorus flame retardants in house dust from the Philippines: occurrence and assessment of human exposure. Environmental Science and Pollution Research, 20:812-22.
- Kim, Y., Ha, E. H., Kim, E. J., Park, H., Ha, M., Kim, J. H., Hong, Y. C., Chang, N. and Kim, B. N. 2011. Prenatal exposure to phthalates and infant development at 6 months: prospective Mothers and Children's Environmental Health (MOCEH) study. Environmental Health Perspectives, 119, 1495-1500.
- Kolarik, B., Naydenov, K., Larsson, M., Bornehag, C. -G. and Sundell, J. 2008a. The association between phthalates in dust and allergic diseases among Bulgarian children. Environmental Health Perspectives, 116: 98-103.
- Kolarik, B., Bornehag, C.-G., Naydenov, K., Sundell, J., Stavova, P. and Nielsen, O. F. 2008b. The concentrations of phthalates in settled dust in Bulgarian homes in relation to building characteristic and cleaning habits in the family. Atmospheric Environment, 42: 8553-9.
- Kubwabo, C., Rasmussen, P. E., Fan, X., Kosarac, I., Wu, F., Zidek, A. and Kuchta, S. L. 2013. Analysis of selected phthalates in Canadian indoor dust collected using household vacuum and standardized sampling techniques. Indoor Air, 23: 506-14.
- Latini, G., De Felice, C., Presta, G., Del Vecchio, A., Paris, I., Ruggieri, F. and Mazzeo, P. 2003. In utero exposure to di-(2-ethylhexyl) phthalate and duration of human pregnancy. Environmental Health Perspectives, 111: 1783-5.
- Lee, S., Kannan, K. and Moon, H.-B. 2013. Assessment of exposure to polybrominated diphenyl ethers (PBDEs) via seafood consumption and dust ingestion in Korea. Science of the Total Environment, 443: 24-30.
- Lioy, P. J., Freeman, N. C. and Millette, J. R. 2002. Dust: a metric for use in residential and building exposure assessment and

- source characterization. Environmental Health Perspectives, 110: 969-83.
- Liu, L., Bao, H., Liu, F., Zhang, J. and Shen, H. 2012. Phthalates exposure of Chinese reproductive age couples and its effect on male semen quality, a primary study. Environmental International, 42: 78-83.
- Ma, J., Addink, R., Yun, S. H., Cheng, J., Wang, W. and Kannan, K. 2009. Polybrominated dibenzo-p-dioxins/ dibenzofurans and polybrominated diphenyl ethers in soil, vegetation, workshop-floor dust, and electronic shredder residue from an electronic waste recycling facility and in soils from a chemical industrial complex in eastern China. Environmental Science and Technology, 43: 7350-6.
- Main, K. M., Mortensen, G. K., Kaleva, M. M., Boisen, K. A., Damgaard, I. N., Chellakooty, M., Schmidt, I. M., Suomi, A., Virtanen, H. E., Petersen, J. H., Andersson, A., Toppari, J. and Skakkebaek, N. E. 2006. Human breast milk contamination with phthalates and alteration of endogenous reproductive hormones in infants three months of age. Environmental Health Perspectives, 114: 270-6.
- Marklund, A., Andersson, B. and Haglund, P. 2005. Organophosphorus flame retardants and plasticizers in air From various indoor environments. Journal of Environmental Monitoring, 7: 814-9.
- Marklund, A., Andersson, B. and Haglund, P. 2003. Screening of organophosphorus compounds and their distribution in various indoor environments. Chemosphere, 53: 1137-46.
- McDonald, T. A. 2002. A perspective on the potential health risks of PBDEs. Chemosphere, 46: 745-55.
- Meeker, J. D., Calafat, A. M. and Hauser, R. 2012. Urinary phthalate metabolites and their biotransformation products: predictors and temporal variability among men and women. Journal of Exposure Science and Environmental Epidemiology, 22: 376-85.
- Meeker, J. D. and Stapleton, H. M. 2010. House dust concentrations of organophosphate flame retardants in relation to hormone levels and semen quality parameters. Environmental Health Perspectives, 118: 318-23.
- Mendiola, J., Jorgensen, N., Andersson, A.-M., Calafat, A. M., Silva, M. J., Redmon, J.B., Sparks, A., Drobnis, E.Z., Wang, C., Liu, F. and Swan, S.H. 2011. Associations between urinary

- metabolites of di (2-ethylhexyl) phthalate and reproductive hormones in fertile men. International Journal of Andrology, 34: 369-78.
- Mercier, F., Glorennec, P., Thomas, O. and Le Bot, B. 2011. Organic contamination of settled house dust, a review for exposure assessment purposes. Environmental Science and Technology, 45: 6716-27.
- Morgenroth, V. III. 1993. Scientific evaluation of the data-derived safety factors for the acceptable daily intake. Case study: diethylhexylphthalate. Food Additives and Contaminants, 10, 363-73.
- Morris, P. J., Medina-Cleghorn, D., Heslin, A., King, S. M., Orr, J., Mulvihill, M. M., Krauss, R. M. and Nomura, D. K. 2014. Organophosphorus flame retardants inhibit specific liver carboxylesterases and cause serum hypertriglyceridemia. ACS Chemical Biology, 9: 1097-1103.
- Muenhor, D., Harrad, S., Ali, N. and Covaci, A. 2010. Brominated flame retardants (BFRs) in air and dust from electronic waste storage facilities in Thailand. Environment International, 36: 690-8.
- Muenhor, D. and Harrad, S. 2012. Within-room and within-building temporal and spatial variations in concentrations of polybrominated diphenyl ethers (PBDEs) in indoor dust. Environment International, 47: 23-7.
- North, M. L., Takaro, T. K., Diamond, M. L. and Ellis, A. K. 2014. Effects of phthalates on the development and expression of allergic disease and asthma. Annals of Allergy, Asthma and Immunology, 112: 496-502.
- Noyes, P. D., Lema, S. C., Macaulay, L. J., Douglas, N. K. and Stapleton, H. M., 2013. Low level exposure to the flame retardant BDE-209 reduces thyroid hormone levels and disrupts thyroid signaling in fathead minnows. Environmental Science and Technology, 47: 10012-21.
- Oie, L., Hersoug, L. G. and Madsen, J. O. 1997. Residential exposure to plasticizers and its possible role in the pathogenesis of asthma. Environmental Health Perspectives, 105: 972-78.
- Pollution Control Department (PCD). 2008. Household hazardous waste and waste electrical and electronic equipment inventories, July 2008. Ministry of Natural Resources and Environment, Bangkok, Thailand.

- Saito, I., Onuki, A. and Seto, H. 2007. Indoor organophosphate and polybrominated flame retardants in Tokyo. Indoor Air, 17: 28-36.
- Sathyanarayana, S. 2008. Phthalates and children's health. Current Problems in Pediatric and Adolescent Health Care, 38: 34-49.
- Sato, T., Watanabe, K., Nagase, H., Kito, H., Niikawa, M. and Yoshioka, Y., 1997. Investigation of the hemolytic effects of various organophosphoric acid triesters (OPEs) and their structure-activity relationship. Toxicological and Environmental Chemistry, 59: 305-13.
- Size Thailand. <http://www.sizethailand.org> (Accessed: 19 May 2015).
- Solbu, K., Thorud, S., Hersson, M., Ovrebø, S., Ellingsen, D. G., Lundanes, E. and Molander, P. 2007. Journal of Chromatography A, 1161: 275-83.
- Stapleton, H. M., Sjodin, A., Jones, R. S., Niehuser, S., Zhang, Y. and Patterson, D. G., Jr. 2008a. Serum levels of polybrominated diphenyl ethers (PBDEs) in foam recyclers and carpet installers working in the United States. Environmental Science and Technology, 42(9): 3453-8.
- Stapleton, H. M., Allen, J. G., Kelly, S. M., Konstantinov, A., Klosterhaus, S., Watkins, D. H., McClean, M. D. and Webster, T. F. 2008b. Alternate and new brominated flame retardants detected in U.S. house dust. Environmental Science and Technology, 42: 6910-6.
- Stapleton, H. M., Klosterhaus, S., Eagle, S., Fuh, J., Meekers, J. D., Blum, A. and Webster, T. F. 2009. Detection of organophosphate flame retardants in furniture foam and U.S. house dust. Environmental Science and Technology, 43: 7490-5.
- Stapleton, H. M., Misenheimer, J., Hoffman, K. and Webster, T. F. 2014. Flame retardant associations between children's handwipes and house dust. Chemosphere, 116: 54-60.
- Swan, S. H., Main, K. M., Liu, F., Stewart, S. L., Kruse, R. L., Calafat, A. M., Mao, C. S., Redmon, J. B., Ternand, C. L., Sullivan, S. and Tague, J. L. 2005. Decrease in anogenital distance among male infants with prenatal phthalate exposure. Environmental Health Perspectives, 113: 1056-61.
- Tajima, S., Araki, A., Kawai, T., Tsuboi, T. Ait Bamai, Y., Yoshioka, E., Kanazawa, A., Cong, S. and Kishi, R. 2014. Detection and intake assessment of organophosphate flame

- retardants in house dust in Japanese dwellings. Science of the Total Environment, 478: 190-9
- Takaro, T. K., Diamond, M., Gobas, F., Otton, V. and Shu, H. 2010. Critical Review of Phthalates in Canadian Indoor Environments. Ottawa, Ontario: Health Canada, Safe Environments Program; 31 March 2010: 1-128. Available online: <http://research.rem.sfu.ca/papers/gobas/FinalReportFIN-1.pdf> (Accessed: 29 May 2015).
- Takigami, H., Suzuki, G. Hirai, Y. and Sakai, S.-I. 2009. Brominated flame retardants and other polyhalogenated compounds in indoor air and dust from two houses in Japan. Chemosphere, 76: 270-7.
- Testa, C., Nuti, F., Hayek, J., De Felice, C., Chelli, M., Rovero, P. Latini, G. and Papini, A. M. 2012. Di-(2-ethylhexyl) phthalate and autism spectrum disorders. Asn Neuro, 4: 223-9.
- Tina Organics (P) Ltd. (TOPL), Plasticizers & Allied Chemicals. 2015. Phosphate Esters. [www.pac-india.com/organo-phosphate-esters.html](http://www.pac-india.com/organo-phosphate-esters.html) (accessed 27 May 2015).
- Toft, G., Jonsson, B. A. G, Lindh, C. H., Jensen, T. K., Hjollund, N. H., Vested, A. and Bonde, J. P. 2012. Association between pregnancy loss and urinary phthalate levels around the time of conception. Environmental Health Perspectives, 120: 458-63.
- Toms, L.-M. L., Hearn, L., Kennedy, K., Harden, F. and Bartkow, M. 2009a. Concentrations of polybrominated diphenyl ethers (PBDEs) in matched samples of human milk, dust and indoor air. Environment International, 35: 864-9.
- Toms, L.-M. L., Bartkow, M. E., Symons, R., Paepke, O. and Mueller, J. F. 2009b. Assessment of polybrominated diphenyl ethers (PBDEs) in samples collected from indoor environments in South East Queensland, Australia. Chemosphere, 76: 173-8.
- U.S. EPA. 2005. Furniture Flame Retardancy Partnership: Environmental Profiles of Chemical Flame-Retardant Alternative for Low-Density Polyurethane Foam. EPA 742-R-05-002, United States Environmental Protection Agency; Washington, D.C., The United States. Available online: <http://www.epa.gov/dfe/pubs/flameret/ffr-alt.htm> (Accessed: 19 October 2014).
- U.S. EPA. 2008. Toxicological Review of Decabromodiphenyl Ether (BDE-209): In Support of Summary Information on the

- Integrated Risk Information System (IRIS). EPA/635/R-07/008F. United States Environmental Protection Agency; Washington, D.C., The United States; 2008. June. Available online:  
<http://cfpub.epa.gov/ncea/cfm/recordisplay.cfm?deid=190307>  
(Accessed: 25 May 2015).
- van der Veen, I. and de Boer, J. 2012. Phosphorus flame retardants: Properties, production, environmental occurrence, toxicity and analysis. Chemosphere, 88: 1119-53.
- Wensing, M., Uhde, E. and Salthammer, T. 2005. Plastics additives in the indoor environment-flame retardants and plasticizers. Science of the Total Environment, 339:19-40.
- Weschler, C. J. and Nazaroff, W. W. 2008. Semivolatile organic compounds in indoor environments, Atmospheric Environment, 42: 9018-40.
- Wilford, B. H., Harner, T., Zhu, J., Shoeib, M. and Jones, K. C. 2004. Passive sampling survey of polybrominated diphenyl ether flame retardants in indoor and outdoor air in Ottawa, Canada: implications for sources and exposure. Environmental Science and Technology, 38: 5312-8.
- Wilford, B. H., Shoeib, M., Harner, T., Zhu, J. and Jones, K. C. 2005. Polybrominated diphenyl ethers in indoor dust in Ottawa, Canada: Implications for sources and exposure. Environmental Science and Technology, 39(18): 7027-35.
- Wolff, M. S., Teitelbaum, S. L., Pinney, S. M., Windham, G., Liao, L., Biro, F., Kushi, L. H., Erdmann, C., Hiatt, R. A., Rybak, M. E. and Calafat, A. M. 2010. Investigation of relationships between urinary biomarkers of phytoestrogens, phthalates, and phenols and pubertal stages in girls, Environmental Health Perspectives, 118, 1039-46.
- World Health Organization/ International Programme on Chemical Safety (WHO/IPCS). 1990. Tricresyl phosphate. Environmental Health Criteria 110. World Health Organization; Geneva, Switzerland.
- WHO/IPCS. 1991a. Tri-n-butyl phosphate. Environmental Health Criteria 112. World Health Organization; Geneva, Switzerland.
- WHO/IPCS. 1991b. Triphenyl phosphate. Environmental Health Criteria 111. World Health Organization; Geneva, Switzerland.
- WHO/IPCS. 1992. Diethylhexyl Phthalate, Environmental Health Criteria 131. World Health Organization; Geneva, Switzerland.

- WHO/IPCS. 1998. Flame Retardants: Tris (chloropropyl) phosphate and tris (2-chloroethyl) phosphate. Environmental Health Criteria 209. World Health Organization; Geneva, Switzerland.
- WHO/IPCS. 2000. Flame Retardants: Tris (2-butoxyethyl) phosphate, tris (2-ethylhexyl) phosphate, tetrakis (hydroxymethyl) phosphonium salts. Environmental Health Criteria 218. World Health Organization; Geneva, Switzerland.
- Wormuth, M., Scheringer, M., Vollenweider, M. and Hungerbühler, K. 2006. What are the sources of exposure to eight frequently used phthalic acid esters in Europeans? Risk Analysis, 26: 803-24.
- Xu, Y., Hubal, E. A. C., Clausen, P. A., and Little, J. C. 2009. Predicting residential exposure to phthalate plasticizer emitted from vinyl flooring: A mechanistic analysis. Environmental Science and Technology, 43(7): 2374-80.

## **Eating Disorders and Weight Issues in Adolescents**

***FRIMA ELDA***

*Ph.D. Student in Public Health Faculty,  
Universitas Indonesia*

## 1. Background

In adolescents, changes in physical appearance and body shape during puberty can be a sensitive and important subject. Issues with body image and body satisfaction can influence eating behaviors and motivation toward weight control. Body image distortion and dissatisfaction in adolescents may play a crucial role in the development of pathogenic behaviors such as excessive dieting, exercising, and purging. They can lead to serious psychological and medical problems such as eating disorders (anorexia nervosa and bulimia nervosa) (1)

Body image is a construct determined by a series of individual and socio-cultural factors that intervenes decisively in several aspects of our lives in Western society. Amongst the broader socio-cultural determinants of body image development are ideal body representations transmitted through various socialisation agents such as the mass media, which clearly stands out as spokespeople for these cultural values. Thus, it can be argued that the mass media not only reinforces cultural stereotypes but also strengthens gender behaviour patterns. From a multidimensional perspective, body image is formed through the dynamic interaction of several of these sociocultural and individual factors; the alteration of one of these necessarily affects the rest of the factors in the cycle. (2)

The relationship between positive body image and self-esteem among adolescents has been well documented in correlational studies, and it is found regardless of age and gender. Furthermore, the association between body image and self-esteem has been found to be higher than those between self-esteem and other domains of life experience such as scholastic competence, social acceptance, and athletic competence, across age groups from children to middle-aged adults, and across countries (2-4) Body image distortion is considered as a multidimensional pattern consisting of cognitive and affective components (concerns and feelings about the body) and behaviors related to own body perception. Body image distortion can have two meanings: one is

to have a distorted image of one's body, which is a problem of recognition, and the other is to have an emotional response about one's physical condition ie, not happy.<sup>2</sup> Body image distortion is recognized to be a core and often persistent symptom in EDs defined as disorders in which there is extreme concern with the control of body weight and shape, followed by grossly inadequate, capricious, or hectic food intake. (1)

Socialisation agents such as television, internet, cinema and printed media project the idea that ideal body images can be reached through body control and change and that it is solely up to a person's resolve to realize these ideals. This implies moving from the representation of ideal bodies to providing information on how to achieve them. However, in many cases the images presented as ideal prove to be unachievable (unless through aggressive methods such as cosmetic surgery) as they have probably, prior to their publication, been airbrushed and retouched, and thus become unreal.

The variable that continues to be unalterable in content analysis of body control in women is weight. Obesity stereotypes tend to include the belief that weight is controllable and overweight people tend to be portrayed as greedy, weak and lazy, whilst miracle weight-loss results are normalized by experts. (5) Recent criticism in this direction led to weight loss advice stressing more the importance of health, which was thus associated with thinness (Calado, 2010). Wiseman et al. (1992) found that since 1981 joint weight loss and exercise magazine articles had increased indicating a possible cultural redefinition of methods for weight loss. Previous studies had reported articles based solely on dieting as a weight loss mechanism (5)

The association between an ideal body and social values must be pointed out. Ideal body shapes are associated with personality traits and positive values, enhancing even more their desirability. The beauty ideal becomes a value in itself and trends that move in different directions are frowned upon. Thin women are therefore associated with wealth. (2, 5)

Given that problems with negative body image and low self-esteem are common during adolescence and commonly co occur, it is important to understand the association between these two domains of subjective personal experience, especially with a goal of developing preventive and therapeutic interventions.(4, 6)

The issues of 'health and well-being' have been common concerns for all generations and times. Especially, in modern society, these concerns are related to controlling lifestyle and life satisfaction as a concept of well-being. Therefore, well-being is subjective with regards to satisfaction with life and advanced level of health needs in modern society. (7)

Well-being considers integrative health promotion that includes physical and psychological aspects of nursing care. Generally, people realize the importance of health and its values in middle age and have had experiences of health-related problems. For college students, the concerns are appearance rather than health. Youths in their college years are sensitive to the latest fashion and try to pursue new ideas. However, the formation of healthy habits would be a good foundation for health and well-being in later years and could lead to a healthy lifespan. Therefore, for youths in their college years, health management must be appealing. (8, 9)

Generally, as we grew older, the ratio of muscle gradually decreases but fat increases. However, in modern society, all for ages it appears that the range of body weight is normal, but the fat ratio is related with activities. Especially when studying and preparing for jobs, college students are more likely to have decreased activities and an increased ratio of body fats. Female college students concerned about looks tend to decrease their weight by food, not by exercise. These tendencies of inactivity in female students can add to body fat. (8-10)

Eating disorders are psychiatric syndromes that manifest themselves in nutrition related symptoms. Anorexia and bulimia nervosa are not distinct disorders, rather the symptoms appear in several combinations along a continuum of disorders eating. (11)

The incidence and prevalence of eating disorders in children and adolescents has increased significantly in recent decades, making it essential for pediatricians to consider these disorders in appropriate clinical settings, to evaluate patients suspected of having these disorders, and to manage (or refer) patients in whom eating disorders are diagnosed. (11-14)

Anorexia nervosa (AN) is an eating disorder that leads to a number of medical sequel in adult women and has a mortality rate of 5.6% per decade; known complications include effects on hematologic, biochemical, bone density, and body composition parameters. Bulimia nervosa is the ingestion and subsequent purging of copious amounts of food, has been part of human society, sporadically, since the Roman orgies. (13, 15, 16)

Binge eating is a common problem among people who are overweight and obese. Besides consuming unusually large amounts of food in a single sitting, binge eaters generally suffer from low mood and low alertness, and experience uncontrollable compulsions to eat.(12, 17)

Binge eating and purging is dangerous. In rare cases, bingeing can cause esophageal ruptures, and purging can result in life-threatening cardiac (heart) conditions because the body loses vital minerals. The acid in vomit wears down too the name land the stomach lining and can cause scarring on the hands when fingers are pushed down the throat to induce vomiting. The esophagus may become inflamed, and glands in the neck may become swollen.(18)

Eating disorders appear to center on preoccupations with food and weight; however, mental health professionals believe these disorders are often about more than simply food. Besides psychological factors that may predispose people to eating disorders, including diminished self-esteem, depression, anxiety, loneliness, or feelings of lack of control, a variety of inter personal and social factors have been implicated as causal factors for these disorders. (18, 19)

Interpersonal issues that may increase the risk for developing eating disorders include troubled family and personal relationships; difficulty expressing emotions; a history of physical or sexual abuse or the experience of being teased, taunted, or ridiculed about body size, shape, or weight. (20) Social factors that may contribute to eating disorders include sharply restricted, rigid definitions of beauty that exclude people who do not conform to a particular body weight and shape, cultures that glorify thinness and overemphasize the importance of obtaining a “perfect body”, and cultures that judge and value people based on external physical appearance rather than on internal qualities such as character, intellect, generosity, and kindness. Appearance driven concerns, rather than health needs, continue to motivate many obese individuals to lose weight. Societal pressures reinforce these appearance driven concerns by portraying obese individuals in a negative manner.(18-20)

## **2. Conceptual Framework**

A proposed etiologic model for eating disorders is based on the current cultural emphasis on thinness combined with a predisposition toward a stockier build and a greater tendency toward emotional reactivity resulting in consequent dietary restraint. (12)

Most eating disorders can be traced to a “first” diet in response to body size dissatisfaction. Genetic make-up predisposes some individuals to obesity. Environmental influences such as the type of food available, the opportunity to become involved in athletics, and the examples set by parents and other significant adults have an effect on the diet and exercise patterns developed. In society, “thin ideal” places the chubby child in a position to be teased, ridiculed, and excluded, all of which can be very damaging to self-esteem. As the child enters puberty and adolescence, the desire to be thin overrides common sense and spurs adherence to whatever fad diet is “in” and promises quick results. (21)

Excessive dietary restraint leads to energy deprivation and hunger. This hunger, if combined with added stress, depression, anxiety, or just impatience with a diet that is not working fast enough, leads to frustration and overeating. In the person who will develop an eating disorder, this overeating is rapidly followed by guilt and worry over potential weight gain. Reaction to this guilt may include giving up on dieting and becoming obese, chronic dieting, subsequent fasting, or purging of food. (19)

The conceptual framework of eating disorders will explain in figure 1.

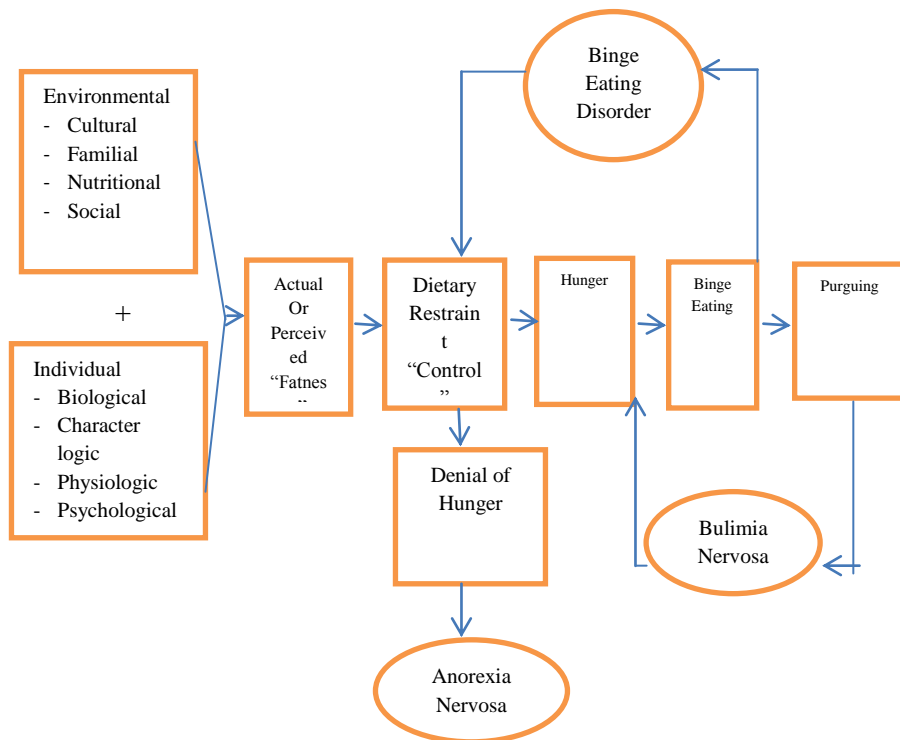


Figure 1. Framework of Etiologic Cycle for Eating Disorders (Krummel, 1996).

### 3. Research Method

This study utilized a cross-sectional design. Participants are informed that they have a right to refuse to participate or to withdraw from the study at any time. This study is completely anonymous. This study using two designs are quantitative and qualitative. The participants are 379 girls. The age of the participants ranged from 15 to 19 years. For qualitative participants in Korea, there are 5 college students.

All the participants completed a questionnaire that contained the following measures:

The Eating Attitudes Test from DSM IV, is a psychological measure of anorexic/bulimic-like attitudes and beliefs. We used the 40-item self-report version, in which the frequencies of attitudes and beliefs are rated using a 6-point scale. The EAT has been validated to show a high level of concurrent validity and a consistent predictive validity across

independent samples and controls; the test also demonstrates a high degree of internal reliability. We used the Self-Esteem Scale (Rosenberg, 1965) to assess self-esteem. The Self-Esteem Scale is a widely used measure with acceptable reliability and validity.

For body image, we used the Contour Drawing Rating Scale (CDRS; Thompson & Gray, 1991) to assess body dissatisfaction. The CDRS consists of nine drawings of a female figure (for female participants) or a male figure (for male participants). Each drawing increases in size from extremely thin (1) to very obese (9). Participants are asked to rate their ideal figure (what they ideally wanted to look like) and their current size (perceived figure). The discrepancy between the ideal and current size scores is an index of body size dissatisfaction.

We gathered background information on a confidential information sheet that included sex, age, height, present weight, ideal weight, highest past weight, lowest past weight, parents' occupation, and current school. The information given on weight provided another measure of body dissatisfaction: the difference between the students' current weight and ideal weight indicated the number of kilograms they desired to lose or gain. Thus weight dissatisfaction was a second measure of body image dissatisfaction.

Questionnaires are counterbalanced, to control for order effects. Study personnel (myself or trained undergraduate research assistants) are available to answer questions during this time. Expected risks are minimal, and no participants appeared distressed during survey administration.

Statistical Procedures is used for data entry and descriptive analyses. Anova is used to evaluate the model. In most cases, parcels, which served as observed variables in the models, are created from questionnaire items, as described above. Parceling multidimensional constructs so that each indicator is a stand-alone measure of the latent factor maximizes the correlations among observed variables. Items are rank-ordered according to their reliability and then distributed across parcels. Data are cleaned prior to analysis. Specifically, item-level frequencies are examined to determine whether there are any inconsistent values or mistakes in coding. No missing data are imputed. Several steps are involved in estimating structural equations models.

#### **4. Research Objective**

Participants will recruit from urban society with higher education, 15-19 years old, and meet once for a period of approximately 45-60 minutes to complete the questionnaires. Informed consent is obtained prior to survey administration. All questions will answer during the informed consent discussion.

Participants who meet DSM-IV criteria for Anorexia Nervosa (AN), Bulimia Nervosa (BN) or Eating Disorder Not Otherwise Specified (EDNOS) are eligible for participation. EDNOS was defined as recurrent episodes of binge eating and/or compensatory behaviors that occurred less than 24 times during the previous 3 months or an ED where the abstinence period between episodes was greater than 2 weeks. This included cases with purging disorder.

#### **5. Hypothesis**

The hypotheses of this research are;

1. There is a relationship between eating disorders with weight issues in adolescences?
2. There is a relationship between eating disorders with nutrition in adolescences?
3. There is a relationship between nutrition with weight issues in adolescences?
4. What are the most influential factors in the incidence of eating disorders in adolescences?

#### **6. Public Benefit**

Conventional public health definitions describe primary prevention as the prevention of new cases and secondary prevention as the prevention of recurrence of a disease or prevention of its progression. Primary prevention measures fall into two categories: actions to protect against disease and disability and actions to promote health such as good nutrition and hygiene, adequate exercise and rest, avoidance of environmental and health risks. Health promotion also includes education about other interdependent dimensions of health known as wellness. Examples of health promotion programs aimed at preventing eating disorders include programs to enhance self-esteem, nutrition education classes, and programs to support children and teens to resist

unhealthy pressures to conform to unrealistic body weight.

Secondary prevention programs are intended to identify and detect disease in its earliest stages, when it is most likely to be successfully treated. With early detection and diagnosis, it may be possible to cure the disease, slow its progression, prevent or minimize complications, and limit disability. Secondary prevention of eating disorders includes efforts to identify affected individuals to intervene early and prevent the development of serious and potentially life-threatening consequences.

## **7. Outline of Topic**

That diet and eating behaviors are closely linked to psychological health and emotional well-being is widely recognized. Psychological factors often influence eating habits. Many people overeat when they are bored, stressed, angry, depressed, or anxious. Psychological distress can aggravate weight problems by triggering impulses to overeat. Emotional discomfort drives many people over eat as a way to relieve anxiety and improve mood. Some people revert to the “comfort foods of their youth”, the meals or treats of fared to them when they were sick or foods that evoke memories of the care free days of childhood. Others rely on chocolate and other sweets, which actually contain chemicals known to have a soothing effect on mood. Over time, the associations between emotions, food and eating can become firmly fixed.

## **8. Result**

There are three categories of Eating Disorders (ED) namely anorexia nervosa, bulimia nervosa, eating disorder Not Otherwise Specified (EDNOS) includes binge eating. participants are home to the specifications of binge eating as much as 8%, bulimia nervosa as much as 4.3%, anorexia nervosa as much as 2.7%. Anorexic tendencies to as much as 31% and 13.3% as much as EDNOS. On the tendency of anorexia, researchers take the criteria respondents who had the IMT or 17.5 respondents < passes 3 times a menstrual period in the last 3 months. For EDNOS criteria used if it meets all of the criteria for anorexia nervosa, but still having regular menstrual periods or if you experience episodes of binge eating and purging, but not too put on weight and body shape in evaluating yourself, then it is classified into Eating Disorders Not Otherwise Specified (EDNOS)

There is a significant relationship between dietary behaviors, body image, self confidence, physical violence, knowledge of nutrition. This can happen because research among adolescent who are indeed very high risk occurs ED Adolescents are required to have a skinny body and trim as it will help draw attention and success and can improve the quality of work. A desire to perform flawlessly and has a perfect body make their perform various attempts, one of them by doing a strict diet which eventually leads to a less good eating habits that will eventually cause a ED.

The most abundant type of trend experienced by the respondents are the kind of EDNOS. This is similar to statements of Fairburn and Hill (2005) that half of people with anorexia or bulimia is not a anorexia nervosa but EDNOS. Respondents who belong EDNOS types into the trend of having each criteria from the ED, as an example of someone who experienced episodes of binge eating but have a fear of gaining weight.

For most compensation behavior is done is using a laxative or diuretic that is as much as 13%. In people with anorexia nervosa found that respondents have found as many as 17.5 < IMT 9.7%. Respondents who never misses a menstrual period 3 times in 3 months was as much as 24%. According to Stice et al. (2000) questions mengenai amenorrhea is a strong indicator to diagnose whether a person is experiencing anorexia or not.

Safarino (1998) stated that many years ago, a beautiful and ideal woman is a woman who is more round with size chest and hips are bigger. After the 1960s, the ideal figure of a woman becoming thinner and social pressure on women to be slim increases.

The prevalence of ED has been discovered since 1930 in the world. Research conducted by Theander (1970) in Keel (2005) conducted in 1931-1960 expressed as much as 0.24% of the people in Sweden have anorexia nervosa. Pagsberg and Wang (1994) in Keel (2005) stated that as many as 0.7% of adolescents have bulimia nervosa in Denmark. Keel (2005) has conducted research in the UK in 1988-1993, obtained results 12.2% of adolescents have bulimia nervosa.(18, 22)

This study identified that as much as 43% of the respondents never go on a diet in the past year. Demands among flight attendants have to get skinny and slender body that will lead them to do a strict diet to get the perfect body shape. It supported the onset of diet behavior among flight attendants that the level of competition or rivalry in the work is quite high. The competition competition or encourage the formation of specific methods for the flight attendants to control weight loss such as diet or avoid a meal. In this study illustrated that most participant start dieting at work.

Based on the results of the cross-tabulations revealed a significant relationship exists between dietary behavior with ED. The results of this research in line with the theory of Tiemeyer (2008) stating that they are moderately Dieter has the possibility of 5 times more likely to experience the ED compared to people who are not dieting. They are very strict diets has the possibility of 18 times bigger

In Indonesia, Tantiani (2007) proved that 34.8% of adolescents in Jakarta have ED specification 11.6% adolescents suffer from anorexia nervosa and 27% suffer from bulimia nervosa. Kurnia (2008) mentions as many as 88.5% teens have a tendency ED specification tends to 11.8% in anorexia. (23)

Genetic factors, low self confidence, eating and body image are also some of the factors causing the ED. (24) Women tend to be very concerned about body shape and according to their perception of body shape that is both thin and slender body. Understanding of the behavior perception proper diet and body image is something that is important to note. From these results expected to emerge other studies to explore the ED. Understanding of the behavior perception proper diet and body image is something that is important to note.

The participants stated that they had concerns about their figures and desired to be slim. Although they had no concerns about health, they were perceived to have a high ratio of body fat through body composition testing. On discovering this, they reflected on their lifestyle relating to health. Finally they realized that they had no regular habits or exercise regimes; they were inactive.

The female ideal of being extremely thin, as presented through advertising by the diet industry, can be seen as a breeding ground for disordered eating and negative reasons for exercise. Dieting is a more common behavior among women who report that the way they feel about their bodies is important to the way they feel about themselves in general; this relationship was not found for the men in their study. Results of our present study would support this view. There is considerable evidence that men are more visually interested in the bodies of the opposite sex than are women (see Mazur, 1986, for a review). As a result, women have traditionally displayed a greater commitment to the pursuit of cultural standards of beauty than have men. In an era that cherishes a very slender body for women, those for whom body satisfaction is a central aspect for self-esteem are more likely to be preoccupied with weight and prone to negative eating attitudes. (6)

The notion of these ideals has been supported by the results of the present study and would thus suggest that neither men nor women can escape the sociocultural pressure to achieve the ideal body shape.

The participants had problems such as studies, friendships, and other relationships. These stressors can be settled over time. However, these positions affect lifestyle. Students perceived they have more stressors with social relationships than of their own. These stressors impact on activities and diet patterns in daily lifestyle. Especially, introverted students tended to block external relationships and take nutritional unbalanced foods as they please. (2)

Settling stress included: sleeping, staying in their own place, smoking, drinking, sweet foods or binge eating. The more stressful the life, the more irregular the diet patterns. From depth interview with some Korean students, most of them agree that body image is very important for their performance. Peer group and media as some of their reasons. In Indonesia, some of Indonesian adolescents make the Korean girls as their role model.

In Korea, some of participants like vegetables and fruits like Korean noodles, gimbab, Kimchi, and fried foods. Most of them follows an irregular pattern; that eat out and skip breakfast daily, while eating at night when doing their task, same like Indonesia girls.

When they are stressed, they take snacks and cookies instead of three meals. They usually take cold foods and fast foods. Some of them drink at night and they also like spend time at coffee shop.

## **9. Discussion**

Anorexia nervosa is a clinical syndrome in which a person experiencing an unnatural fear of fatness. This is attributed by the distortions in the rough of the shadow body, think of air-wasters of food and refusal to eat. Anorexia Nervosa means lack of appetite, but true anorexia nervosa sufferers him feel hungry and too tasteful to food, learn about food and calories; Stockpiling; hiding and deliberately wasting food. (13)

The criteria of anorexia nervosa, according to Diagnostic and Statistical Manual of (DSM-IV American Psychiatric Association, 1994) there are four diagnostic criteria for anorexia nervosa, i.e.: 1) is very afraid of becoming fat although weight had been under par. 2) encountered an error in accepting the weight or shape of the body, which in turn affects the assessment of body weight or shape her body. Disturbances in the received weight or body shape also affects the assessment of patients with anorexia nervosa against risks that will arise when her weight remains below normal (3) refused to concern weight in accordance with age and height body. 4) women experienced a disruption on the menstruation cycle usually occurs before any drastic weight loss. The disorder is characterized by the presence of no menstruation at least 3 times the cycle accordingly. (12, 18, 19)

A tendency to internalize media messages regarding ideals for attractiveness has been suggested as one potential mediator between exposure to those messages and the development of eating and shape-related disturbances developed the Sociocultural Attitudes Towards Appearance Questionnaire (SATAQ), which contains two scales: internalization (endorsement or acceptance of media and societally based pressures regarding appearance) and awareness (acknowledgement that such pressures exist). In a series of studies, we found that internalization is a significant correlate of body dissatisfaction and eating disturbance and predicts variance beyond that associated with simple awareness of pressures and other risk factors, such as negative feed- back (teasing) about appearance (3)

Similar findings have been demonstrated using structural equation modeling. For instance, measured media exposure (print media and television exposure), gender role endorsement, ideal-body stereotype internalization, body dissatisfaction, and eating disordered symptomatology among undergraduate women. In addition to finding a direct path between media exposure and eating disordered behaviors, the researchers discovered that media exposure led to internalization of a slender ideal body shape, which in turn led to body dissatisfaction and eating-disordered symptoms (25)

Theoretical explanations for the specific mechanisms by which the media produce their negative effects are just beginning to appear in the literature. Stice and colleagues have proposed a Dual-Pathway Model that asserts that maladaptive messages in the mass media predispose individuals to bulimia nervosa when those messages are condoned and reinforced by family and peers and when this occurs in the setting of low self-esteem, a poorly developed self-concept, and perceptions of being above an ideal weight. In addition, it is proposed that media influence may play a secondary role by providing information on problematic means of achieving the idealized body size, such as fasting, over exercising, and purgative techniques (26)

A second theory is derived from the work of Levine (1998), whose Developmental Transitions Model suggests that childhood predispositions such as beliefs about the importance of thinness are developed and maintained by teasing and by family and peer modeling of weight concerns. At adolescence, these predispositions interact with simultaneous developmental changes (e.g., weight increase at puberty, academic stress). In turn, a social context of messages about the importance of thinness, the societal support of dieting for weight control, and further teasing may lead to the development of disordered eating(26)

A third approach emphasizes Social Comparison Processes as a possible mechanism connecting media exposure or pressures to the development of heightened internalization of media values or, possibly, body dissatisfaction and eating disturbance(3). Levine have emphasized the importance of multifactorial models for understanding the complex connection between disparate media influences and negative sequel related to eating disturbed cognitions and behaviors. More empirical work in this area is certainly indicated. (3)

## 10. Conclusion

Existing research over the past few years indicates the high tendency of anorexia nervosa is mainly on young women. When this happens continuously then it will appear negative effects in the short and long term for the young women. According to the existing research Summit occurrence tendency of anorexia nervosa appears at the age of 15 to 20 years, the age at which the young women began to leave home and enter secondary education up even in college.

Tendency to anorexia nervosa an early indications from anorexia that intention or the wishes of the person who marked the attitude or behavior that lead to emotional disorders, have a critically against was

nowhere, any change of body image and the refusal to maintain a normal body weight who appointed it with restrictions on eating in excess or by doing certain things in order to lose weight quickly. Confidence is a positive attitude and the belief that individual to develop a positive judgment against yourself or against the environment or situation that exposes itself as well as to receive all the advantages and disadvantages of belonging so that it can actualization. While body image source feed feelings, experiences, attitudes and evaluations, owned one of her body covering body shape, body size and body weight that leads to physical appearance which may be positive or negative. Imagers' slim body can still in dream woman. This phenomenon make folding duplicate case anorexia the drain. For the ladies there is a tendency to use all means in order to have the ideal body. The population in this study are all the young women students

Based on the results of the study pointed out that there's a negative relationship between the confidence with the tendency of anorexia nervosa in young women, there is a negative relationship between body image anorexia nervosa on trend with young women, there is a negative relationship between confidence and body image anorexia nervosa on trend with young women.

Distortion was assessed via self-reporting by the subjects, and more structured clinical measures are needed to more accurately evaluate subjects' body image distortion. High risk for eating disorder and depression were also determined from self-reported data. Self-report measures may lead to under-reporting or underestimation of symptoms.

The target schools were conveniently selected, and therefore the study findings may not be representative of all Korean adolescents. The cross-sectional nature of the study design limited the interpretation of the results and was not optimal for the investigation of the direction of causal inference. These findings should be considered as preliminary findings, and clarification of the direction of the relationship using prospective research is needed in order to contribute to understanding of the related area of body image distortion in adolescence.

## References

1. hyun M-Y, Jung Y-e. Factors associated with body image distortion in Korean adolescents. *Neuropsychiatric Disease and Treatment* 2014;10:797–802.
2. Sepulveda AR, Calado M. Westernization: The Role of Mass Media on Body Image and Eating Disorders. <http://www.intechopen.com/books/relevant-topics-in-eating-disorders/westernization-the-role-of-mass-media-on-body-image-and-eating-disorders> 2012.
3. Thompson JK, Heinberg LJ. The Media's Influence on Body Image Disturbance and Eating Disorders: We've Reviled Them, Now Can We Rehabilitate Them? *Journal of Social Issues*. 1999;5: 339–53.
4. Park W, Epstein NB. The longitudinal causal directionality between body image distress and self-esteem among Korean adolescents: The moderating effect of relationships with parents. *Journal of Adolescence*. 2013;36(2):403-11.
5. Calado M, Lameiras M, Sepulveda AR, Rodriguez Y, Carrera MV. The Association Between Exposure to Mass Media and Body Dissatisfaction Among Spanish Adolescents. *Women's Health Issues*. 2011;21(5):390-9.
6. Furnhams A, Badmin N, Sneade I. Body Image Dissatisfaction: Gender Differences in Eating Attitudes, Self-Esteem, and Reasons for Exercise. *The Journal of Psychology*., 2002;581–596.
7. Kim J. Experiences of Health Related Lifestyles in High Body Fat but Non-obese Female College Students in Korea. *Osong Public Health and Research Perspectives*. 2014;5(1):68-73.
8. Kim J. Experiences of Health Related Lifestyles in High Body Fat but Non-obese Female College Students in Korea. *Elsevier*. 2014:68-73.
9. Andrade FCD, Raffaelli M, Teran-Garcia M, Jerman JA, Garcia CA. Weight status misperception among Mexican young adults. *Body Image*. 2012;9(1):184-8.

10. Vogel EA, Rose JP, Roberts LR, Eckles K. Social comparison, social media, and self-esteem. *Psychology of Popular Media Culture*. 2014;3(4):206-22.
11. Quigley, Patricia. . *Eating Disorder, Bulimia* medscape. 2010.
12. Krummel DA, Kris-Etherton PM. *Nutrition in Women's Health*. Gaithersburg, Maryland: An Aspen Publication; 1996.
13. Alison DB. *Handbook Of Assessment Methods For Eating Baheviors and Weight Related Problems. Measures, Theory, and Research*1994.
14. Ata RN, Thompson JK, Small BJ. Effects of exposure to thin-ideal media images on body dissatisfaction: Testing the inclusion of a disclaimer versus warning label. *Body Image*. 2013;10(4):472-80.
15. Brown LB, Larsen KJ, Nyland NK, Eggett DL. Eating Competence of College Students in an Introductory Nutrition Course. *Journal of Nutrition Education and Behavior*. 2013;45(3):269-73.
16. Rice FP, Dolgin KG. *The Aloscent Development, Relationships, and Culture*. Boston: Pearson; 2005.
17. Brown JE. *Nutrition Through The Life cycle*. United States of America: Wadsworth Thomson Learning; 2002.
18. Keel PK. *Eating Disorders*. New Jersey: Pearson Prentice Hall; 2005.
19. Kring AM, Johnson SL, Davidson GC, Neale JM. *Abnormal Psychology*. United States of America: Wiley; 2012.
20. Chang EC, Perera MJ, Kupfermann Y. Predictors of eating disturbances in South Asian American females and males: A look at negative affectivity and contingencies of self-worth. *Asian American Journal of Psychology*. 2014;5(3):172-80.
21. Rakhkovskaya LM, Warren CS. Ethnic identity, thin-ideal internalization, and eating pathology in ethnically diverse college women. *Body Image*. 2014;11(4):438-45.
22. Nasser M. Eating disorders across cultures. *Psychiatry*. 2009;8(9):347-50.
23. Tantiani T, Syafiq A. Perilaku Makan Menyimpang Pada Remaja di Jakarta *Jurnal Kesehatan Masyarakat Nasional* 2008;2.
24. Gibney MJ, Margetts BM, Kearney jM, Arab L. *Public Health Nutrition*. Oxford: Blackwell Publishing Ltd.; 2005.
25. Chang EC, Yu EA, Lin EY. An examination of ethnic variations in perfectionism and interpersonal influences as predictors of eating disturbances: A look at Asian and European American females. *Asian American Journal of Psychology*. 2014;5(3):243-51.

26. Hausenblas HA, Campbell A, Menzel JE, Doughty J, Levine M, Thompson JK. Media effects of experimental presentation of the ideal physique on eating disorder symptoms: A meta-analysis of laboratory studies. *Clinical Psychology Review*. 2013;33(1):168-81.

**Acknowledgment**

*This work was supported by a fellowship exchange students Asean University Network (AUN)- Republic of Korea (ROK)s*

**Resistive Switching Effect in Chromium Oxide Thin Films Probed  
by Conductive Atomic Force Microscopy**

*PHAM KIM NGOC*

## I. Introduction

The chromium oxide has been already exhibited as one of the most important transition metal oxides. There are many phases of chromium oxide such as  $\text{Cr}_2\text{O}$ ,  $\text{CrO}$ ,  $\text{CrO}_2$ ,  $\text{Cr}_2\text{O}_3$ ,  $\text{Cr}_3\text{O}_4$  and  $\text{Cr}_8\text{O}_{11}$ , in which  $\text{Cr}_2\text{O}_3$  is the most stable phase under normal condition [1]. The chromium oxide films have been widely used for protective coatings on read – write heads in digital magnetic recording units and gas- bearing details [2-4], electro – chromic materials [5], solar absorber [6-7], potential cathode for lithium batteries [8] and spintronic devices [9–10]. Recently, chromium oxide films have attracted more attention due to their new promising application in resistive switching random access memory (RRAM) [11-13].

The first study about reversible resistive switching properties on chromium oxide thin films was reported by Chen et al in 2011 [11]. Among two devices of  $\text{Pt}/\text{Cr}_2\text{O}_3/\text{TiN}$  and  $\text{Pt}/\text{Cr}_2\text{O}_3/\text{Pt}$ , only the first one presented the bipolar resistive switching with resistance ratio over  $10^2$  after forming process. The physical model of vacancy filament for formation and rupture is proposed to illustrate the resistive switching mechanism using observation oxygen migration through  $\text{TiN}$  and  $\text{Cr}_2\text{O}_3$  interface by Auger electron spectroscopy analysis. The other report of chromium oxide based RRAM from our study is about influence of electrode materials and thermal treatment process on resistive switching behavior [13]. It is found that the mechanism of resistive switching depends not only on the nature of electrode materials but also on the density of defects and grain boundaries of chromium oxide. Since then, as – prepared  $\text{Ag}/\text{CrO}_x/\text{Pt}$  devices are proposed by metallic filament model involved the electro – chemical redox reaction. However, to further clarify this mechanism, some new techniques should be approached.

The model of filamentary conduction paths in Metal – Insulator – Metal (MIM) has been investigated since 1960s and many scientists have efforts to make it more visible and clearer through laterally resolving techniques such as scanning probe microscopy (SPM) [14-20], scanning electron microscopy (SEM) with photoemission electron microscopy (PEEM) [21], high resolution transmission electron

microscopy (HRTEM) [22-24], electron energy loss spectroscopy (EELS)[25]...Among them, SPM based techniques seem the most effective tool because they can provide information with very high spatial resolution in both horizontal and vertical directions. SPM techniques include scanning tunneling microscopy (STM) and conducting – atomic force microscopy (C – AFM). If STM's principle is based on the tunneling electrical current through the surface to probe tip in the very high vacuum with using conductive substrates, C – AFM can be used more simply by using dc bias during contact mode to measure both topography and current images in the ambient condition without conducting substrates. There are many studies in recent years using C – AFM technique to observe the growth and shrinkage of filamentary paths controlled by bias voltages applied to the materials. C – AFM images has confirmed filamentary conduction in various resistive switching films including  $\text{TiO}_2$  [26-28],  $\text{SrTiO}_3$  [29],  $\text{MoO}_x$  [30],  $\text{NiO}$  [31-33],  $\text{Cu}_x\text{O}$  [34],...However, studies about filamentary model in chromium oxide based RRAM up to now have been till missing.

In this work, chromium oxide thin films are deposited by reactive sputtering technique for  $\text{Ag}/\text{CrO}_x/\text{Pt}$  and  $\text{Ti}/\text{CrO}_x/\text{Pt}$  devices which have been thoroughly investigated mechanism of resistive switching by C – AFM method. The direct observations of conductive filament appearances only appeared in  $\text{Ag}/\text{CrO}_x/\text{Pt}$  devices demonstrated that electro – chemical redox reaction process as the key role for resistive switching properties in chromium oxide films.

## **II. Experiment**

The chromium oxide thin films were deposited by dc reactive sputtering technique at room temperature. To investigate the current – voltage (I – V) characteristics of chromium oxide films,  $\text{Ag}/\text{CrO}_x/\text{Pt}$  and  $\text{Ti}/\text{CrO}_x/\text{Pt}$  devices were prepared with 100 nm – thick  $\text{CrO}_x$  films as in our previous report [13]. The Keithley 4200 Semiconductor Characterization System was used to measure I – V behavior in a dc sweep mode. During electrical measurement, the bias voltage was applied to bottom electrode (Pt) while the top electrode (Ag, Ti) was grounded.

To study the mechanism of resistive switching of devices by C – AFM technique, the reversible structures was prepared with 10 nm – thick  $\text{CrO}_x$  films on bottom electrodes of sputtered Ag, Ti layers on glass substrate. The Pt coated tip of C – AFM plays the role as a top electrode of approximately 20 nm in diameter. The topography and current images of RRAM cells were measured by Veeco Dimension D3100 Atomic Force Microscope. Scan was performed on the surface of  $\text{CrO}_x$  with the sample bias to achieve the set/ reset processes. The XPS spectroscopy was performed using ESCA2000 ((VG microtech - UK) with X – ray source being Al  $K\alpha$  radiation (1486.6 eV) and C 1s peak calibration at 284.5 eV.

### III. Results

1. Current – voltage characteristics of TE/ $\text{CrO}_x$ /Pt devices:

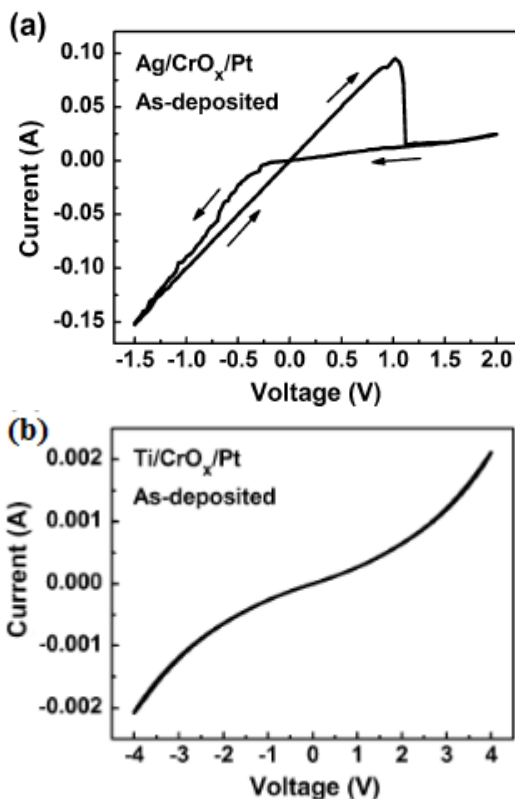


Figure 1. Current – voltage behavior of TE/ $\text{CrO}_x$ /Pt devices (TE: Ag, Ti)

In the previous report, we have investigated the switching behavior of the as-deposited  $\text{CrO}_x$  films with various top electrodes such as Ag and Ti on Pt commercial substrate. As shown in Fig. 1, only the  $\text{Ag}/\text{CrO}_x/\text{Pt}$  device exhibited I-V hysteresis, while no resistance switching was observed in the  $\text{Ti}/\text{CrO}_x/\text{Pt}$  device.

We also suggested that electrochemical redox reaction controlled resistance switching occurred in  $\text{Ag}/\text{CrO}_x/\text{Pt}$  device. When top electrode is applied positive bias, active silver metal atoms oxidize to ions.  $\text{Ag}^+$  ions at the interface of  $\text{Ag}/\text{CrO}_x$  migrate through the grain boundaries or dislocations in  $\text{CrO}_x$  film to the bottom electrode and deoxidize therein. Precipitations of active metal atoms at the electrochemically inert electrode and finally form a highly conductive filament in the cell. When the polarity of the applied voltage is reversed, an electrochemical dissolution of the filament takes place, resetting the system into HRS. The resistive switching operation was controlled by formation/rupture of silver filaments process. These results above were in our previous report [13].

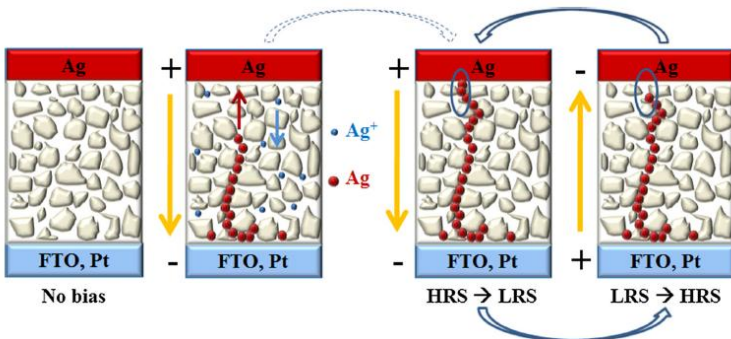


Figure 2. Ag filament conductive paths mediated by electrochemical redox reaction.

### III.2. X – ray photoelectron Spectroscopy:

Figure 3(a) and 1(b) show high – resolution XPS core level spectra at the near surface region of the  $\text{CrO}_x$  films prepared at the room temperature. The Cr 2p<sub>3/2</sub> spectrum in Fig. 1(a) of  $\text{CrO}_x$  films showed three separate peak components at binding energy of 576.1, 577.5 and 579.2 eV, respectively. It can be seen from Fig. 1(a) that the peak of around 574 eV corresponding to metallic Cr was not observed in the chromium oxide films. The Cr 2p<sub>3/2</sub> spectrum at binding energy of

576.1 eV is attributed to  $\text{Cr}^{3+}$  (denote  $\text{Cr}_x^{3+}$ ) in  $\text{Cr}_2\text{O}_3$  phase [35-37]. The lower intensity peak at binding energy of 577.5 eV corresponds to  $\text{Cr}^{3+}$  (denote  $\text{Cr}_y^{3+}$ ) originating from  $\text{CrO(OH)/Cr(OH)}_3$  phases [38]. Besides two peaks of  $\text{O}_{\text{Ox}}^{3+}$  and  $\text{O}_{\text{Oy}}^{3+}$ , there is a low intensity peak positioned at 579.2eV which is identified to  $\text{Cr}^{6+}$  indicating the formation of  $\text{CrO}_3$  phase [39]. The analysis of Cr 2p<sub>3/2</sub> spectrum can be revealed that there are multi-phases of  $\text{Cr}_2\text{O}_3$ ,  $\text{CrO(OH)/Cr(OH)}_3$  and  $\text{CrO}_3$  coexisting in chromium oxide films prepared at room temperature. The relative contents of various phases can be estimated from Gaussian – Lorentzian fitting curves in Fig.1(a). The relative contents are 51.63%, 36.7% and 11.5% corresponding to  $\text{Cr}_2\text{O}_3$ ,  $\text{CrO(OH)/Cr(OH)}_3$  and  $\text{CrO}_3$ , respectively. It is clearly observed that  $\text{Cr}_2\text{O}_3$  phase is dominant in content.

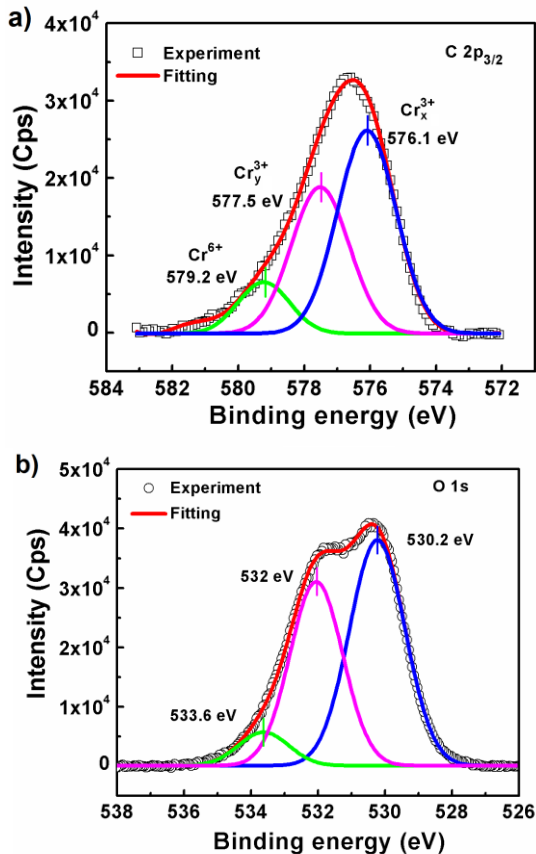


Figure 3. XPS spectra of Cr 2p and O 1s in  $\text{CrO}_x$  film.

The convolution of the O 1s spectrum in Fig. 1(b) resulted in three peaks centered at 530.2, 532 and 533.6 eV. The highest intensity peak 530.2 eV corresponds to oxygen in Cr<sub>2</sub>O<sub>3</sub> phase [40-41]. The lower intensity peak at a binding energy of 532 eV corresponds to absorbed oxygen species ( $O^-$ ,  $O_2^{2-}$ ) on surface in the ambient atmosphere [42-43]. The lowest intensity peak of O 1s at 533.6 eV can be attributed to oxygen related covalent bond. This peak is consistent the existing of CrO(OH) and/or Cr(OH)<sub>3</sub> phases in CrO<sub>x</sub> films prepared at room temperature. Process of thermal treatment at high temperature about 1000<sup>0</sup>C leads to disappear of this peak due to the loss of oxygen [44].

III.3. Conducting – AFM study:

a) Schematic of C – AFM measurement:

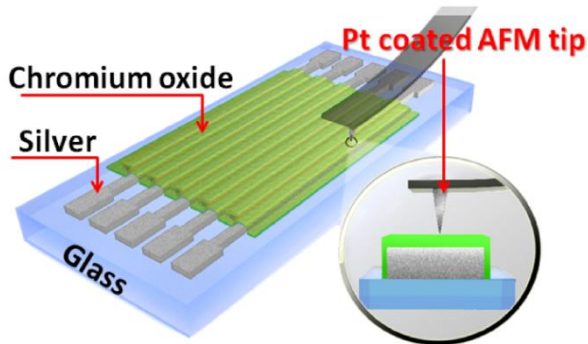


Figure 4. Sketch of schematics of C – AFM measurement.

The schematics of C – AFM measurement was presented in Figure 4. The topography and current images of the RRAM cell were carried out by C-AFM using Pt coated Si probe with curvature radius of 20 nm. Sputtered CrO<sub>x</sub> film was deposited on 1 mm - width silver electrode lines on glass substrate. For the C-AFM measured sample, there were no Pt coating on the top layer. In this case, the C-AFM probe functioned as a mobile top electrode, and the contact area could be estimated to be about 0.5 μm x 0.5 μm. The writing process was performed with a contact-AFM in scan mode by applying 0.5 V on the Pt – coating tip while Ag electrode was ground. The reading process was carried out at a voltage of 0.1 V.

b) Formation/ rupture of conductive filaments:

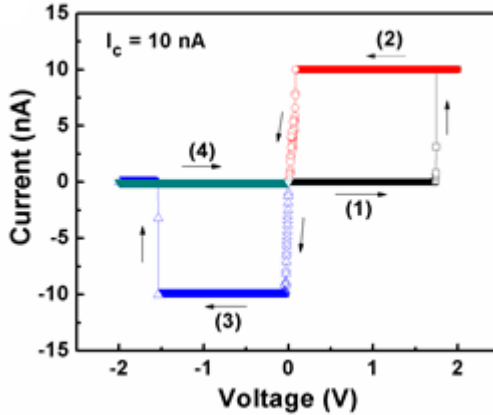
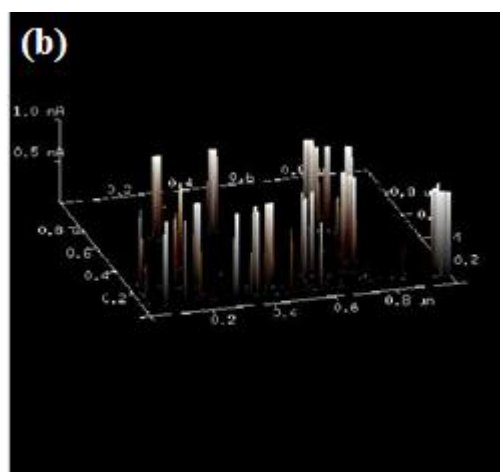
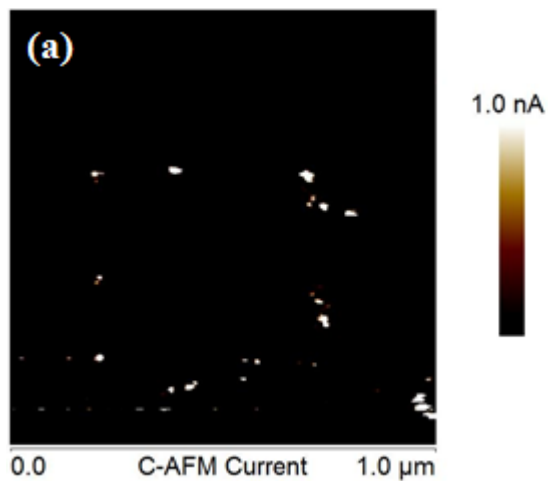
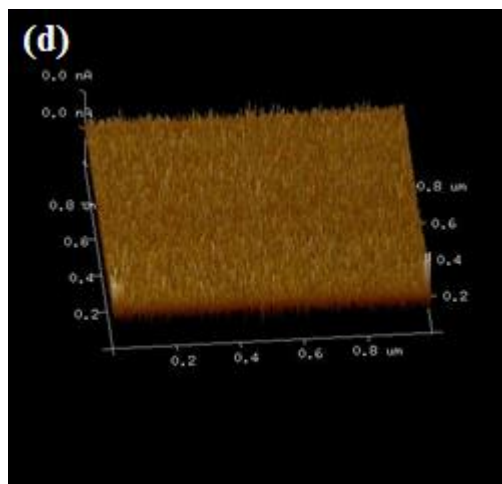
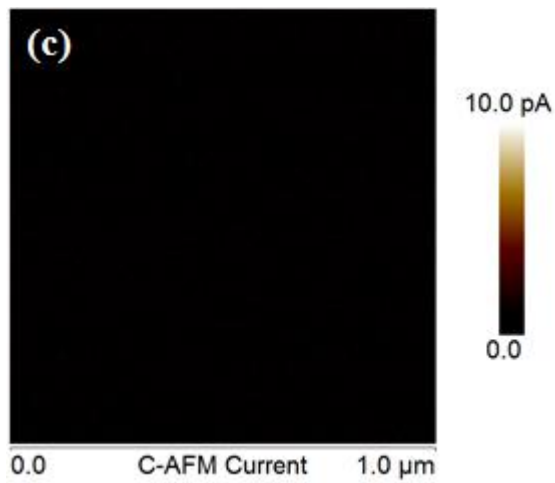


Figure 5. Local I-V hysteresis curve obtained by C – AFM at compliance current of 10 nA, .

Local I–V hysteresis measurements of Ag/10 nm-CrO<sub>x</sub>/Pt structure were carried out using C-AFM technique as shown in Fig.5. The sweeping voltage follows the process of 0 → + 2 V → 0 → - 2 V → 0, repeatedly. A compliance current was used during measurements to protect the C-AFM probe and the structure. In the process 1, the initial high resistance state (HRS) was switched to the low resistance state (LRS) with an applied voltage ( $V_{\text{set}}$ ) of about + 1.7 V. In the subsequent voltage sweep as the process 3, a negatively applied voltage ( $V_{\text{reset}}$ ) of - 1.5 V recovered the structure back to the HRS. It is noted that the large set/reset current hinders the application of TMOs to integrated RRAM devices. However, our Ag/CrO<sub>x</sub>/Pt structure can switch repeatedly with low set/reset current of 10 nA, leading to very small power consumption.





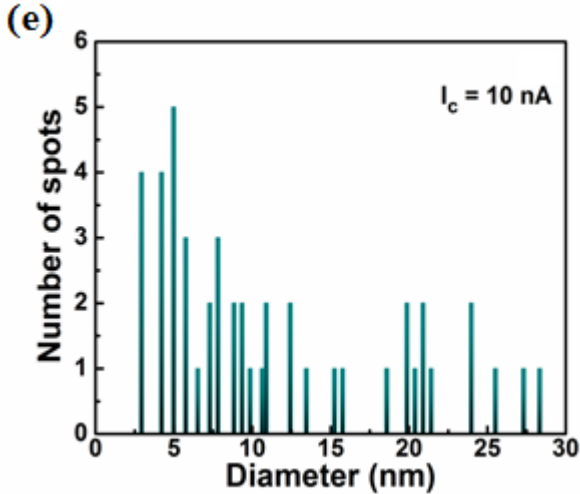


Figure 5: (a) – (d) Current mapping images in 2D and 3D of writing and erasing processes of  $\text{CrO}_x$  thin films, respectively and (e) Statistical distribution in size of silver conductive filaments of the writing process at compliance current of 10 nA.

The conductivity mapping results of the writing and erasing of  $\text{CrO}_x$  films, respectively in 2D and 3D images are shown in Fig. 5a – 5d. In the writing process, a positive voltage of + 0.5 V was applied to the Ag bottom electrode leading to a random presence of bright spots in dark background, which represents conducting spots or multiple filaments. In the erasing process, a negative voltage of – 0.5 V which was applied to the Ag bottom electrode, deletes the current spots completely, resulting in a uniform dark background. The presence of the conducting spots qualitatively confirms the filament model for resistive switching: By applying a positive voltage at the Ag electrode, an electrochemical reaction occurs in the anode (Ag), which oxidizes the Ag metal atoms to Ag ions, the metal ions  $\text{Ag}^+$  start from the bottom interface and easily drift through the  $\text{CrO}_x$  films to the top interface  $\text{CrO}_x/\text{Pt}$  cantilever, an electrochemical reduction and an electro-crystallization of Ag occur. This electro-crystallization process results in the formation of a Ag filament, which grow towards the Ag electrode. As a result, the Ag filaments grow and connect the Ag bottom electrode, leading to HRS to LRS switching. To reset the cell, a negative voltage is applied at the Ag bottom electrode, which leads to a dissolution of the Ag filament and LRS to HRS occurs.

Figure 5e is the statistical distribution in size of conductive filaments obtained from the writing process at compliance current of 10 nA. The lateral size of the bright spots ranged from 2.9 to 30 nm. The spot shape also indicates the spots contain multiple filaments. The dominant size is below 15 nm. The small size of the filaments suggests that the memory cell size can be scaled down to nanometers.

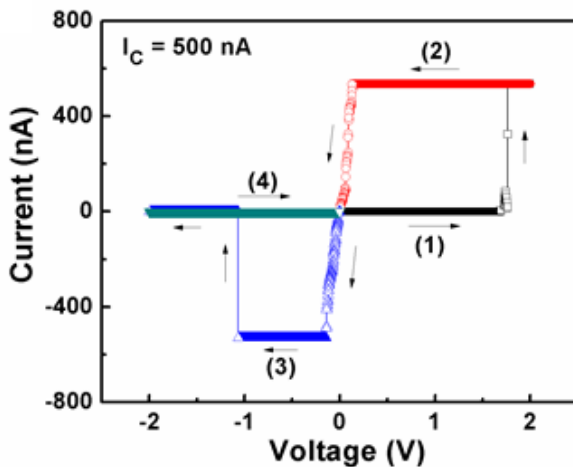
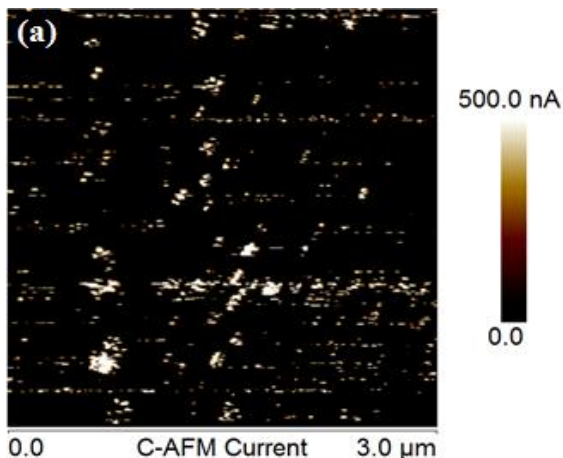
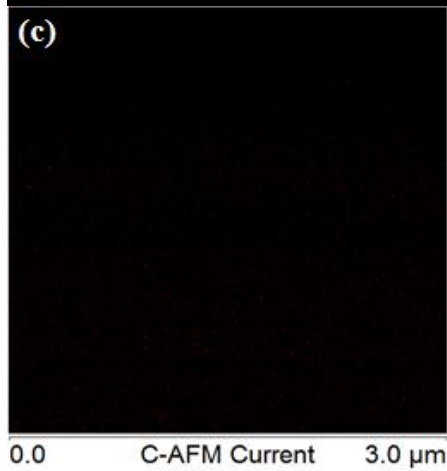
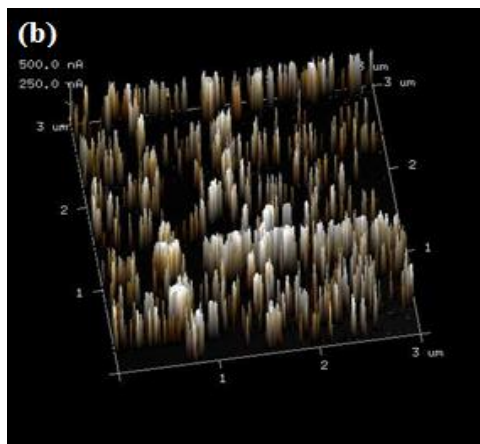


Figure 6. Local current - voltage hysteresis investigated by C - AFM, at  $I_c = 500 \text{ nA}$ .





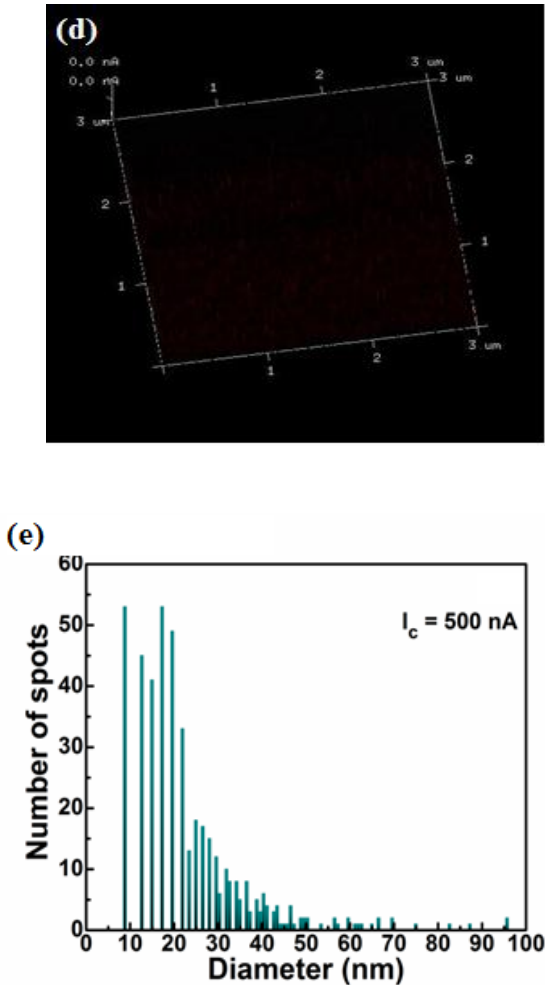


Figure 7: (a)-(d) Current mapping images in 2D and 3D of writing process and (d) statistical distribution in size of conductive filaments at compliance current of 500 nA.

Local I–V hysteresis, current mapping results and statistical distribution of filament sizes obtained from the writing process at the compliance current of 500 nA are shown in Fig. 7a – 7d. In comparison to data obtained at the compliance current of 10 nA, the conductivity mapping indeed shows that there are clear conducting spots with a higher density on the  $\text{CrO}_x$  films. The lateral size of the bright spots ranged from 8.8 nm to 100 nm and the

dominant size is below 20 nm. From the statistical distribution of filament sizes, we found that the minimum diameter of the filaments in the  $\text{CrO}_x$  are 2.9 nm and 8.8 nm for  $I_c = 10$  nA and 500 nA, respectively. These values indicate very clearly that a larger compliance current induces a larger physical diameter and that the larger diameter leads to a lower resistance value. Various compliance currents clearly indicate that filaments with different resistances have been formed. Therefore, controlling the compliance current can modulate the size of the filament and thus the resistance. In addition, the corresponding memory densities are 100 Tbit/sq and 10.6 Tbit/sq for the filament diameter of 2.9 nm and 8.8 nm, respectively.

### **c) Study $\text{CrO}_x/\text{Ti}$ devices by C – AFM technique:**

In order compare to the  $\text{CrO}_x/\text{Ag}$  devices, we also studied the  $\text{CrO}_x/\text{Ti}$  devices by C – AFM technique. Although the measurement parameters and investigated process on to  $\text{CrO}_x/\text{Ti}$  devices are similiar to  $\text{CrO}_x/\text{Ag}$  devices, there are no changes in current images as seen in Fig. 8(a) – (b). The current detected on the  $\text{CrO}_x$  surface is as small as several nanoampere. Eventually applying bias from  $0 \rightarrow +4 \text{ V} \rightarrow 0 \rightarrow -4 \text{ V}$ , we cannot establish any filament through the structure. Generally, Ti electrode is less reactive than Ag electrode in nature. This result again confirmed that mechanism of resistive switching of  $\text{CrO}_x$  films prepared at room temperature controlled by formation/rupture of silver filament via electrochemical redox reaction.

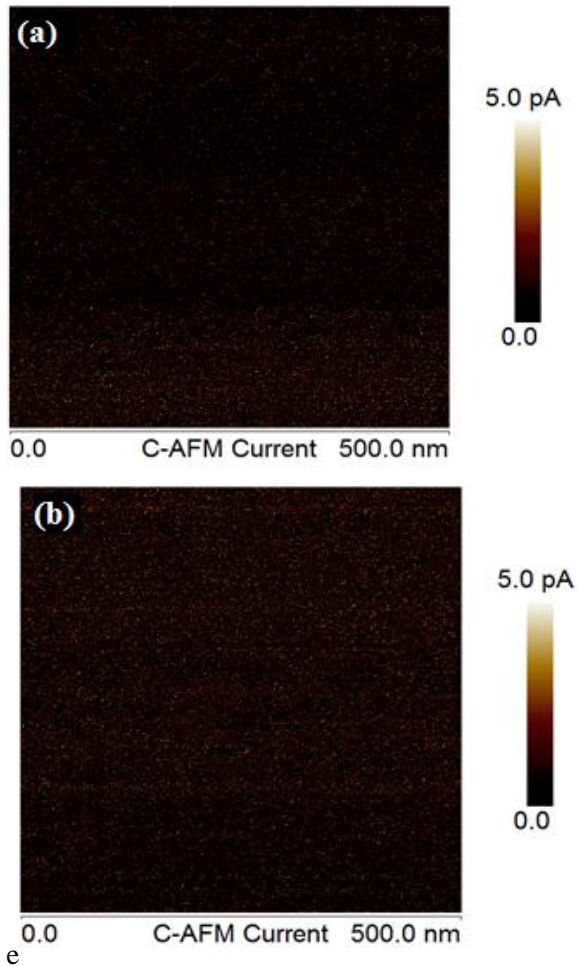


Figure 8. Current mapping images of the  $\text{CrO}_x/\text{Ti}$  device carried by C – AFM technique at positive bias (a) and negative bias (b).

e) C – AFM study of 100 nm  $\text{CrO}_x/\text{Ag}$  device:

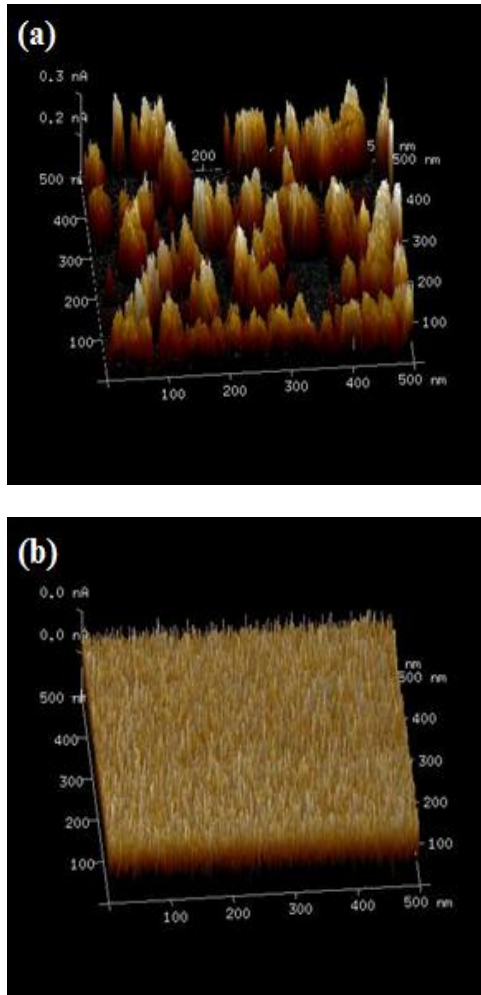
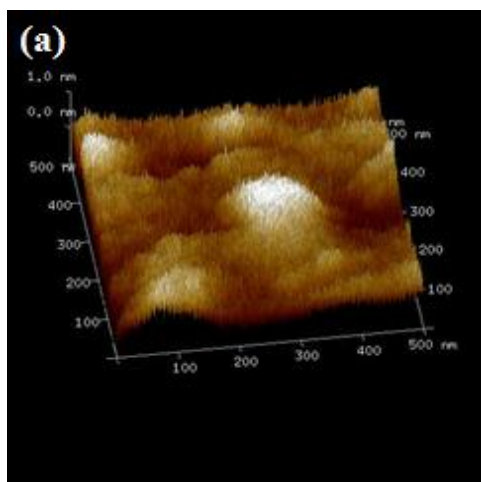


Figure 9. Current mapping images of the 100 nm CrO<sub>x</sub>/Ag device carried by C – AFM technique at LRS (a) and HRS (b).

We have investigated the formation of conductive filaments of 100 nm CrO<sub>x</sub>/Ag device by C – AFM measurement. In this case, the voltage applied to devices from  $0 \rightarrow +2 \text{ V} \rightarrow 0 \rightarrow -2 \text{ V}$ . When thickness of CrO<sub>x</sub> films increases to 100 nm, current of filaments is relative small and decreases lower 0.5 nA at writing process. While intensity of current reduces, the size of filaments increases significantly compared to 10 nm CrO<sub>x</sub>/Ag devices. This suggests that C – AFM technique seems suitable for devices with thin insulator layer.

**f) Relative between topography and distribution of conductive filaments of  $\text{CrO}_x/\text{Ag}$  device:**

As seen in Fig. 9, distribution of silver conductive filament at LRS is closely relative to topography or surface roughness of  $\text{CrO}_x$  film. It is found that both intensity of current and density of filaments are dominant at local region with larger height. This may be due to the easy approach of Pt - coated tip onto higher positions comparing to lower ones. Thus, the smooth surface of  $\text{CrO}_x$  plays a key role on homogeneous distribution of metal filaments.



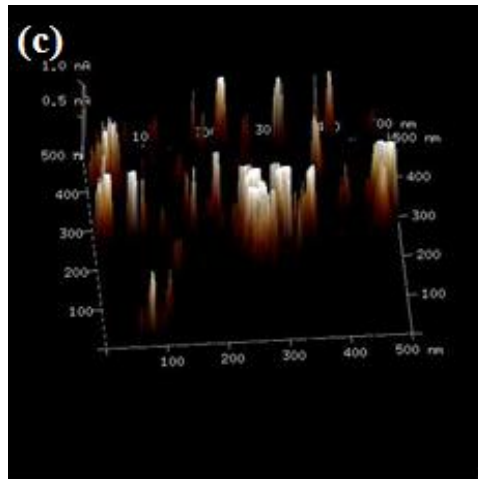
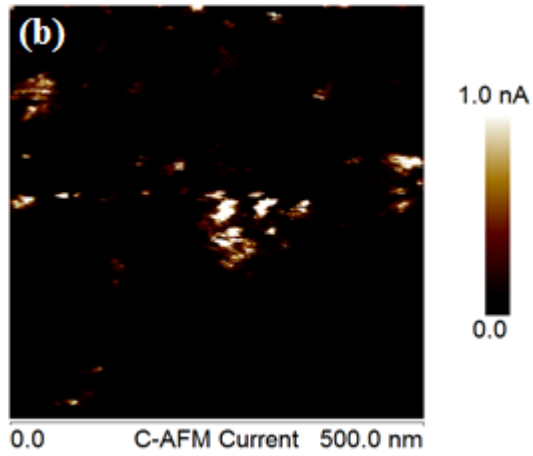


Figure 9: (a) Topography image of  $\text{CrO}_x$  surface (b)–(c) Current mapping images in 2D and 3D of writing process carried out by C – AFM technique.

## IV. Conclusion

In this study, reversible resistive switching of the  $\text{CrO}_x$  films is performed using CAFM. A clear observation of filament controlled bipolar resistance switching through local I-V hysteresis, conductivity and current mapping were observed. Our study demonstrates the correlation between the compliance current with the filament size, the multilevel capability and memory density of  $\text{CrO}_x$ -based RRAM devices. The small compliance current results in small size of filaments, higher memory density, low consumption power and suggests that the memory cell size can be scaled down to tens of nanometers. It was also revealed that the current intensity and distribution of silver conducting filaments influenced by thickness and surface roughness of chromium oxide thin films.

*Results in this study have been reported in manuscript "Resistive switching effect in chromium oxide thin films probed by conductive atomic force microscopy". This manuscript was submitted in Journal of Electronic Materials.*

## References

- [1] A. Khanna, D.G. Bhat, E.A. Payzant, (2006), *J. Vac. Sci. Technol.*, A 24 1870.
- [2] Bharat Bhushan, G. S. A. M. T., Xiaodong Li (1997), *Thin Solid Films*, 311(1-2): 67-80
- [3] P. Hones , M. D., F. Le'vy (1999), *Surface and Coatings Technology*, 120–121: 277–283.
- [4] M. Tabbal, S. K., T.C. Christidis, B. Nsouli, K. Zahraman (2006), *Thin Solid Films*, 515(4): 1976–1984.
- [5] V. Moise, R. C., A. Rulmont (2001), *International Journal of Inorganic Materials* 3: 1323-1329.
- [6] Hutchins, M. G. (1983), *Surface Technology*, 20(4): 301-320.
- [7] Ruihua Cheng, C. N. B., and P.A. Dowben (2000), *Mat. Res. Soc. Symp. Proc*, 614: F10.11.
- [8] R. Koksban, P. N. (1991, *Electrochimica Acta*, 36(1): 127-133.
- [9] N. Popovici, M. L. P., R.C. Da Silva, O. Monnereau<sup>3</sup>, P.M. Sousa, A.J. Silvestre<sup>4</sup> And O. Conde (2004), *Applied Physics A*, 79(4-6): 1409-1411.
- [10] D. Stanoi, G. S., C. Grigorescu, F. Guinneton, O. Monnereau, L. Tortet, T. Zhang, I.N. Mihailescu (2005), *Materials Science and Engineering B*, 118: 74-78.
- [11] S.C. Chen, T.C. Chang, S.Y. Chen, H.W. Li, C.W. Chen, S.M. Sze, F.S.Y. Huang, and Y.H. Tai, (2011), *Electrochem. Solid-State Lett.*, 14, H103.
- [12] S. C. Chen, T. C. Chang, S. Y. Chen, C.W. Chen, S. C. Chen, S. M. Sze, M. J. Tsai, M. J. Kao, F. S. Yeh, (2011), *Solid-State Electronics* , 62, 1, 40-43.
- [13] N. K. Pham, D. T. Nguyen, B. T. T. Dao, K. H. T. Ta, V. C. Tran, V. H. Nguyen, S. S. Kim, S. Maenosono, T. B. Phan, (2014), *Joural of Electronic Materials*, 43, 7, 2747-2752
- [14] Lantz, M. A.; Hug, H. J.; Hoffmann, R.; van Schendel, P. J. A.; Kappenberger, P.; Martin, S.; Baratoff, A.; Guntherodt, (2001), *Science*, 291, 2580–2583.
- [15] Sugimoto, Y.; Pou, P.; Abe, M.; Jelinek, P.; Perez, R.; Morita, S.; Custance, (2007), *Nature*, 446, 64–67.
- [16] Dai, H.; Hafner, J. H.; Rinzler, A. G.; Colbert, D. T.; Smalley, R. E. , (1996), *Nature*, 384, 147–150.
- [17] Hafner, J. H.; Cheung, C. L.; Lieber, C. M.; (1999), *Nature*, 398, 761–762.
- [18] Topinka, M. A.; LeRoy, B. J.; Shaw, S. E. J.; Heller, E. J.; Westervelt, R. M.; Maranowski, K. D.; Gossard, A. C.; (2000), *Science*, 289, 2323– 2326.
- [19] Deng, Z.; Yenilmez, E.; Leu, J.; Hoffman, J. E.; Straver, E. W. J.; Dai, H.; Moler, K. A. ; (2004), *Appl. Phys. Lett.*, 85, 6263.
- [20] De Angelis, F.; Das, G.; Candeloro, P.; Patrini, M.; Galli, M.; Bek, A.; Lazzarino, M.; Maksymov, I.; Liberale, C.; Andreani, L. C.; Di Fabrizio, E. ; (2010), *Nat. Nanotechnol.*, 5, 67–72.
- [21] Yasuhara R, Fujiwara K, Horiba K, (2009), *Appl Phys Lett*, 95(1): 012110
- [22] Yang Y C, Pan F, Liu Q, (2009), *Nano Lett.*, 9(4): 1636–1643

- [23] S. Z. Rahaman, S. Maikap, T. C. Tien, H. Y. Lee, W. S. Chen, F. T. Chen, M. J. Kao and M. J Tsai, (2012), *Nanoscale Research Letters*, 7:345
- [24] D.-H. Kwon, K. M. Kim, J. H. Jang, J. M. Jeon, M. H. Lee, G. H. Kim, X.-S. Li, G.-S. Park, B. Lee, S. Han, M. Kim and C. S. Hwang, (2010), *Nat. Nanotechnol.*, 5, 148.
- [25] G.-S. Park, X.-S. Li, D.-C. Kim, R.-J. Jung, M.-J. Lee and S. Seo (2007), *Appl. Phys. Lett.*, , 91, 222103.
- [26] B. J. Choi, D. S. Jeong, S. K. Kim, C. Rohde, S. Choi, J. H. Oh, H. J. Kim, C. S. Hwang, K. Szot, R. Waser, B. Reichenberg and S. Tiedke, (2005), *J. Appl. Phys.*, 98, 033715.
- [27] K. M. Kim, B. J. Choi, B. W. Koo, S. Choi, D. S. Jeong and C. S. Hwang, (2006), *Electrochem. Solid-State Lett.*, 9, G343.
- [28] R. Münstermann, J. J. Yang, J. P. Strachan, G. Medeiros-Ribeiro, R. Dittmann and R. Waser, (2010), *Phys. Status Solidi RRL*, 4, 16.
- [29] K. Szot, W. Speier, G. Bihlmayer and R. Waser, (2006), *Nat. Mater.*, 5, 312.
- [30] D. Lee, D.-J. Seong, I. Jo, F. Xiang, R. Dong, S. Oh and H. Hwang, (2007), *Appl. Phys. Lett.*, 90, 122104.
- [31] J.-B. Yun, S. Kim, S. Seo, M.-J. Lee, D.-C. Kim, S.-E. Ahn, Y. Park, J. Kim and H. Shin, (2007), *Phys. Status Solidi RRL*, 1, 280.
- [32] J. Y. Son and Y.-H. Shin, (2008), *Appl. Phys. Lett.*, 92, 222106.
- [33] I. Hwang, J. Choi, S. Hong, J.-S. Kim, I.-S. Byun, J. H. Bahng, J.-Y. Koo, S.-O. Kang and B. H. Park, (2010), *Appl. Phys. Lett.*, 96, 053112.
- [34] Q. Zhoua, Q. Lua, X. Zhanga, Y. Songb, Y. Y. Linb, X. Wu, (2013), *Applied Surface Science*, 271, 407– 411.
- [35] X.B. Cox III, R.W. Linton, F.E. Butler, (1985), *Environ. Sci. Technol.*, 19, 345.
- [36] Hassel M, Hemmerich I, Kuhlenbeck H, Freund H-J., (1998), *Surface Sci Spectra*, 4(3).
- [37] Cheng Ruihua, Xu B, Borca CN, Sokolov A, Yang C -S, Yuan L, (2001), *Appl Phys Lett.*,79(19).
- [38] E. Desimoni, C. Malitesta, P.G. Zambonin, J.C. Rivi ere, (1988), *Surf. Interf. Anal.*, 13, 173–179.
- [39] X.B. Cox III, R.W. Linton, F.E. Butler, (1985), *Environ. Sci. Technol.*, 19, 345
- [40] H.C. Barshilia, K.S. Rajam, (2008), *Appl. Surf. Sci.*, 255, 2925.
- [41] S. Agouram, F. Bodart, G. Terwagne, (2004), *Surf. Coat. Technol.*,180–181 164-168.
- [42] K. Tabata, Y. Hirano, E. Suzuki, (1998), *Appl. Catal. A* 170, 245–254.
- [43] H. He, H.X. Dai, (2003), *Appl. Catal. A* 251 61–74.
- [44] D. Yang, A. Velamakanni,G. Bozoklu, S. Park, M. Stoller, R. D. Piner, S. Stankovich, I. Jung, D. A. Field, C. A. Ventrice Jr, R. S. Ruoff, (2009), *Carbon*, 47, 145–152

**A Comprehensive Proteome Analysis of *Acinetobacter baumannii*  
Outer Membrane Vesicles Grown under Biofilm and Planktonic  
Conditions**

*Vanitha Mariapan, PhD*

Department of Medical Microbiology,  
Faculty of Medicine,  
University of Malaya

## Abstract

The secretion of outer membrane vesicles (OMVs) is one of the major mechanisms by which Gram-negative bacteria deliver effector molecules to host cells. *Acinetobacter baumannii* is an important opportunistic and hospital acquired pathogen that causes a high morbidity and mortality rate in infected patients due to resistances different range of antibiotics. This is due to formation of biofilms, where the surface-attached bacterial communities are protected against host defenses and pharmacotherapy by a self-produced matrix that surrounds and strengthens them. *A. baumannii* is known to secrete OMVs into the extracellular milieu during *in vitro* growth. In the present study, we investigated the secretion of *A. baumannii* OMVs and analysed the comprehensive proteome of *A. baumannii*- derived OMVs between the two growth modes (i.e., planktonic and biofilm). We demonstrated that the *A. baumannii*-derived OMVs contain altered proteins within a biofilm that make them uniquely resistant compared to their planktonic (free-living) counterparts. A large number of proteins are present at significantly different abundance levels, with some proteins being unique to a specific growth mode. Furthermore, this information has may be potential for the development of specific therapies and could serve as a novel approach for combating the high-level of antimicrobial resistance in *A. baumannii* biofilms.

## Introduction

*Acinetobacter baumannii*, is an important Gram-negative nosocomial pathogen, that causes various infections especially in immune-compromised patients (Villegas and Hartstein, 2003). Among the human infections caused by this bacterium, include urinary tract infection, secondary meningitis, wound or burn infection, and pneumonia (Chen et al., 2001; Davis et al., 2005). Although this organism is considered as a low-virulent pathogen, it produces numerous virulence factors which include phospholipase D, capsular polysaccharides, serum resistance, biofilm formation, iron acquisition, adherence, invasion and host cell death (Moon et al., 2012). In recent years, infections caused by *A. baumannii* have posed major problems in the clinical setting, due to the development of multidrug resistance to several commonly used antimicrobial agents (Dijkshoorn et al., 2007).

*A. baumannii* is being protected from several extracellular agents, including antibiotics and immune factors by the development of layer of aggregated bacteria attached to a surface and secrete an exopolysaccharide matrix or known as biofilms formation (Denkhaus et al., 2007). The biofilm formed *in vivo* or *in vitro* have been associated with pathogenesis of disease. During infection *A.baumannii* transitions from an independent, free-swimming lifestyle (i.e., planktonic) into sessile aggregates of bacteria (i.e., biofilms). It has been estimated that 65% of all human infectious diseases are biofilm-related (Seneviratne et al., 2012). Microorganisms growing in biofilms exhibit high resistance to the host immune response, environmental stresses, and antimicrobial therapy.

These persistent biofilm populations can serve as a reservoir for chronic and systemic infections, playing an important role in human disease (Costerton et al., 1999; Ramage et al., 2009). The increased resistance demonstrated suggests that cells in biofilms can modulate metabolic activity, dormancy, and stress responses, (Petrova et al., 2012; Yeom et al., 2013), which highlights the importance of understanding the biofilm-forming properties of *A.*

*baumannii*.The biofilms also contain great quantity of outer membrane vesicles (OMVs) and it is also believed that the OMVs have a significant role in the formation of biofilms.

A wide variety of Gram-negative bacteria, which include *A. baumannii*, *Escherichia coli*, *Neisseria meningitidis*, *Pseudomonas aeruginosa*, *Shigella flexneri*, and *Helicobacter pylori* are known to secrete OMVs during their growth cycle (Beveridge, 1999; Lee et al., 2008). However, to date, the secretion of OMVs and their contribution to pathogenesis under biofilm condition have not been reported in the *Acinetobacter* species. Secreted OMVs can disseminate far from the cell and impart biological functions on the environment and on other cells, including playing a role in pathogenesis, quorum signaling, nutrient acquisition, and horizontal gene transfer (Mayrand and Grenier, 1989; Mashburn and Whiteley, 2005). The bacteria constitutively secrete OMVs that contain biologically active proteins and perform diverse biological processes into the extracellular milieu.

Unlike other secretion mechanisms, OMVs enable bacteria to secrete insoluble molecules in addition to and in complex with soluble materials. OMVs allow enzymes to reach distant targets in a concentrated, protected and targeted form. Many virulence factors of pathogenic bacteria, such as heat-labile toxin and cytolysin A of *E. coli*;  $\beta$ -lactamase, hemolytic phospholipase C, alkaline phosphatase of *P. aeruginosa*; and VacA of *H. pylori*, are enriched in OMVs, and their roles in bacterial pathogenesis, have been relatively well characterised (Kwon et al., 2009). Understanding of OMVs can help us comprehend how other domains of life produce similar secreted structures, and *vice versa*. Such comparisons will yield insight into the general principles involved in forming a vesicle from a biological membrane. Recent research in this area has revealed that OMVs may act as intercellular communicosomes in polyspecies communities by enhancing bacterial survival and pathogenesis in hosts. Our recent proteomics data revealed presence of outer membrane (OM) proteins in the bacterial secretome and it was proven not to be due to bacterial lysis (Mariappan et al., 2011). The question that remains is

whether the bacteria themselves undergo specific changes within the biofilm that make them more resistant than their planktonic counterparts.

Thus, important considerations for OMVs include the role of diverse functions of OMVs, the mechanisms of vesicle formation and of protein sorting into OMVs, as well as the pathophysiology of OMVs, which remain yet to be defined. To address these issues, vesicular proteins should be comprehensively identified. Proteomics offers a powerful approach to decode the protein components of OMVs. This study hypothesises that the *A. baumannii* OMVs generated during different condition of growth play important roles in the pathogenesis of diseases.

Therefore, the aim of this study is to identify the *A. baumannii* OMVs under planktonic and biofilm conditions using proteomic approaches. This may provide future directions for high- throughput and comparative proteomic studies of OMVs that originate under different growth conditions. The identification of OMV proteins may stimulate further efforts to construct a comprehensive proteome database of bacterial OMVs that will help us not only to elucidate the

biogenesis and functions of OMVs but also to develop diagnostic tools, vaccines, and antibiotics effective against pathogenic bacteria.

## **MATERIALS AND METHODS**

### **Bacterial strains and culture growth conditions**

A total of four *A.baumannii* isolates, *A.baumannii* ATCC19606 (wild-type), *A. baumannii* ATCC19606<sub>Mut</sub> (deletion of OmpA), clinical isolate *A. baumannii*<sub>DU202</sub> and *A. baumannii*<sub>DU202IM</sub> were used in this study. All the strains were grown overnight in Luria Bertani (LB) broth (except DU202<sub>IM</sub>, was grown in LB broth supplemented with 50µg/ml of imipenem) at 37°C under shaking condition (180rpm) until it reaches OD<sub>600nm</sub> 0.8-1.0. The optical density of the cultures were normalised to OD<sub>600nm</sub> 1.0 prior to further processing.

### **Bacterial growth and biofilm formation assay**

The quantitative biofilm formation assay was performed using crystal violet staining method as described previously by Ramli et al. (2012) with slight modifications. The planktonic cultures (OD<sub>600nm</sub>1.0) were diluted with fresh LB broth to 1:100 (~OD<sub>600nm</sub> 0.01). Briefly, 100 µl of the culture was added into each well of a sterile 96-well plate and incubated at 37°C for 24, 48 and 72 hours. For the control wells, bacterial cultures were substituted with fresh the LB. Following incubation, the culture supernatant was transferred into a new sterile 96-well plate and the absorbance was measured at OD<sub>600nm</sub> for bacterial growth during biofilm condition. The empty wells containing biofilm were stained with 150 µl of 1% crystal violet (w/v) and further incubated for 30 mins at room temperature. The excessive staining was removed by washing the wells twice with 175 µl sterile distilled water. Finally, 175 µl dimethyl sulfoxide (DMSO) was added to each well and the absorbance was measured at OD<sub>570nm</sub> after 10 mins incubation at room temperature. The experiment was repeated in triplicates and the average OD<sub>600nm</sub> was measured.

### **Preparation of secretory proteins**

The *A. baumannii*, ATCC19606 culture was transferred into fresh LB and grown under shaking condition until OD<sub>600nm</sub> 1.0 (180rpm; 37°C) (planktonic condition) is reached or the bacterial culture was spread on a LB agar and incubated at 37°C overnight (biofilm condition). The biofilm bacteria were scraped and suspended in fresh LB broth (OD<sub>600nm</sub> 1.0). The planktonic or biofilm culture of ATCC19606 was centrifuged for 30 mins at 8,000 rpm, 4°C. The

remaining bacterial culture supernatant was filtered through 0.2  $\mu\text{m}$  vacuum filter to remove the debris and bacterial residues. The secretory proteins were also prepared from the culture supernatant using trichloroacetic acid (TCA) precipitation method as described by Mariappan et al. (2010; 2011) with minor modifications. The filtered culture supernatant was then precipitated using pre-chilled 50% TCA diluted in 100% acetone (w/v) with 4:1 dilution. The mixture was then incubated on ice for an hour and centrifuged for 1 hour at  $40,000 \times g$  at  $4^\circ\text{C}$ . The pellet was dissolved in cold acetone and washed twice, air dried and stored at  $-80^\circ\text{C}$ .

### **Preparation of outer membrane vesicles**

The OMV was purified according to the method described by Kwon et al. (2009) with slight modifications. Briefly, the bacterial free culture supernatant of different growth modes was concentrated and ultra-filtered using a QuixStand Benchtop System (GE Healthcare) with a 500 kDa hollow fiber membrane column (GE Healthcare). The column was washed with phosphate buffered saline (PBS) and the OMVs were collected following ultracentrifugation for 3 hours at  $150,000g$ ,  $4^\circ\text{C}$ . The pellets containing OMVs were re-suspended in 1.5 ml of PBS. The purity of OMVs was validated and the sample was stored at  $-80^\circ\text{C}$  until further use following protein concentration determination using the modified BCA assay (Thermo Scientific).

### **Sodium dodecyl sulfate polyacrylamide gel electrophoresis (SDS-PAGE) and in-gel digestion**

A total of 15  $\mu\text{g}$  protein samples (secretory proteins and OMVs) were loaded and separated on a 12% SDS-PAGE (Laemmli, 1970). The gels were stained and visualised with Coomassie Brilliant Blue R-250. The peptides from the gels were released using the in-gel digestion method as previously described by Choi et al. (2014) with minor alteration. Briefly, the gels were partitioned into six different fractions according to the molecular size, after which, the gels were diced into cubes and the staining was removed using 50% acetonitrile (ACN) and 10 mM ammonium bicarbonate (ABC). The gels were washed with distilled water, prior to removal of the de-staining solution using 100% ACN. The protein reduction was performed using 10 mM dithiothreitol (DTT) and 100 mM ABC, followed by 55 mM iodoacetamide. The gels were rinsed with distilled water and dried. Trypsin digestion (in 50 mM ABC with final concentration of 10 ng/ml) was carried out for 16-18 hours at  $37^\circ\text{C}$ . The tryptic peptide extraction was transferred into a new tube and the remaining

gels were treated with 50% ACN containing 5% formic acid [FA]), followed by 100% ACN. The peptides were then pooled and lyophilised. The peptides were reconstituted in 0.5% FA prior to LC-MS/MS analysis.

### **Protein identification**

The proteins were identified by LC-MS/MS in triplicates using LTQ mass spectrometry according to Park et al. (2006). The proteins were identified using the MS/MS spectra which were searched using MASCOT software ver. 2.3 (Matrix Science Inc. USA). The genome data of *A. baumannii* ATCC 17978T from NCBI nr was used to decoy sequence database. The following search parameters were allowed: oxidation of methionine (+16Da); carbamidomethylation (+57 Da); propionamidation of cysteine (+71 Da); missed trypsin cleavage: 1; a peptide tolerance and a fragment mass tolerance: within 0.8 Da. Using the MASCOT software, the exponentially modified protein abundance index (emPAI) was generated, with 1% mol calculated according to the emPAI values (Ishihama et al., 2005). The MS/MS analysis was performed more than three times for each sample and the data were filtered according to false discovery rate (FDR) 1% criteria. Functional class assignment proteins were identified based on Cluster of Orthologous Groups (COG) of proteins functional categories (<http://www.ncbi.nlm.nih.gov/COG/old/palox.cgi?fun=all>). The presence of transmembrane  $\alpha$ -helices was inspected with the TMHMM (<http://www.cbs.dtu.dk/services/TMHMM/>) and PSortb (<http://www.psort.org/psortb/>) and results were interpreted using a most-votes approach.

## RESULTS

### Growth profile of *Acinetobacter baumannii* biofilm condition

The biofilm growth profiles of the *A. baumannii* (wild-type, clinical and mutant) strains were studied and revealed almost similar trend in a nutrient rich medium under aerobic condition (Fig. 1). In general, the growth rates of all the strains were almost identical and the density of the bacterial cultures increased significantly ( $p < 0.05$ ) and gradually. Eventually, the strains reached the highest peak ( $OD_{600nm}$  1.0 - 1.2) at 72 hours of growth. Overall, the bacterial density was relatively similar and the growths were found to correlate well with each other.

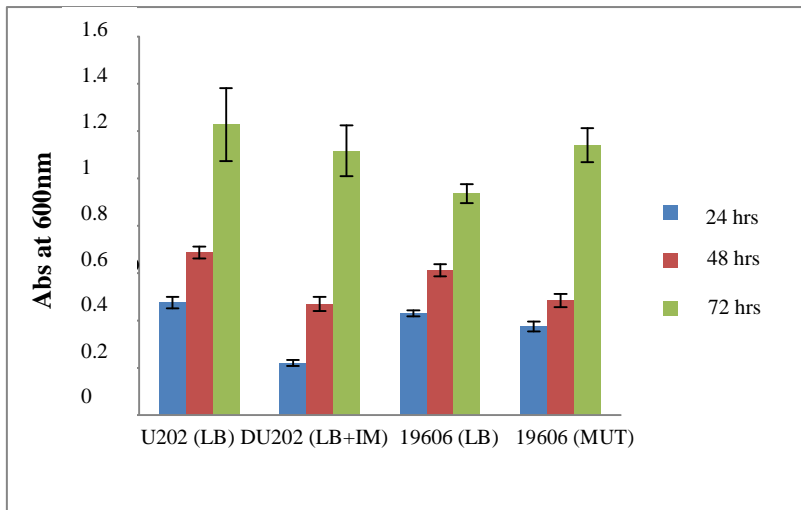


Figure 1: Biofilm growth curve of *Acinetobacter baumannii* strains. The bacterial cultures were inoculated in LB medium and grown at 37°C from 0 h to 72 hrs under a non-shaking condition. The bacterial density was determined at  $OD_{600nm}$ . The experiment was conducted as three independent replicates (e error bars indicate the standard deviation).

### Aptitude of *Acinetobacter baumannii* strains to produce biofilm

To investigate whether the *A. baumannii* strains are able to form biofilm, we determine the production of biofilm by the different *A. baumannii* strains using the colorimetric method (Fig. 2). In general, all the strains (except *A. baumannii*DU202IM) were found to have a similar trend of biofilm production from 24 – 72 hours, whereby these strains were found to yield the highest production of biofilm at 48 hour (OD<sub>570nm</sub> 2.4 – 1.0). However, the biofilm eventually reduced at 72-hour of growth. *A. baumannii* DU202IM was found to produce biofilm progressively from 24 – 72 hours (OD<sub>570nm</sub> 0.8 – 1.6) and peaked at 72 hours of growth. Overall, *A. baumannii*DU202 was found to be the highest biofilm producer (OD<sub>570nm</sub> 1.8 – 2.4) and *A. baumannii* ATCC19606Mut strain was the lowest (OD<sub>570nm</sub>0.6–1.0).

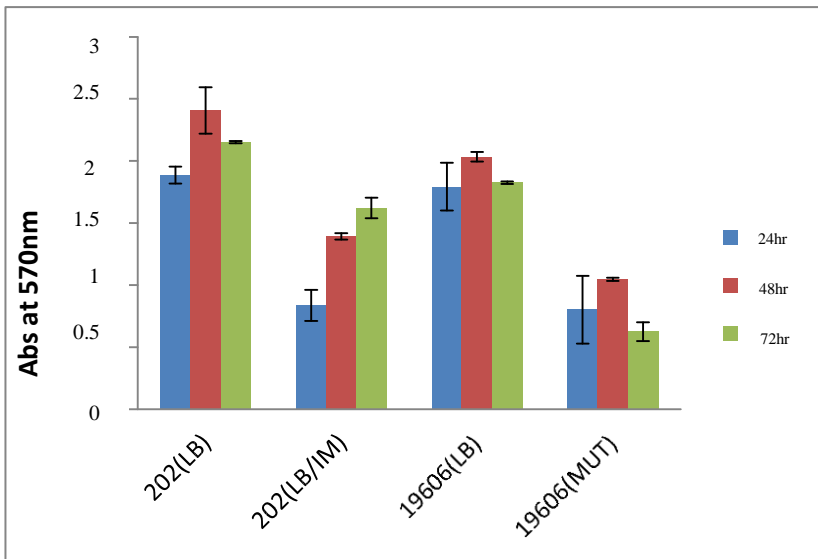


Figure 2: Biofilm formation of *Acinetobacter baumannii* at 37°C using crystal violet method. The experiments were conducted as three independent replicates (error bars indicate the standard deviation)

## **Overview and comparative proteome analysis of *Acinetobacter baumannii* grown under planktonic and bio-film conditions**

In order to determine the different protein profile of OMVs grown during planktonic and biofilm condition, *A.baumannii* ATCC19606 was grown *in vitro* in LB broth under both conditions and secreted OMVs were prepared from the cell-free culture supernatant. To determine whether the vesicles carried bacterial proteins, the secretory proteins and OMVs fractions were subjected to SDS-PAGE. Figure 3 shows the comparative overview of *A. baumannii* secretory proteins and OMVs (planktonic and biofilm) protein profiles using SDS-PAGE analysis.

Many protein bands were detected in the secretory proteins and OMVs fractions. A high similarity between the protein bands of the culture supernatant and the OMVs fraction in both planktonic and biofilm conditions were observed, suggesting that the vesicles were largely responsible for the extracellular proteome of *A. baumannii*. It is also apparent that several of the protein bands were found to be missing at the OMVs fractions. The results indicated that the protein band profile of *A.baumannii* ATCC19606 planktonic OMVs (PO) mostly shared similar bands, with the biofilm OMVs (BO) of the same strain.

However, obvious differences in terms of protein expression were observed between both the PO and the BO. The molecular weight of the identified proteins was in the range of 4,995 - 216,332 in PO and 4,262 - 216,332 in BO. However, the BO was found to have a broader range of pI (3.41 - 12.02) as compared to PO (4.47 - 11.63). To further investigate these differences, LC-MS/MS was used to identify proteins within the purified OMVs from each condition. MS analysis was performed on two biological replicates from each strain. However, only the PO and BO proteins were analysed using LC-MS/MS. The method of LC-MS/MS analysis chosen greatly reduces the potential overlap from abundant peptides within a sample and allowed to examine differences in detectable proteins identified with high probability in the duplicate samples.

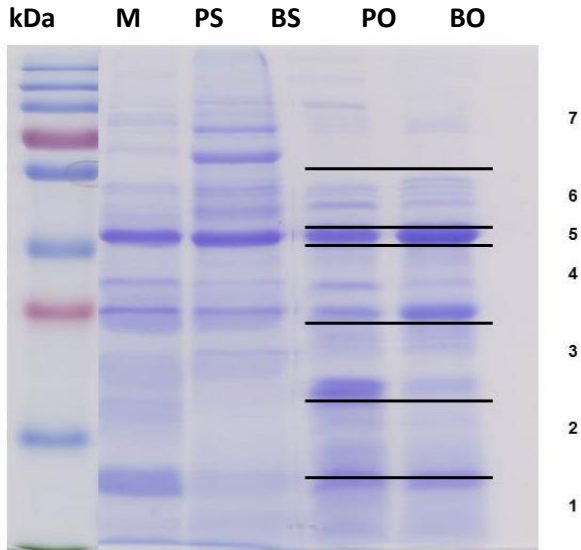


Figure 3: Protein analysis of *A. baumannii* ATCC19606 outer membrane vesicle and secretory proteins (15 $\mu$ g) grown during planktonic and bio-film conditions, on a 12% SDS-PAGE. The separated proteins were detected by CBB G-250 staining [lane 1, marker; lane 2, planktonic secretory proteins (PS); lane 3, biofilm secretory proteins (BS); lane 4, planktonic OMVs (PO); lane 5, biofilm OMVs (BO)]

### ***Acinetobacter baumannii* biofilm and planktonic outer membrane vesicles contain pools of shared and exclusive proteins**

Venn diagrams were used to compare the overlapping and unique OMVs proteins in the biofilm and planktonic conditions (Figure 4). A total of 455 proteins were identified from the BO and 400 were identified from the PO condition. The majority of those proteins were common to both conditions (253), while 147 (44.4%) were identified only in the PO and 202 (50.5%) were exclusive to the OMVs grown in biofilm.

The PO and BO produced from *A. baumannii* ATCC19606 cells were enriched in outer membrane, inner membrane and periplasmic proteins but also contained a large number of cytoplasmic and extracellular proteins (Figure 5). Among the 455 proteins identified in the BO, 172 proteins (37.80%) were identified to be located in the cytoplasmic region, 110 proteins (24.18%) from the periplasmic compartment, 82 proteins (18.02%) were found to be at the outer membrane and 58 proteins (12.75%) located at the inner membrane. However, only 33 proteins were predicted to be found at the extracellular localisation (7.25%). In contrary, of the 400 proteins recognised in the PO, 33.25 % proteins were found to be located at the periplasmic region, followed by 23.25% proteins predicted at both the cytoplasmic and outer membrane compartment. However, only 11.25% and 8.75% were found to be at the inner membrane and extracellular localisation, respectively.

It was also interesting to mention that, of the 202 proteins exclusively found in the OMVs grown under the biofilm condition, more than 50% (n=113) were located in the cytoplasmic region. Roughly, 10% - 15% of the proteins were found to be at the periplasmic (n= 31), inner membrane (n=28) and outer membrane (n=22) location. Only a small number of protein (n=3) were found to be secreted as extracellular protein. However, the proteins found uniquely in the planktonic OMVs (n= 147) were well distributed at all the cell regions (36% - 6.8%) (Figure 6).

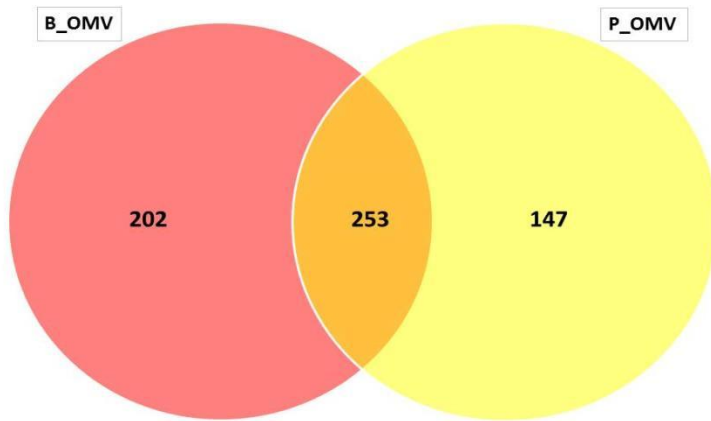
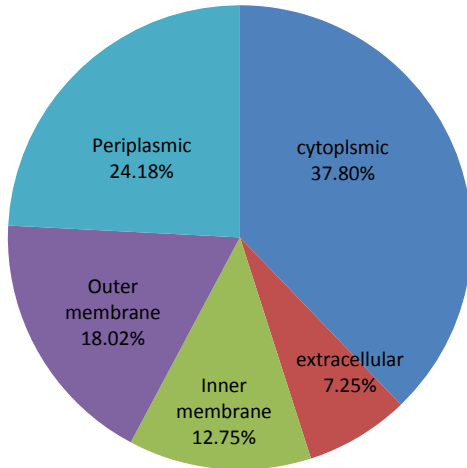


Figure 4: Venn diagram showing the proteins identified across the outer membrane vesicles of *A. baumannii* grown under planktonic and bio-film conditions.

A)



B)

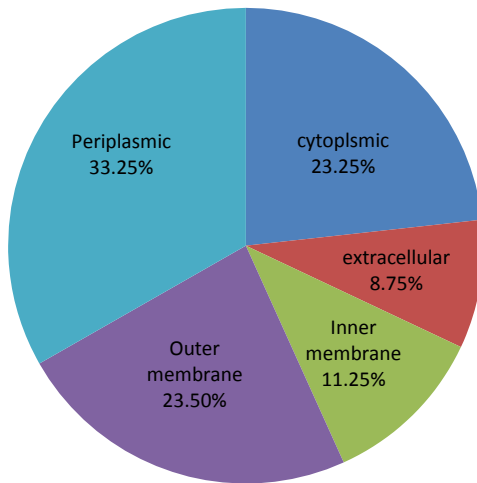
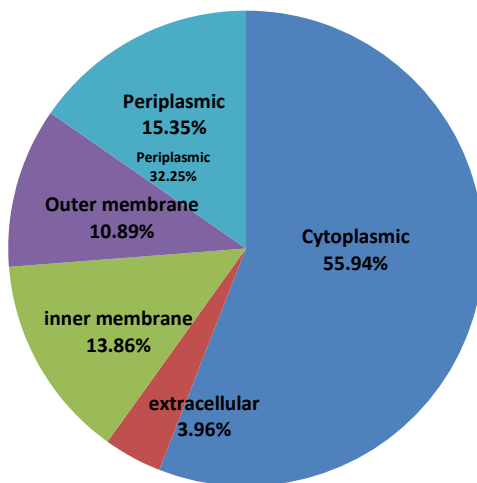


Figure 5: Localisation of common proteins identified in the OMVs of *A. baumannii* grown under (A) biofilm (B) planktonic conditions

A)



B)

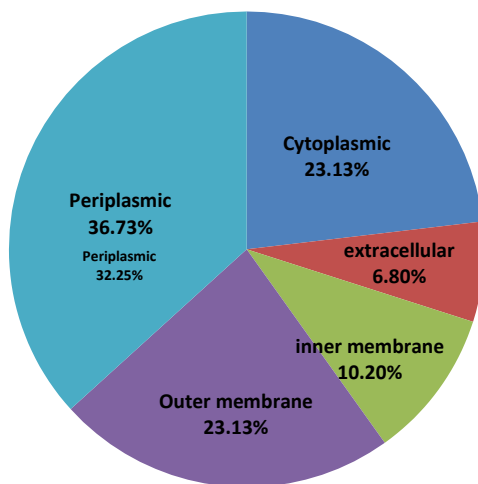


Figure 6: Localisation of unique proteins identified in the OMVs *A. baumannii* under (A) biofilm (B) planktonic conditions.

## **Kyoto Encyclopedia of Genes and Genomes (KEGG) Pathway Analysis**

Recent works have indicated that bacterial biofilm have an active but altered metabolism (Petrova et al., 2012; Yeom et al., 2013). In order to identify the pathways affected by biofilm formation of *A. baumannii*, KEGG pathway analysis was used to observe the differences between the PO and BO. In general, pathways involved in metabolism, genetic information processing, environmental information processing, cellular processes and poorly characterised proteins were found to be altered under both the conditions. Analysing the results in a wider view, it was noticeable that a huge number of BO proteins were involved in pathways related to the metabolism, biosynthesis of secondary metabolites, microbial metabolism in diverse environments, carbon metabolism, biosynthesis of amino acids, citrate cycle (TCA cycle), pyruvate metabolism, glyoxylate and dicarboxylate metabolism, oxidative phosphorylation, ribosome, folding, sorting and degradation, RNA degradation compared to the PO proteins. However, PO proteins do not exhibit higher number of proteins than the BO proteins.

Some pathways were represented only by BO: 2-oxocarboxylic acid metabolism, methane metabolism, nitrogen metabolism, valine, leucine and isoleucine biosynthesis, histidine metabolism, selenocompound metabolism, pantothenate and CoA biosynthesis, one carbon pool by folate, penicillin and cephalosporin biosynthesis, aminobenzoate degradation, ethylbenzene degradation, and nucleotide excision repair; represented only by PO: galactose metabolism, amino sugar and nucleotide sugar metabolism, phenylpropanoid biosynthesis, protein processing in endoplasmic reticulum, sulfur relay system, PI3K-Akt signaling pathway and apoptosis. The remaining pathways had a similar number of proteins present in both the PO and BO. A large set of protein, totaling 153 and 152 proteins identified were classified as hypothetical proteins in the differentially expressed and unique protein sets in the bio-film and planktonic condition, respectively

Table 1: Functional proteins of *Acinetobacter baumannii* ATCC 19606 biofilm and planktonic outer membrane vesicles using KEGG pathway analysis

Functional category <sup>a</sup>	Number of proteins identified	
	Biofilm OMVs	Planktonic OMVs
<b>METABOLISM</b>		
Biosynthesis of secondary metabolites	35	24
Microbial metabolism in diverse environments	28	18
Carbon metabolism	21	15
2-Oxocarboxylic acid metabolism	3	0
Fatty acid metabolism	8	5
Biosynthesis of amino acids	10	3
Degradation of aromatic compounds	1	1
<b><u>Carbohydrate metabolism</u></b>		
Glycolysis / Gluconeogenesis	5	5
Citrate cycle (TCA cycle)	16	10
Pentose phosphate pathway	1	1
Galactose metabolism	0	1
Amino sugar and nucleotide sugar metabolism	0	1
Pyruvate metabolism	10	7
Glyoxylate and dicarboxylate metabolism	5	2
Propanoate metabolism	4	4
Butanoate metabolism	6	7
C5-Branched dibasic acid metabolism	1	1

### **Energy metabolism**

Oxidative phosphorylation	25	16
Photosynthesis	8	5
Carbon fixation in photosynthetic organisms	3	1
Carbon fixation pathways in prokaryotes	9	6
Methane metabolism	1	0
Nitrogen metabolism	2	0
Sulfur metabolism	1	1

### **Lipid metabolism**

Fatty acid biosynthesis	4	3
Fatty acid degradation	5	3
Glycerolipid metabolism	1	1
Glycerophospholipid metabolism	5	2
Ether lipid metabolism	1	1
Arachidonic acid metabolism	1	1
Linoleic acid metabolism	2	1
alpha-Linolenic acid metabolism	2	1
Biosynthesis of unsaturated fatty acids	3	3

### **Nucleotide metabolism**

Pyrimidine metabolism	6	4
-----------------------	---	---

### **Amino acid metabolism**

Glycine, serine and threonine metabolism	2	1
Cysteine and methionine metabolism	4	1
Valine, leucine and isoleucine degradation	4	4
Valine, leucine and isoleucine biosynthesis	1	0
Lysine degradation	4	1
Arginine and proline metabolism	3	2
Phenylpropanoid biosynthesis	0	1
Benzoate degradation	3	1
Aminobenzoate degradation	1	0
Ethylbenzene degradation	1	0
Caprolactam degradation	2	1

Polycyclic aromatic hydrocarbon degradation	1	1
<b>GENETIC INFORMATION PROCESSING</b>		
Transcription		
Translation		
Aminoacyl-tRNA biosynthesis	2	1
Folding, sorting and degradation		
Protein processing in endoplasmic reticulum	0	1
Sulfur relay system	0	1
RNA degradation	5	1
Replication and repair		
Nucleotide excision repair	1	0
Mismatch repair	1	1
Homologous recombination	1	1
<b>ENVIRONMENTAL INFORMATION PROCESSING</b>		
Membrane transport		
Bacterial secretion system	9	8
Signal transduction		
HIF-1 signaling pathway	2	1
FoxO signaling pathway	2	2
PI3K-Akt signaling pathway	0	1
<b>CELLULAR PROCESSES</b>		
Transport and catabolism		
Cell growth and death	5	4
Drug resistance		
POORLY CHARACTERISED	5	7
General metabolic functions	1	150

<sup>a</sup> Functional category based on Kyoto Encyclopedia of Genes and Genomes (KEGG) Pathway Analysis

### **Changes in *Acinetobacter baumannii* ATCC 19606 outer membrane vesicles proteins that are differentially expressed under biofilm and planktonic condition**

The abundance of the proteins associated with OMVs was determined according to the emPAI values. Table 1 shows the 20 most abundant OMVs proteins of *A. baumannii* ATCC 19606 proteins that are differentially expressed under biofilm and planktonic condition. The most abundant proteins present in both the conditions were ompA family protein, (emPAI: BO, 172.17 and PO149.65) and beta-lactamase (emPAI: BO, 119.57 and PO, 149.41).

Of the 20 vast abundance proteins, only 12 were expressed in both growth modes. Remaining eight proteins were expressed uniquely in each condition. Ribosomal protein L22 was found to be uniquely and highly (emPAI: 160.25) expressed in the OMVs under biofilm condition. However, in the planktonic condition, type VI secretion system effector, Hcp1 family (emPAI: PO, 101.18) was present exclusively. Many hypothetical and outer membrane proteins were expressed in OMVs grown under both modes. It is also noticeable that ribosomal proteins were expressed only the in the OMVs biofilm.

Table 2: Identification of most abundant *Acinetobacter baumannii* ATCC 19606 outer membrane vesicles proteins that are differentially expressed under biofilm and planktonic condition (top 20 proteins in each condition) using Mascot search engine data from liquid chromatography mass spectrometry analysis

Accession	Protein name <sup>a</sup>	MW	pI	Score	Peptide	Coverage (%)	emPAI	
							BO	PO
gi 260410686	OmpA family protein	22472	9.3	17335	29	98.2	172.17	149.65
gi 260409638	ribosomal protein L22	11930	10.2	1601	37	100	160.25	-
gi 260409976	beta-lactamase	43179	9.37	19353	42	81.7	119.57	149.41
gi 260412037	hypothetical protein HMPREF0010_01099	15709	8.83	1202	24	98.6	71.87	32.41
gi 260409659	ribosomal protein L17	13986	10.95	648	33	99.2	49.76	-
gi 260411007	hypothetical protein HMPREF0010_00069	13274	8.99	3211	22	98.4	47.55	120.03
gi 260409322	entericidin EcnA/B family protein	4995	9.43	399	10	100	46.04	-
gi 260408569	hypothetical protein HMPREF0010_03374	25678	4.49	1394	21	76.7	33.82	33.82
gi 260408711	hypothetical protein HMPREF0010_03516	27633	4.59	3138	23	82.7	33.10	94.02
gi 260411292	outer membrane protein	18699	9.52	450	31	100	31.78	62.72

gi 260409655	30S ribosomal protein S13	13258	11.12	853	34	100	30.58	-
gi 260409393	ribosomal protein L21	11467	10.07	345	22	100	29.65	-
gi 260409570	copper/zinc superoxide dismutase	21009	9.28	1269	23	74.6	29.42	21.61
gi 260408956	hypothetical protein HMPREF0010_02928	25132	9.17	2041	27	96.9	28.25	-
gi 260411855	hypothetical protein HMPREF0010_00917	35016	6.25	1902	51	100	27.57	33.25
gi 260410243	ribosomal protein L28	9098	11.29	272	23	98.7	24.68	-
gi 260409289	outer membrane protein Omp38	38396	5.32	25759	39	59	24.14	66.79
gi 260409820	hypothetical protein HMPREF0010_02162	14696	9.54	388	30	100	21.93	21.93
gi 260408384	OmpA family protein	17981	9.42	736	29	100	21.12	25.28
gi 260408639	6,7-dimethyl-8-riboylumazine synthase	16483	5.93	1142	16	100	19.07	-
gi 260412061	type VI secretion system effector, Hcp1 family	18731	6.52	4653	26	97	-	101.18
gi 260410945	hypothetical protein HMPREF0010_00007	18798	8.87	2066	24	95.2	-	85.62

gi 260411050	protein CsuC	30624	9.34	5337	49	98.9	-	74.76
gi 260409040	curli production assembly/transport component CsgG	24195	9.12	3192	31	99.1	-	47.6
gi 480139631	hypothetical protein F911_00608	23499	9.84	2973	22	83.6	-	46.29
gi 260410843	hypothetical protein HMPREF0010_01535	53061	5.2	4064	54	93.3	-	40.86
gi 260409991	secretory lipase	46362	5.47	8246	39	83.4	-	37.15
gi 260410071	hypothetical protein HMPREF0010_02413	39534	5.2	4730	37	79.7	-	33.39

<sup>a</sup> Accession number btained from NCBI

## Discussion

Bacterial outer membrane is the envelope layer of Gram-negative cells that is exposed to the extracellular environment and thus, serves as the essential scaffold for extracellular organelles and polymers as well as a barrier to the diffusion of toxic molecules (Schooling and Beveridge, 2006). The extracellular processes that depend on the integrity of the outer membrane include those involved in pathogenesis such as assembly of adhesive organelles and protein secretion systems (Chatterjee and Chaudhuri, 2012). Thus, a comprehensive understanding of the protein composition of bacterial outer membranes could influence efforts to develop anti-infective drugs as well as vaccines that target pathogenic Gram-negative bacteria. Here we show that proteomic analysis of OMVs of *A. baumannii* grown under different growth modes can efficiently provide insights into the protein composition of this organism's outer membrane and, to a lesser degree, its periplasmic space.

Previous study has demonstrated that OMVs were observed in the culture supernatant of a biofilm culture. The OMV structures have been shown to play a role in biofilm formation (Yonezawa et al., 2009), toxin packaging and delivery (Kesty et al., 2004; Bauman and Kuehn, 2009; Bomberger et al., 2009; Haurat et al., 2011), induction of inflammatory responses (Bauman and Kuehn, 2006; Jun et al., 2013; Kim et al., 2013; Park et al., 2013; Thay et al., 2013), cell-cell communication (Berleman and Auer, 2012), and bacterial survival (Manning and Kuehn, 2011). In addition, Yonezawa et al. (2010) reported that biofilm formation by *H. pylori* strain TK1402 was strongly correlated with the production of OMV and suggested that the OMVs produced may serve as an EPS matrix for these biofilms.

Our initial SDS-PAGE analysis revealed considerable differences in the protein contents of OMVs isolated from various growth modes, while the protein contents of the OMVs from the corresponding secretory proteins remained constant. This indicates that the differences in protein contents observed in OMVs were not a result of differences in the production of these proteins within the secretory proteins.

However, the secretion systems used for the secretion of these extracellular proteins were not determined in this study. Among the almost 455 proteins detected, 202 proteins were found to be unique or more abundant in the biofilm state. Meanwhile, about 400 proteins were identified, of which 147 proteins were exclusively detected in the planktonic condition. By performing systematic comparisons with various functional genomic databases, we also showed that a moderate number of the OMVs associated proteins were apparently also involved in several key metabolic processes that were previously identified in studies of bacterial biofilms.

Activation of the metabolic pathways could be due to increased cellular physiological structure in microbial biofilms. We also postulate that other metabolic pathways related to amino acid metabolism could be used as a precursor for energy production. These metabolism pathways could be used for bacterial protection. Surprisingly, many hypothetical proteins were also identified in the OMVs. These are interesting because they suggest that the overall composition of cell surface sugars influences the architecture of OMVs, and this in turn could be related to mechanisms involving OMV biogenesis. Together, these proteins provide potential and interesting targets for further studies.

Interestingly, a large number of ribosomal proteins were identified in the biofilm OMVs. This protein may be released by the cells due to the stressor response and an enhanced permeability of the membrane. Similarly, Park et al., 2014 have also identified several ribosomal proteins in the *P. aeruginosa* OMVs associated with biofilm. These ribosomal proteins were found to be bounded by antibiotics classes and only a few of these targets appear in the planktonic OMVs, suggesting that this may be a potential mechanism of resistance that is specific to established biofilms. In line with this thought, Schooling and Beveridge (2006) reported that in *P. aeruginosa*, OMVs have multifunctional biological roles including functions in microbial interaction and host infection as well as maintenance of the structure of biofilm.

Many researchers have demonstrated that pathogen-associated molecular patterns, such as lipopolysaccharide, OMP, and lipoproteins, modulate innate and adaptive immune responses via their interaction with pattern recognition receptors in the host cells (Kuehn & Kesty, 2005; Bauman & Kuehn, 2006). OMVs of *P. aeruginosa* have also been reported to deliver multiple enzymes and virulence factors, such as beta-lactamase, into the host cytoplasm via fusion of OMV with lipid rafts in the host plasma membrane (Bomberger et al., 2009). The OmpA family protein, most abundant protein found in both the biofilm and planktonic growth mode, has been shown to be associated with a Toll-like receptor 2 and modulated immune response in epithelial cells and dendritic cells (Lee et al., 2007; Kim et al., 2008). Moreover, there are reports which demonstrated that OmpA mediated the adherence and invasion of *A. baumannii* in epithelial cells and eventually suggest that OMVs act as a vehicle for the transport of effector molecules into host cells (Choi et al., 2008c). In addition, Kwon et al. (2009) have reported that there was no significant effect on the viability of cells treated with OMVs, but the morphological change such as cellular elongation was observed.

These results suggest that the OMVs aid to deliver virulence factors into host cells and alter the physiology of the cells. OMV proteins that are essential for cell growth represent intriguing drug targets, simply because small molecules that interfere with their function may be less susceptible to cytosolic membrane processes such as drug efflux or impermeability (Altindis et al., 2014). OMV proteins that are essential for host colonisation included components of known virulence factors but also novel proteins whose functions are not fully understood. Similarly, Schooling and Beveridge (2006) reported that OMVs derived from *P.aeruginosa* PAO1 biofilms were consistently different than their planktonically derived counterparts. In another study, Haurat et al. (2011) proposed that the human oral pathogen *Porphyromonas gingivalis*, specific virulence factors are preferentially packaged into OMVs and those abundant OMPs are excluded

Based on the proteomic data, were found that majority of the identified proteins are located at the cytosol, outer and inner membrane compartment. Similarly, many investigators also reported the presence of proteins associated with the cytosol, outer and inner membrane in the OMVs (Nevot et al., 2006; Lee et al., 2008; Sidhu et al., 2008). Similar to the finding by Kwon et al. (2009), among the proteins associated with biofilm and planktonic *A. baumannii*-derived OMVs, several known virulence associated proteins were identified: AbOmpA, putative serine protease, putative Zn-dependent protease, putative protease, putative phospholipase A1 precursor, bacterioferritin, Cu/Zn superoxide dismutase, catalase, and ferrichrome–iron receptor. Interestingly, the planktonic OMVs contained Csu/C protein, a similar to fimbrial chaperone proteins (chaperone-usher pili assembly system) as the most abundant, but this particular protein was found to be absent in the biofilm OMVs. This could be as a result of the bacteria swimming freely in the *in vitro* condition.

In summary, *A. baumannii* secretes OMVs during *in vitro* biofilm and planktonic growth. These OMVs from different mode of growth contain various altered proteins. The changes in protein expression in the biofilm revealed important insights related to energy acquisition, as indicated by the metabolic pathways analyses, linking the resistance to a persistent infective behavior, a feature also seen in bacterial biofilms. *A. baumannii*-derived OMVs simultaneously deliver multiple virulence-associated proteins and pathogen-associated molecular patterns to host cells. The lack of similarity between the pathogen-specific proteins with human proteins makes these good potential targets for therapeutic intervention. Further studies of the virulence attributes of each virulence factor in OMVs are expected to provide insights into the association of *A. baumannii* pathogenesis and alterations of host cell biology.

## References

1. Altindis E, Fu Y, Mekalanos JJ. (2014) Proteomic analysis of *Vibrio cholerae* outer membrane vesicles. *Proc Natl Acad Sci* 111: E1548–E1556.
2. Bauman SJ, Kuehn MJ. (2006) Purification of outer membrane vesicles from *Pseudomonas aeruginosa* and their activation of an IL-8 response. *Microbes Infect.* 8: 2400–2408.
3. Bauman SJ, Kuehn MJ.(2009). *Pseudomonas aeruginosa* vesicles associate with and are internalized by human lung epithelial cells. *BMC Microbiol.* 9: 26 10.1186/1471-2180-9-26.
4. Berleman J, Auer M. (2012) The role of bacterial outer membrane vesicles for intra- and interspecies delivery. *Environ. Microbiol.* 15 347–354
5. Bishop DG, Work E. (1965) An extracellular glycolipid produced by *Escherichia coli* grown under lysine limiting conditions. *Biochem. J.* 96: 567–576
6. Bomberger JM, MacEachran DP, Coutermarsh BA, Ye S, O’Toole GA, Stanton BA. (2009) Long-distance delivery of bacterial virulence factors by *Pseudomonas aeruginosa* outer membrane vesicles. *PLoS Pathog.* 5:e1000382.10.1371/journal.ppat.1000382.s004
7. Bos MP, Robert V, Tommassen J. (2007) Biogenesis of the Gram-negative bacterial outer membrane. *Annu. Rev. Microbiol.* 61: 191–214
8. Chatterjee SN, Chaudhuri K. (2012) Outer membrane vesicles of bacteria. *Springer Briefs in Microbiol.* DOI: 10.1007/978-3-642-30526-9\_5
9. Chen MZ, Hsueh PR, Lee LN, Yu CJ, Yang PC, Luh KT. (2001) Severe community-acquired pneumonia due to *Acinetobacter baumannii*. *Chest* 120: 1072-1077.
10. Costerton JW, Stewart PS, Greenberg EP. (1999) Bacterial biofilms: a common cause of persistent infections *Science.* 284: 1318–1322
11. Davis KA, Moran KA, McAllister CK, Gray PJ. (2005) Multidrug-resistant *Acinetobacter* extremity infections in soldiers. *Emerg. Infect.* 11: 1218-1224.

12. Denkhaus E, Meisen S, Telgheder U, Wingender J. (2007) Chemical and physical methods for characterisation of biofilms. *Microchim Acta* 158, 1–27
13. Dijkshoorn L, Nemec A, Seifert H. (2007) An increase threat in hospitals: multidrug-resistant *Acinetobacter baumannii*. *Nat Rev Microbiol.* 5: 939-951
14. Haurat MF, Aduse-Opoku J, Rangarajan M, Dorobantu L, Gray MR, Curtis MA, Feldman MF. (2011) Selective sorting of cargo proteins into bacterial membrane vesicles. *J. Biol. Chem.* 286: 1269–1276.
15. Jun SH, Lee JH, Kim BR, Kim SI, Park TI, Lee JC, et al. (2013) *Acinetobacter baumannii* outer membrane vesicles elicit a potent innate immune response via membrane proteins. *PLoS ONE* 8: e71751
16. Kesty NC, Mason KM, Reedy M, Miller SE, Kuehn MJ. (2004) Enterotoxigenic *Escherichia coli* vesicles target toxin delivery into mammalian cells. *EMBO J.* 23: 4538–4549
17. Kim JH, Yoon YJ, Lee J, Choi EJ, Yi N, Park KS, et al. (2013) Outer membrane vesicles derived from *Escherichia coli* up-regulate expression of endothelial cell adhesion molecules *in vitro* and *in vivo*. *PLoS ONE* 8: e59276 10.1371/
18. Kwon SO, Gho YS, Lee JC, Kim SI. (2009) Proteome analysis of outer membrane vesicles from a clinical *Acinetobacter baumannii* isolate. *FEMS Microbiol Lett.* 297: 150-6. doi: 10.1111/j.1574-6968.2009.01669.
19. Lee EY, Choi DS, Kim KP, and Gho YS. (2008) Proteomics in Gram-negative bacterial outer membrane vesicles. *Mass Spec. Rev.* 27: 535-555
20. Manning AJ, Kuehn MJ. (2011) Contribution of bacterial outer membrane vesicles to innate bacterial defense. *BMC Microbiol.* 11: 258
21. Mariappan V, Vellasamy KM, Onn H, Vadivelu J. (2012) Profiling of *Burkholderia cepacia* secretome at mid-logarithmic and early-stationary phases of growth. *PLoS One.* 6: e26518. doi: 10.1371/journal.pone.0026518.
22. Mashburn LM, Whiteley M. (2005) Membrane vesicles traffic signals and facilitate group activities in a prokaryote. *Nature* 437: 422–42

23. Mayrand D, Grenier D. (1989) Biological activities of outer membrane vesicles. *Can. J. Microbiol.* 35: 607– 613
24. Moon DC, Choi CH, Lee JH, Choi CW, Kim HY et al. (2012) *Acinetobacter baumannii* outer membrane protein A modulates the biogenesis of outer membrane vesicles. *J Microbiol.* 50: 155-160. doi: 10.1007/s12275-012-1589-4.
25. Nevot M, Deroncele V, Messner P, Guinea J & Mercade E. (2006) Characterization of outer membrane vesicles released by the psychrotolerant bacterium *Pseudoalteromonas antarctica* NF3. *Environ Microbiol* 8: 1523–1533
26. Petrova OE, Schurr JR, Schurr MJ, Sauer K. (2012) Microcolony formation by the opportunistic pathogen *Pseudomonas aeruginosa* requires pyruvate and pyruvate fermentation. *Mol. Microbiol.* 86: 819–835.
27. Park AJ, Surrette MD, Khursigara CM. (2014) Antimicrobial targets localize the extracellular vesicle-associated proteome of *Pseudomonas aeruginosa* grown in a biofilm. *Frontier in Microbiol.* 5: doi:10.3389/fmicb.2014.00464.
28. Park KS, Lee J, Jang SC, Kim SR, Jang MH, Lötvall J., et al. (2013) Pulmonary inflammation induced by bacteria-free outer membrane vesicles from *Pseudomonas aeruginosa*. *Am. J. Respir. Cell Mol. Biol.* 49: 637–645
29. Ramage G, Mowat E, Jones B, Williams C, Lopez-Ribot J. (2009) Our current understanding of fungal biofilms. *Crit. Rev. Microbiol.* 35: 340–355
30. Ramli NS, Eng GC, Nathan S, Vadivelu J. (2012) The effect of environmental conditions on biofilm formation of *Burkholderia pseudomallei* clinical isolates. *PLoS One.* 7: e44104. doi: 10.1371/journal.pone.0044104.
31. Schooling SR, Beveridge TJ. (2006) Membrane vesicles: an overlooked component of the matrices of biofilms. *J. Bacteriol.* 188: 5945–5957
32. Seneviratne CJ, Wang Y, Jin L, Wong SS, Herath TD, Samaranyake LP. (2012) Unraveling the resistance of microbial biofilms: has proteomics been helpful? *Proteomics* 12: 651–665
33. Sidhu VK, Vorholter FJ, Niehaus K, Watt SA (2008) Analysis of outer membrane vesicle associated proteins isolated from the plant pathogenic bacterium *Xanthomonas campestris* pv. *Campestris*. *BMC Microbiol* 8: 87

34. Thay B, Wai SN, Oscarsson J. (2013) *Staphylococcus aureus*  $\alpha$  toxin-dependent induction of host cell death by membrane-derived vesicles. *PLoS ONE* 8: e54661
35. Villegas MV, Hartstein AI. (2003) *Acinetobacter* outbreaks, 1977-2000. *Infect. Control. Hosp. Epidemiol.* 24: 284-295.
36. Yeom J, Shin JH, Yang JY, Kim J, Hwang GS. (2013) 1H NMR-based metabolite profiling of planktonic and biofilm cells in *Acinetobacter baumannii*. *PLoS One* 8: e57730.
37. Yonezawa H, Osaki T, Kurata S, Fukuda M, Kawakami H, Ochiai K., et al. (2009) Outer membrane vesicles of *Helicobacter pylori* TK1402 are involved in biofilm formation. *BMC Microbiol.* 9: 197
38. Yonezawa H, Osaki T, Kurata S, Zaman C, Hanawa T, Kamiya S. (2010) "Assessment of *in vitro* biofilm formation by *Helicobacter pylori*," *J. Gastroenterol. Hepatol.* 25: supplement1, pp. S90–S94, 2010.
39. Yun SH, Chio CW, Park SH, Lee JC, Leam SH et al. (2008) Proteomic analysis of outer membrane proteins from *Acinetobacter baumannii* DU202 in tetracycline stress condition. *J Microbiol.* 46: 720-727. doi: 10.1007/s12275-008-0202

